PHOTONIC GENERATION OF MICROWAVE AND MILLIMETER WAVE SIGNALS

Wangzhe Li

Thesis submitted to the Faculty of Graduate and Postdoctoral Studies in partial fulfillment of the requirements for a doctoral degree in Electrical and Computer Engineering

School of Electrical Engineering and Computer Science

Faculty of Engineering

University of Ottawa

uOttawa

ACKNOWLEDGMENTS

This thesis is the end of my journey in obtaining my Ph.D. In this journey, there were moments of frustration and moments of happy and finally, truly, a moment of enjoying the scientific research. This thesis would have been impossible without the help of many people who contributed in many ways and made it an unforgettable experience for me. I would like to express my heartfelt thanks to all of them. I will cherish forever.

First and foremost, I would like to express my deepest gratitude to my supervisor, Professor Jianping Yao for the immeasurable amount of support and guidance he has provided throughout my study. His constant encouragement and patience are deeply appreciated. Without his trust and advice, this work would have never been possible.

I would also like to thank Yitang Dai, Qing Wang, Chao Wang, Honglei Guo, and Xihua Zou for their invaluable help inside and outside the laboratory when I first came to Ottawa to start my PhD study. With their help, I was able to start my research as quickly and smoothly as possible.

I would also like to thank Sebastian Blais, Hao Chi, Shilong Pan, Ming Li, Ze Li, Weilin Liu, and Hiva Shahoei for their constant help. Inspiring insights from them and fruitful discussion with them aided dissertation research a great deal.

I would also like to thank the following people, who are current or former colleagues working with me in the Microwave Photonics Research Laboratory at the School of Electrical Engineering and Computer Science, University of Ottawa: Yichen Han, Haiyun Xia, Hongqian

Mu, Weifeng Zhan, Shawn Kostyk, Montasir Qasymeh, Muguang Wang, Peiwen Chen and Wentao Cui. Their strong supports and generous help greatly improved my research work. I will always cherish the good memories of working with them.

Finally, I would like to thank my beloved mother Shuhe Wang and father Yaocai Li, for their immeasurable love and the support, materially and spiritually, throughout my life.

It is impossible to remember all, and I apologize to those I have inadvertently left out.

Again, thank you all!

ABSTRACT

Photonic generation of ultra-low phase noise and frequency-tunable microwave or millimeter-wave (mm-wave) signals has been a topic of interest in the last few years. Advanced photonic techniques, especially the recent advancement in photonic components, have enabled the generation of microwave and mm-wave signals at high frequencies with a large tunable range and ultra-low phase noise. In this thesis, techniques to generate microwave and mm-wave signals in the optical domain are investigated, with an emphasis on system architectures to achieve large frequency tunability and low phase noise.

The thesis consists of two parts. In the first part, techniques to generate microwave and mm-wave signals based on microwave frequency multiplication are investigated. Microwave frequency multiplication can be realized in the optical domain based on external modulation using a Mach-Zehnder modulator (MZM), but with limited multiplication factor. Microwave frequency multiplication based on external modulation using two cascaded MZMs to provide a larger multiplication factor has been proposed, but no generalized approach has been developed. In this thesis, a generalized approach to achieving microwave frequency multiplication using two cascaded MZMs is presented. A theoretical analysis leading to the operating conditions to achieve frequency quadrupling, sextupling or octupling is developed. The system performance in terms of phase noise, tunability and stability is investigated. To achieve microwave generation with a frequency multiplication factor (FMF) of 12, a technique based on a joint operation of polarization modulation, four-wave mixing and stimulated-Brillouin-scattering-assisted filtering is also proposed. The generation of a frequency-tunable

mm-wave signal from 48 to 132 GHz is demonstrated. The proposed architecture can even potentially boost the FMF up to 24.

In the second part, techniques to generate ultra-low phase noise and frequency-tunable microwave and mm-wave signals based on an optoelectronic oscillator (OEO) are studied. The key component in an OEO to achieve low phase noise and large frequency-tunable operation is the microwave bandpass filter. In the thesis, we first develop a microwave photonic filter with an ultra-narrow passband and large tunability based on a phase-shifted fiber Bragg grating (PS-FBG). Then, an OEO incorporating such a microwave photonic filter is developed. The performance including the tunable range and phase noise is evaluated. To further increase the frequency tunable range, a technique to achieve microwave frequency multiplication in an OEO is proposed. An mm-wave signal with a tunable range more than 40 GHz is demonstrated.

TABLE OF CONTENTS

LIST OF FIGURES

LIST OF TABLES

LIST OF ACRONYMS

BAWR	Bulk acoustic wave resonator
CCR	Ceramic coaxial resonator
CW	Continuous wave
DFB	Distributed feedback
DR	Dielectric resonator
DR	Dynamic range
DSF	Dispersion-shifted fiber
EDFA	Erbium-doped fiber amplifier
EO	Electro-optic
ESSR	Electrical spurious suppression ratio
FBG	Fiber Bragg grating
FIR	Finite impulse response
FMF	Frequency multiplication factor
FP-LD	Fabry-Perot laser diode
FSR	Free spectral range
FWHM	Full-width at half-maximum
FWM	Four wave mixing
HNLF	Highly nonlinear fiber
IIR	Infinite impulse response
IMPATT	Impact ionization avalanche transit time
MATP	Maximum transmission point
MDSL	Mminimum detectable signal level
MITP	Minimum transmission point
MM	Millimeter
MPF	Microwave photonic filter
MSFET	Metal semiconductor field-effect transistor
MZM	Mach-Zehnder modulator
OC	Optical circulator

OEO	Optoelectronic oscillator
OIL	Optical injection locking
OIP3	Output third-order intercept point
OIPLL	Optical injection phase-lock loop
ONF	Optical notch filter
OPLL	Optical phase-lock loop
OSSR	Optical sideband suppression ratio
PA	Power amplifier
PC	Polarization controller
PD	Photodetector
PM	Phase modulator
PMI	Phase modulation index
PM-IM	Phase-modulation to intensity-modulation
PolM	Polarization modulator
PS-FBG	Phase-shifted fiber Bragg grating
QTP	Quadrature transmission point
RIN	Relative intensity noise
ROM	Reciprocating optical modulator
SAW	Surface acoustic wave
SBS	Stimulated Brillouin scattering
SFDR	Spurious free dynamic range
SLCR	Sapphire-loaded cavity resonator
SLM	Single-longitudinal-mode
SMF	Single-mode fiber
SOA	Semiconductor optical amplifier
TE	Transverse electric
TEPS	Tunable electrical phase shifter
TLS	Tunable laser source
TM	Transverse magnetic
TOPS	Tunable optical phase shifter
UTC	Uni-traveling carrier

VNA	Vector network analyzer
WGM	Whispering gallery mode
YIG	Yttrium-iron-garnet

CHAPTER 1 INTRODUCTION

1.1. Background

Microwave and millimeter waves (mm-waves) are electromagnetic waves with wavelengths ranging from as long as centimeters to as short as millimeters, or equivalently, with frequencies between about 3 GHz and 300 GHz. Generation of a microwave or mm-wave signal can find extensive applications, ranging from emerging wireless communications [1-3] including high-speed, point-to-point wireless local area networks, nomadic broadband wireless systems, and inter-satellite links, to high speed optical communications, such as radio-over-fiber networks [4-6], from military radar systems [7, 8] to high resolution automotive radars in transportation areas [9-11], from bio-imaging for identifying cancers [12, 13] to test instruments. Markets for microwave and mm-wave equipment are growing rapidly, which is estimated a 63% compound annual growth rate 2011 to 2016. The global microwave and mm-wave market is forecast to total $5.6 billion in 2016 [14].

Irrespective of various applications, a microwave or mm-wave source provides the heartbeat of a microwave or mm-wave system, and the characteristics of a microwave or mm-wave source play a crucial role in determining the performance of the applications. The most important characteristics include wide operation band, large frequency tunability and ultra-low phase noise performance. For example, in an advanced frequency hopping spread spectrum communication system [15, 16], wide operation band and large frequency tunability can enhance the anti-interference capabilities, the security and the communication capacity of the system. For microwave measurement instruments, large operation band and frequency

tunability can undoubtedly enhance the measurement integrity. The ultra-low phase noise performance is also indispensable for many applications. For instance, in a radar system, phase noise at an offset frequency ranging from tens of Hz to tens of MHz is important. For a Doppler radar which identifies a moving target by measuring very small frequency changes in the reflected microwave signal, detections of targets are affected greatly by phase noise [17]. Specifically, if a hostile target is traveling head-on towards radars at about 500 km/h and a pulse in the X-band (10 GHz) is transmitted to identify the target, a difference in frequency from the transmitted and the reflected of approximately 10 kHz could be produced. Practically, given the power of the received is very small compared to that of the original signal, and to be able to detect the target requires that the phase noise of the original signal at the 10 kHz offset frequency must be lower than the power of the received signal. Otherwise, the returned signal could be hidden in the phase noise of the carrier, and the probability of detection could be low. For an airborne radar system, a severe issue is the echo from the ground, referred as "clutter" [17]. The ratio of the clutter to the reflected signal from the desired target could be as high as 80 dB; therefore, a high phase noise in either a microwave transmitter or receiver would aggravate significantly the difficulty in separating the useful signal from the "clutter". Phase noise can also affect a microwave data communications system [18, 19]. Since phase noise also appears in the time domain as an undesirable timing jitter, phase noise on clock and data signals would lead to high bit error rates. Reducing phase noise over an offset frequency from a few kHz to tens or hundreds of MHz is significant in high speed data systems to increase communication capacity and data rates.

Therefore, a microwave or mm-wave source with wide operation band, large frequency-tunability and ultra-low phase noise is a key module in various microwave and mm-wave

systems. Conventionally, a microwave or mm-wave signal is generated using an electrical oscillator [20, 21], consisting of an active gain device and a passive frequency-determining resonant cavity. The active devices include a Gunn diode, an impact ionization avalanche transit time (IMPATT) diode, a junction bipolar transistor, and a metal semiconductor field-effect transistor (MSFET), providing sufficient gain in a oscillator loop and covering frequencies up to 100 GHz or beyond. The high frequency limitation of these diodes is caused by the relatively high junction capacitance, parasitic capacitance, and stray capacitance in electrical circuits. Thus, the design and package of a high frequency diode become very sophisticated and difficult. The passive resonant cavity is used to determine the oscillation frequency. In a typical multiplied-up low-noise quartz oscillator, the resonant element is a quartz crystal with a low resonant frequency of around 10 MHz. Thus, the oscillator's frequency must be multiplied by a factor of 1000 to operate at the X-band or the K-band. Such a large multiplication factor unavoidably leads to a significant increase in the phase noise of the generated signal [22]. Other resonators used in the microwave oscillators, like dielectric resonators (DRs) [23], sapphire-loaded cavity resonators (SLCRs) [24], ceramic coaxial resonators (CCRs) [20], surface acoustic waves (SAWs) [25], and bulk acoustic wave resonators (BAWRs) [26]. Such oscillators can commonly enable the generation a microwave signal with ultra-low phase noise. For example, microwave signals with the lowest phase noise of -100 dBc/Hz at 1 Hz offset frequency ever reported have been achieved by a cryogenic sapphire oscillator using high-Q whispering gallery mode sapphire resonators [27, 28]; however, to achieve ultra-low phase noise, complex laboratory-based equipment is required and strict environmental conditions are also demanded. In addition, these oscillators have a limited range of frequency tunability and usually generate a low-frequency signal. To enhance the frequency tunability and the operation band, an yttrium-iron-garnet (YIG) resonator whose

resonant frequency in a uniform magnetic field is a linear function of the magnetic field strength is employed in the cavity. By changing the magnetic field strength, YIG-tuned [29, 30] oscillators are capable of enabling wideband frequency tuning and low phase noise simultaneously. To achieve ultra-high frequency mm-wave signals, frequency multipliers could be cascaded with YIG-tuned oscillators. However, the drawbacks of a YIG-tuned oscillator include low tuning speed, heavy weight, large footprint, high power consumption, and relatively high cost [31]. To reduce power consumption, a permanent magnet is commonly employed to boost magnetic field strength; however, such a permanent magnet bias could narrow the tuning range of an oscillator. In addition, the relatively slow tuning response and heavy weight could restrict the application of a YIG-tuned oscillator in certain practical areas.

Given the fact that it is difficult to fulfill the generation of ultra-low phase noise, wideband frequency-tunable, and high-frequency microwave or mm-wave signals based on electrical techniques, seeking photonic solutions has attracted a great attention in the past few years [32-36]. Thanks to the unique advantages of high speed, ultra-broad bandwidth, low loss (the loss in an optical fiber is in the order of 0.1 $dB \cdot km^{-1}$, whereas in a coaxial cable the loss is almost 1 dB per 30 cm), low weight (optical fiber weighs only 2 $kg \cdot km^{-1}$, whereas coaxial cable, in contrast, weighs around 560 $kg \cdot km^{-1}$.) and strong immunity to electromagnetic interference offered by photonics [37], advanced photonic techniques have enabled the generation of microwave and mm-wave signals at high frequencies with a large tunable range and ultra-low phase noise. Various photonic approaches have been proposed to realize the generation of microwave and mm-wave signals during the past a few years.

1.2. Photonic generation of microwave and millimeter wave signals

In the optical domain, a high frequency and wideband frequency-tunable microwave or mm-wave signal can be generated by simply heterodyning two optical waves of different wavelengths at a photodetector (PD), as shown in Fig. 1.1. Assume the two optical wave are given by

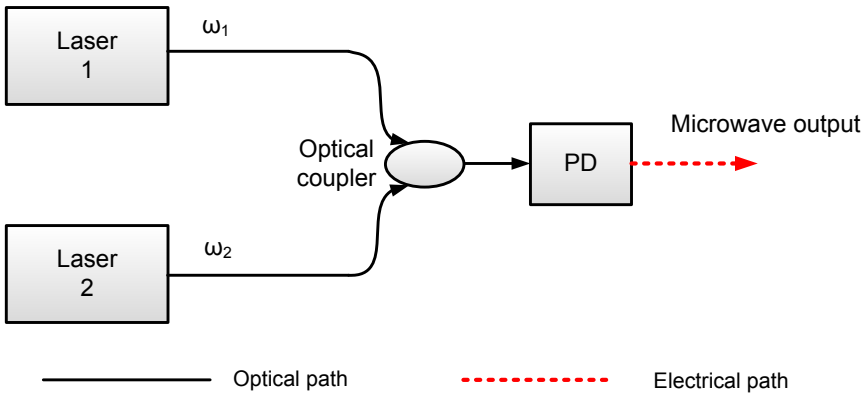

Fig. 1.1 Heterodyning of two optical waves of different wavelengths at a PD for the generation of a microwave or mm-wave signal.

$$E_1(t) = E_{01}\cos(\omega_1 t + \phi_1), \tag{1-1}$$

and

$$E_2(t) = E_{02}\cos(\omega_2 t + \phi_2), \tag{1-2}$$

where E_{01} and E_{02} are the amplitude terms, ω_1 and ω_2 are the angular frequencies, ϕ_1 and ϕ_2 are the phase terms of the two optical waves. The signal at the output of the PD can be written as

$$I(t) = \Re\left|E(t)\right|^2 = \Re\left|E_1(t) + E_2(t)\right|^2$$
$$= \Re P_1 + \Re P_2 + 2\Re\sqrt{P_1 P_2}\cos\left[\left(\omega_1 - \omega_2\right)t + \left(\phi_1 - \phi_2\right)\right], \quad (1\text{-}3)$$

where $\Re$ is the responsivity of the PD, P_1 and P_2 are the average power of the two optical waves given the bandwidth of the PD is limited. Thus, the current at the output of the PD can be expressed as

$$I_M(t) = 2\Re\sqrt{P_1 P_2}\cos\left[\left(\omega_1 - \omega_2\right)t + \left(\phi_1 - \phi_2\right)\right] \quad (1\text{-}4)$$

As can be seen from (1-4), a microwave or mm-wave signal with a frequency $\left|\omega_1 - \omega_2\right|$ is generated. Thanks to the availability of laser diodes covering a wide wavelength range, a signal with a frequency up to the THz band can be generated at the output of the PD. By tuning the wavelength/frequency difference between two laser diodes, the frequency of the generated signal is also changed. Given that the wavelengths of the laser diodes are at the 1550-nm window, 1 nm in wavelength difference corresponds approximately to a frequency difference of 125 GHz. Thus to generate a 10 GHz microwave signal, a wavelength spacing of 0.08 nm is needed.

However, due to fact that the phase terms of the two optical waves from two independent free-running laser sources are not correlated, the generated microwave or mm-wave signal would have high phase noise since the heterodyning process will transfer the relative phase fluctuations between the two optical waves to the generated microwave or mm-wave signal. To improve the quality of the generated signal, the relative optical phase fluctuations must be eliminated by making the phase terms of two laser sources or two wavelengths correlated. Numerous photonic techniques to generate microwave or mm-wave signals with low phase

noise have been proposed in the last few years. All these techniques can be classified into four categories [35]: 1) Optical injection locking (OIL), 2) Optical phase-lock loop (OPLL), 3) Microwave generation using external modulation, 4) Dual-wavelength single-longitudinal-mode (SLM) lasers. In addition, an ultra-low phase noise microwave signal can also be generated using an optoelectronic oscillator (OEO).

1.2.1. Optical injection locking

To obtain a high-quality microwave or mm-wave signal based on optical heterodyning, the phase terms of the two optical waves must be highly correlated which can be achieved through phase locking. An approach to locking the two phase terms of the two independent free-running lasers is optical injection locking (OIL) [38-42]. An OIL system typically includes a master laser, two slaver lasers, an EO modulator, a reference RF source and a PD. Fig. 1.2 shows the schematic of an OIL system.

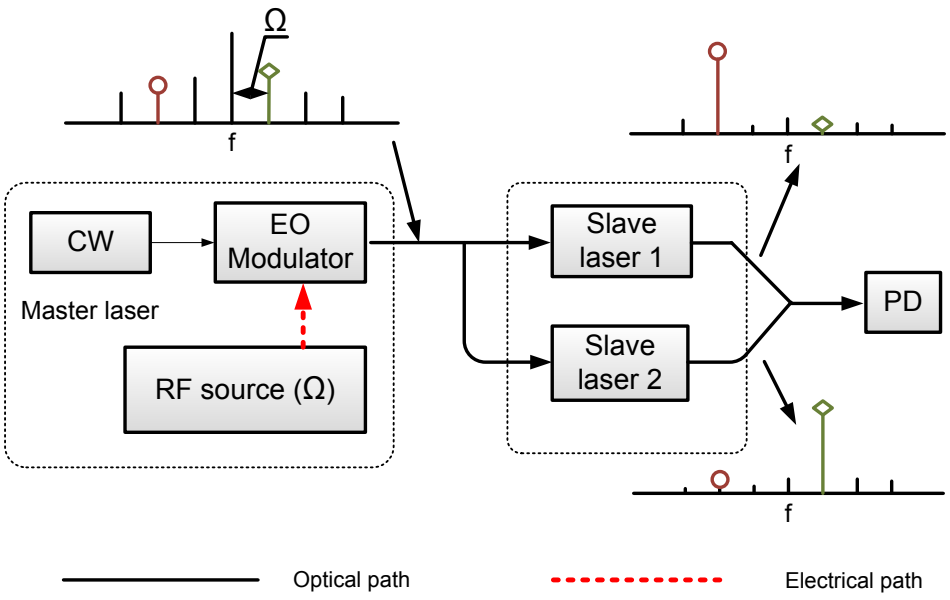

Fig. 1.2 Schematic of an optical injection locking system.

As can be seen, the light wave from a CW laser source is sent to an electro-optic (EO) modulator and is modulated by a RF signal applied to the modulator. Due to the nonlinearity of the modulation, the signal at the output the EO modulator has several pairs of optical sidebands. The signal from the EO modulator is then split into two paths, and the light wave of each path is then sent into a slave laser. If the lasing mode (the laser sources are usually single longitudinal mode lasers) of each of the free-running slave lasers is close to a certain sideband, the lasing wavelength of the slave laser is then locked to that sideband, and the two slave lasers are injection locked. For an OIL system, there are two important parameters which determine the performance of the injection locking: the frequency detuning and the injection ratio. The frequency detuning is the frequency difference between the frequencies of the injection sideband and the free-running slave laser. The larger the frequency detuning is, the more difficult the wavelength can be locked. The injection ratio is defined as a ratio between the injected power from the master laser and that of the free-running slave laser. A higher injection ratio would ensure a more stable injection locking.

1.2.2. Optical phase-lock loop

Another photonic technique for correlating the phase terms of the two free-running laser sources is to use a phase lock loop [43-51]. Fig. 1.3 shows a scheme to achieve optical phase locking of two free-running lasers. The system of the optical phase-lock loop includes two lasers, a PD, a mixer, a reference RF source, and a low-pass filter.

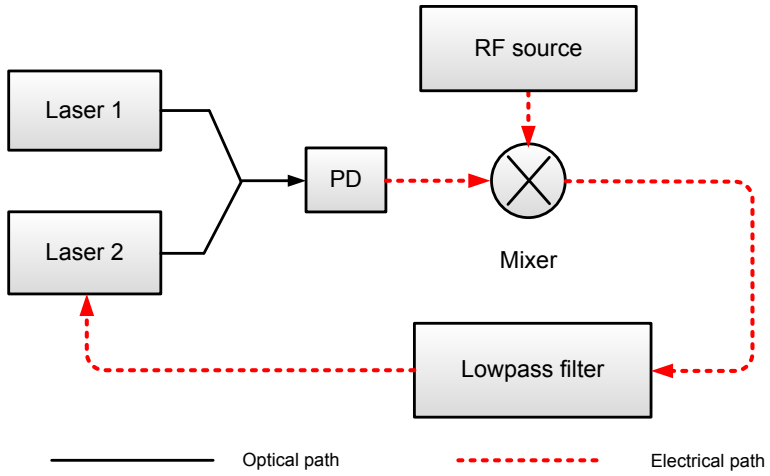

Fig. 1.3 Setup of a typical OPLL system.

As can be seen from Fig. 1.3, two optical waves are sent to the PD. At the output of the PD, a beat note with a frequency equal to the frequency difference of the two lasers is generated. The generated microwave signal is then mixed with a reference signal from the RF source and filtered by the lowpass filter. The output of the filter, which is proportional to the phase difference between the generated microwave signal and the reference signal, is then send to one of two lasers to control its injection current for cancelling the relative phase fluctuation between the two lasers.

Therefore, the phase terms of the two lasers are phase-locked and the beat note at the output of the PD is phase-locked to the RF signal. To obtain effective phase locking, the feedback loop should be short so that the feedback signal is capable of tracking the fast phase changes. Otherwise, the rapid relative phase fluctuations between the two lasers would not be cancelled and high phase noise at high offset frequency range would appear. In addition, the linewidth of the two lasers should be narrow; otherwise the high frequency components in the relative phase fluctuation of the two lasers would not be suppressed given a certain length of the loop.

Similar to the OIL scheme, the optical signal can be distributed over an optical fiber for remote distribution of a microwave signal. Note that the frequency of the RF reference source is not necessarily identical to the frequency of the generated microwave signal. In fact, if a harmonic mixer is used, then the generated microwave signal could mix with a high order harmonic of the RF reference signal, thus a relatively low frequency RF reference signal can be used. For example, to generate a 60 GHz microwave signal, one may use a 10-GHz reference source, and the sixth-order harmonic will be mixed with the beat note to produce a voltage signal to control the phase of one laser.

Comparing the two methods, OIL and OPLL, we can see that OIL has no loop delay restriction and the level of phase noise can be controlled by the injection levels into the two slave lasers, but cannot follow long-term wavelength drift of the master laser; OPLL requires a very small loop propagation delay to get an acceptable phase noise reduction if the linewidths of two lasers are relatively wide. Thus, the combination of the two schemes, an optical injection phase-lock loop (OIPLL) system, has been proposed [52-54] as a solution to increase the locking range and to reduce the phase noise, with better performance than using a single OIL or OPLL system.

Fig. 1.4 shows a block diagram that is a combination of OIL and OPLL. The light from the master laser is modulated first and then split into two paths: one is injected into the slave laser through the OIL path for injection locking; the other one combined with the light wave from the injection-locked slave laser is launched into a PD. The output of the PD is then processed in exactly the same way in a typical OPLL. The idea of the marriage of OIL and OPLL is to phase lock the slave laser to the master laser through injection locking and use the phase-locked loop to minimize the relative phase fluctuation between the master laser and the

injection locked slave laser. Both advantages of OIL and OPLL are kept, allowing the locking of wide-linewidth lasers with a wide locking range, even with considerable phase-lock loop delay. However, it is obvious that using OIPLL would greatly increase the cost and complexity of the microwave generation system.

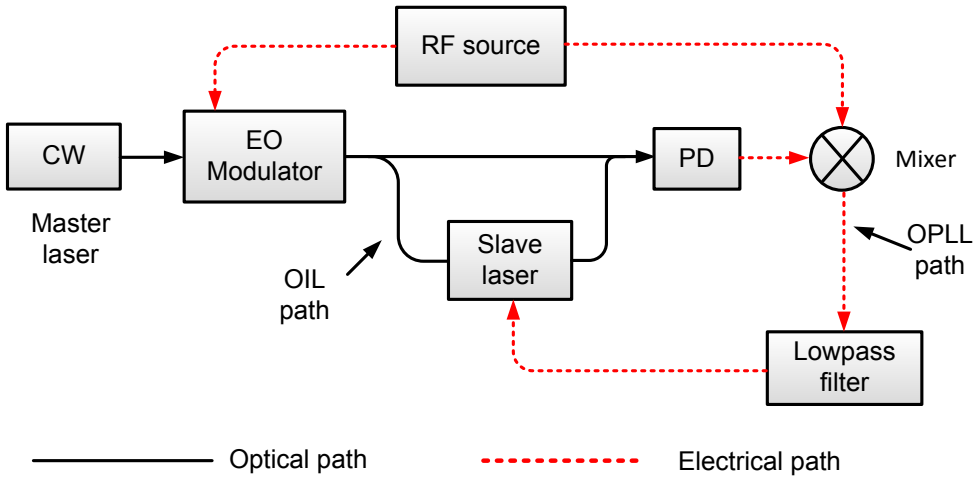

Fig. 1.4 Block diagram of a photonic microwave generation system that combines of OIL and OPLL.

1.2.3. External modulation

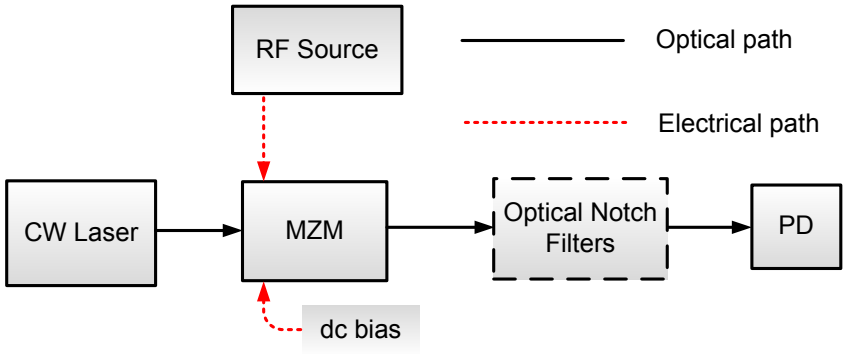

Fig. 1.5 Block diagram of external modulation for microwave generation.

Photonic generation of a microwave or mm-wave signal can also be achieved based on external modulation [57, 58], by which the frequency of a low-frequency microwave signal

can be multiplied up to a high frequency through frequency multiplication in the optical domain. Fig. 1.5 shows a basic scheme of external modulation using one Mach-Zehnder modulator (MZM) to achieve frequency doubling or quadrupling. A RF signal is applied to the MZM via the RF port. The MZM is biased at the minimum transmission point (MITP) to suppress the optical carrier when the phase modulation index is small. At the output of the MZM, only two first-order sidebands are generated. By beating the first-order sidebands at a PD, a frequency-doubled microwave signal is generated. If the MZM is biased at the maximum transmission point (MATP), at the output of the MZM, an optical signal with the optical carrier and two second-order sidebands are generated. By using an optical notch filter which is typically a Mach-Zehnder interferometer [58] or a FBG [59] to remove the optical carrier, and to beat the two sidebands at the PD, a frequency-quadrupled microwave signal is generated. The key significance of external modulation is that the frequency of the generated microwave or mm-wave signal can be continuously tuned by simply changing the frequency of the RF source. Replacing the MZM in Fig. 1.5 with a phase modulator (PM) to achieve microwave frequency doubling has also been proposed [60]. Since no bias is needed for the PM, the system is immune to the dc bias drifting problem associated with an MZM, leading to better long-term stability. The phase modulation index (PMI) must be small, otherwise, due to the existence of high order sidebands when operating at a large PMI, undesired electrical harmonics can be observed and the power penalty due to fiber chromatic dispersion would occur when optical distribution of microwave signals over fibers are required

To generate a microwave or mm-wave signal with a higher frequency multiplication factor (FMF), employing two cascaded [61-67] or paralleled [68, 69] MZMs, or two cascaded dual-parallel MZMs [70-72] has been proposed. The multiplication factor can be as high as 8, which

enables the generation of a high frequency microwave or mm-wave signal using a low-frequency microwave source. By comparing these architectures, we know that the complexity and the stability of external modulation using two cascaded MZMs are the smallest and the best, respectively. A theoretical analysis and experimental demonstration leading to the operating conditions to achieve frequency quadrupling, sextupling, and octupling using two cascaded MZMs will be presented in Chapter 3 of the thesis.

Another configuration to achieve the generation of a high-frequency microwave signal is to use a special EO modulator which is called a reciprocating optical modulator (ROM) [73, 74].

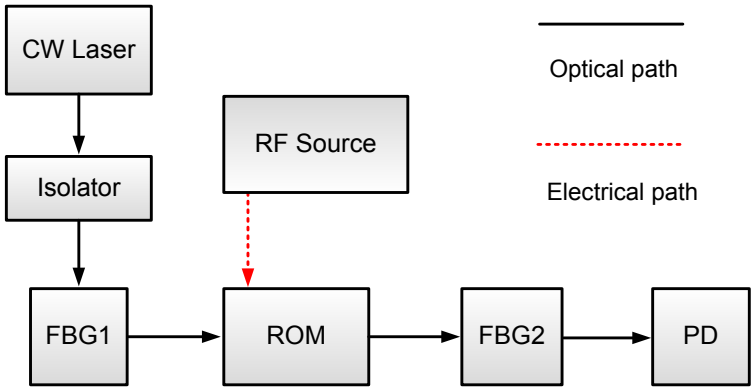

Fig. 1.6 Block diagram of a photonic microwave generation system based on external modulation using a reciprocating optical modulator.

Fig. 1.6 shows the scheme of an external modulation based system using a reciprocating modulator. The ROM has two independent sets of electrodes, enabling the modulator to modulate bidirectional light waves. Two fiber Bragg gratings (FBG1 and FBG2) are placed at each end of the ROM. FBG1 transmits the input light wave from a CW light source, but reflects light waves in a specific optical frequency range; FBG2 also reflects light waves in a specific optical frequency range, but transmits the sidebands which we aim to obtain. Thanks to the two FBGs, the light wave goes through the modulator back and forth many times and is

modulated multiple times to produce a larger number of sidebands. At the output of FBG2, two sidebands with a large frequency difference can be generated, which enables a higher frequency multiplication factor. However, due to the fact that the spectra of the FBGs are fixed, the frequency tunability of the ROM-based external modulation is limited.

The generation of a microwave or mm-wave signal with a higher FMF can also be realized by taking advantage of optical nonlinear effects in optical fibers [75-77] or semiconductor optical amplifiers (SOAs) [78, 79]. In Fig. 1.5, if an erbium-doped fiber amplifier (EDFA) and a highly nonlinear fiber (HNLF) or an SOA are placed between the modulator and the PD, the power of the modulated light wave is boosted by the EDFA, leading to the occurrence of various nonlinear phenomena [80] in the HNLF or the SOA, and consequently the generation of a large number of the sidebands of the modulated light wave can be achieved. By beating two sidebands with a large frequency difference at a high speed PD or photomixer [81-85], a high frequency microwave or mm-wave signal can be generated with a large FMF. Thus, a two-channel optical filter is required to select two desired sidebands and suppress all the other sidebands. Such a two-channel optical filter is either wavelength fixed, resulting in small frequency tunability, or very sophisticated to realize wavelength tunable, causing the increase of the complexity of the system.

1.2.4. Dual-wavelength single-longitudinal-mode laser

A dual-wavelength SLM laser has the capability of directly producing two light waves of different wavelengths. The phase correlation is better than two wavelengths generated using two independent laser sources since the two light waves are generated in the same optical cavity. An obvious advantage of using a dual-wavelength SLM laser is that the system is

simpler. Based on the gain material of the laser cavity, a dual-wavelength SLM laser could be a semiconductor laser [86-94] or a fiber laser [95-109].

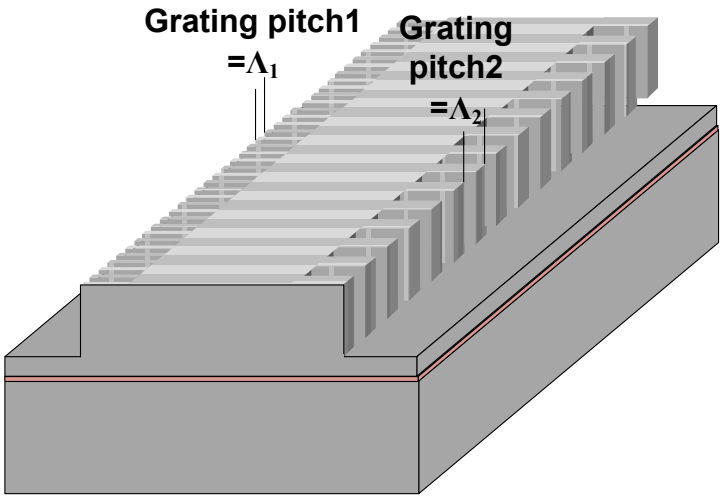

Fig. 1.7 Schematic of a typical dual-wavelength laterally coupled distributed feedback laser.

In a typical dual-wavelength SLM semiconductor laser, two FBGs with different grating pitch are fabricated in the cavity [93]. The transmission peaks of the FBGs are different but fall into the range of the gain spectrum of the laser, which guarantees that only two longitudinal modes with different wavelengths can oscillate in the laser cavity. A typical schematic picture of the dual-wavelength SLM semiconductor laser cavity is shown in Fig. 1.7, which is a laterally coupled distributed feedback (DFB) laser cavity. Two gratings are on each side of the rib waveguide. Because the two oscillating longitudinal modes are in the same cavity, two modes are affected by much the same electrical, thermal and mechanical fluctuations, also known as the common-mode-noise rejection effect. Therefore, the beat note of two modes can be expected to be of narrow bandwidth and low phase noise. Additionally, by setting the values of the two grating pitches, the frequency of the generated microwave or mm-wave signal can be as high as several THz. However, as a compact and integrated semiconductor device, the

frequency spacing of the two modes of the dual-wavelength SLM semiconductor laser cannot be adjusted flexibly. In other words, the dual-wavelength SLM semiconductor laser can be designed and fabricated for generating a frequency-fixed signal but with no or very small frequency tunability.

A dual-wavelength SLM fiber laser can also be implemented using optical fiber with a ring or a linear cavity structure. Based on different gain mechanisms in the loop, dual-wavelength SLMs can be mainly divided into three categories: 1) EDFA-based dual-wavelength SLM fiber lasers [95, 101] , 2) SOA-based dual-wavelength SLM fiber laser [102-104], and 3) stimulated Brillouin scattering (SBS) gain-based dual-wavelength SLM fiber laser [105-109]. For all these fiber lasers, the length of the ring is normally more than tens of meters, which gives a very small longitudinal mode interval. For example, in a fiber ring laser if the length of the whole ring is 20 meter, the longitudinal mode interval is only about 10 MHz. Thus, very densely-spaced longitudinal modes could exist in the fiber loop, and a two-channel ultra-narrow optical filter must be used to select only two modes to ensure a dual-wavelength SLM oscillation.

In an EDFA- or an SOA-based dual-wavelength SLM fiber laser, to pick out the desired two modes and to suppress all the other modes, various optical filtering solutions have been proposed, such as the use of two ultra-narrow band FBGs [96, 97] based on an equivalent phase shift technique [110, 111], a self-tracking ultra-narrow multi-passband filter based on a fiber loop mirror with a saturable absorber [98], external optical feedback with different diffraction gratings [99], or cascaded fiber-ring resonators with different free spectral range (FSR) [102]. Note that for all these filtering solutions, a regular bandpass filter like a fiber Fabry–Perot filter or a uniform FBG is always used to effectively suppress undesired modes.

Due to various optical filters are incorporated in the fiber loop, tuning the wavelengths of the two modes are difficult; therefore, the tunability of the frequency of the generated microwave or mm-wave signal is accordingly limited.

The homogeneous line broadening of an EDFA that causes strong gain competitions at room temperature [112] is another serious obstacle for achieving high performance microwave generation. The powers of two longitudinal modes are not stable, and consequently, the generated microwave or mm-wave signal becomes unstable. One solution is to cool the erbium doped fiber down to cryogenic temperature in liquid nitrogen [113]. However, this technique is not easy to fulfill for practical applications. Another solution is to jointly use an EDFA and an SOA. The SOA is biased in its low-gain regime. Since an SOA has much weaker homogeneous line broadening as compared with an EDFA, the incorporation of an SOA in the laser cavity would greatly reduce the gain competition of the two modes [103]. A fiber laser can also be implemented using only an SOA to provide the gain. The gain competition is again much smaller. The major limitation of using an SOA as the sole gain medium is the high optical noise generated by the SOA, which will be translated to the generated microwave signal. In addition, the heat caused by the pump current may make the gain fluctuate, which would deteriorate the quality of the generated microwave or mm-wave signal.

Therefore, microwave generation using either an EDFA-based or an SOA-based dual-wavelength SLM fiber laser has some clear drawbacks such as poor stability, small frequency tunability, and high noise.

For an SBS-gain-based dual-wavelength SLM fiber laser, on the other hand, no optical filters with ultra-narrow bandwidths are required because the bandwidth of the SBS-gain spectrum is

intrinsically narrow, only several or tens of MHz [80]. Fig. 1.8 shows schematic of a typical SBS dual-wavelength SLM fiber laser. As can be seen the fiber loop is pumped by two CW laser sources through an optical circulator (OC). The two pump waves provide two SBS gains with different central wavelength determined by the wavelengths of the pump waves. Thanks to the narrow bandwidths of the SBS gain spectra, two longitudinal modes will be generated in the loop. A key advantage of using an SBS-gain-based dual-wavelength SLM fiber laser for microwave signal generation is that the frequency of the generated microwave or the mm-wave signal can be easily controlled by changing the wavelengths of the two pump waves. A drawback of this method is the frequency drift of the generated microwave signal, since the wavelength drifts of the pump waves will be directly reflected as the frequency drifts of the two lasing modes.

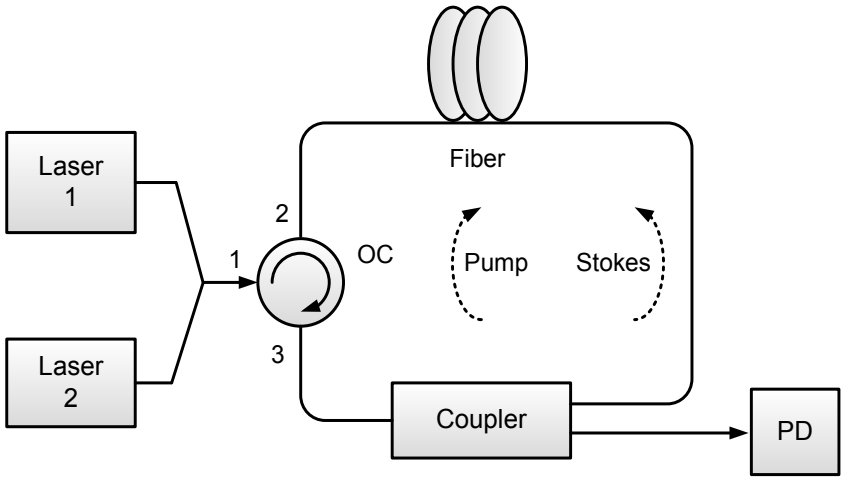

Fig. 1.8 Schematic of a typical SBS dual-wavelength SLM fiber laser.

1.2.5. Optoelectronic oscillator

In addition to the techniques to heterodyne two optical waves at a PD to generate a microwave or mm-wave signal, a microwave or mm-wave signal with a high spectral purity can also be

generated using an optoelectronic oscillator (OEO) [114-117]. Compared with the techniques using injection locking, phase-lock loop, or external modulation, the use of an OEO can generate a microwave or mm-wave signal without the need of a reference microwave source. A typical OEO is shown in Fig. 1.9, which consists of a CW laser source, an OE modulator, a single-mode fiber (SMF), a PD, an electrical bandpass filter and a microwave power amplifier (PA). The length of SMF can be very long to increase the Q factor.

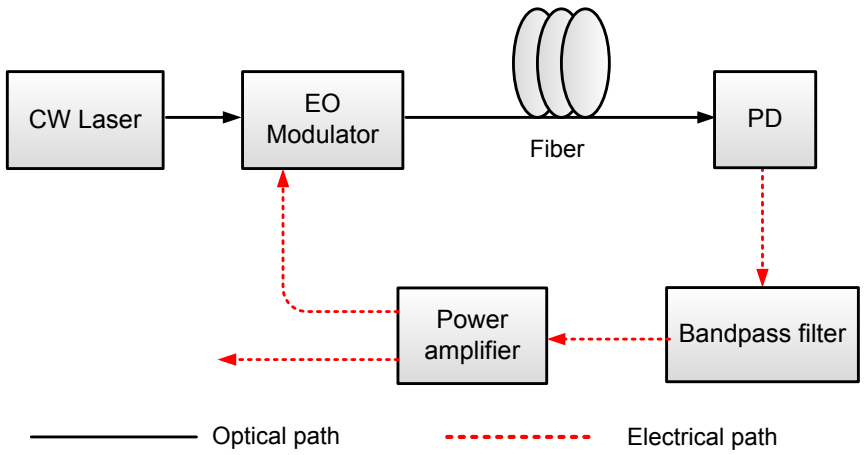

Fig. 1.9 A typical optoelectronic oscillator.

The light wave from the CW laser source is introduced into the EO modulator and modulated by the noise signal from the PA. The output of the modulator is passed through the long SMF and detected with the PD. The output of the PD, which is the recovered modulation signal, is filtered by the bandpass filter, amplified by the PA and fed back to the EO modulator. For certain frequencies, if the loop gain exceeds the loss for the circulating signals in the loop and the phase increments of these frequencies are multiples of 2π after each circulation; these frequencies will be sustained in the OEO loop. Once the OEO starts a self-sustained oscillation, a microwave or mm-wave signal can be generated. The phase noise performance of the generated signal is determined by the Q factor of the OEO loop. Due to the low loss of a

SMF, a long SMF loop up to tens of km could be used in an OEO to generate a microwave or mm-wave signal with an ultra-low phase noise. However, a long SMF would cause a large number of closely-spaced eigenmodes. To ensure a single-frequency oscillation, an electrical bandpass filter of an ultra-narrow passband (~kHz), or a high-Q filter, is required to select a desired frequency and to suppress the others. To ease the requirement for a high-Q electrical bandpass filter, the use of multiple loops in an OEO has been proposed [118-123]. Thanks to the Vernier effect, the effective mode spacing can be significantly increased. However, due to the multiple loop nature of the configuration, such an OEO would have higher system complexity and poorer system stability. More importantly, the frequency tunability would become complicated due to the fact that many loops are incorporated in the OEO. Another solution to suppress undesired modes and ensure a single-frequency oscillation is to use an injection-locked dual-OEO [124-127]. The injection-locked dual-OEO uses a master long-loop multi-mode OEO to injection lock into a slave short-loop signal-mode OEO. At the output of the slave OEO, a single-frequency microwave signal with a significantly reduced phase noise can be achieved. However, similar to a multi-loop OEO, the frequency tunability is limited.

To achieve a high-Q OEO without using a long fiber, a solution is to use a whispering gallery mode (WGM) resonator [128-134]. Thanks to the ultra-high Q factor offered by the WGM resonator, a microwave or mm-wave signal with ultra-low phase noise can be generated. Due to the small size of the WGM, the size of the OEO can be controlled small. Fig. 1.10 shows a miniaturized OEO developed by OEwaves in which a lithium niobate WGM resonator is employed.

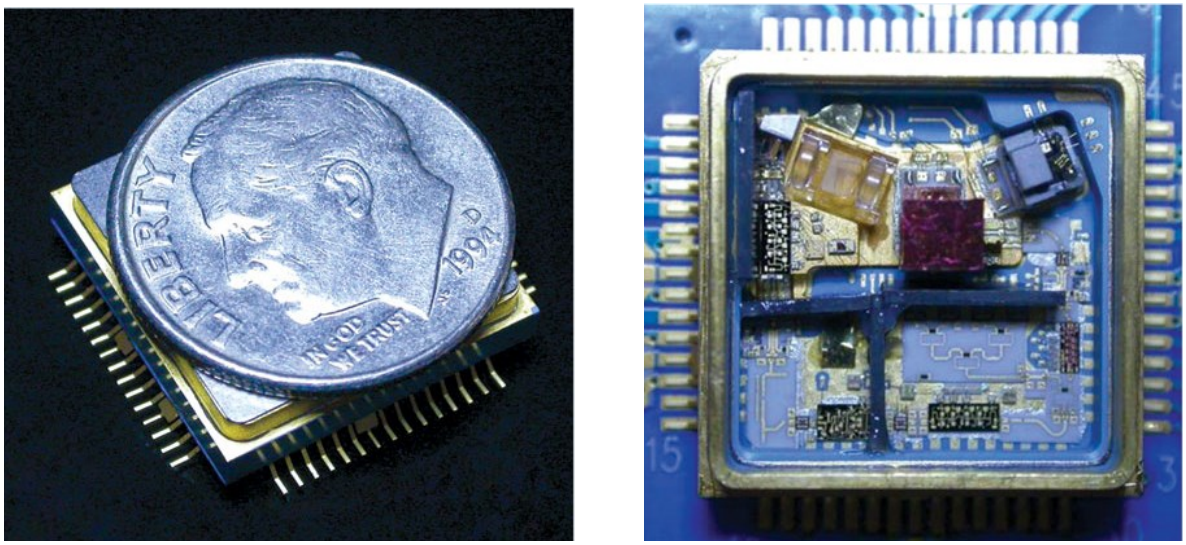

Fig. 1.10 Miniature OEO incorporating a lithium niobate WGM resonator (from OEwaves [133, 134]).

Since an electrical bandpass filter has to be used in these approaches, there are two limitations. First, the tunability is limited. Since an electrical bandpass filter is usually not tunable or the filter becomes very complicated and costly, the OEO using an electrical bandpass filter has a small frequency tunable range. The tuning is usually realized by slightly changing the mode spacing of the OEO [135-137], realized by changing the loop delay using a dispersive optical fiber [135], or a slow light element [136]. The tuning can also be realized by using a Fabry-Perot etalon [137]. The frequency tunable range can be several or tens of MHz, limited by the narrow bandwidth of the electrical bandpass filter in the loop. Another solution is to utilize a magnetically tunable filter such as an yttrium-iron-garnet (YIG) filter [138], with a center frequency tunable over a much wider frequency range of tens of GHz by varying the strength of the magnetic field. However, the bandwidth of the YIG filter is usually tens of MHz, so that a multiple loop structure has to be employed to avoid multiple eigenmode generation [139]. In addition, the fluctuations of the magnetic field strength would lead to the variations of the center frequency of the filter, leading to the frequency fluctuations of the generated microwave

or mm-wave signal. To avoid using an electrical or magnetic filter, an equivalent frequency-tunable microwave photonic filter in an OEO has been proposed [140-145]. For example, a Fabry-Perot laser diode (FP-LD) is employed to serve as a tunable high-Q microwave photonic bandpass filter [140]. Due to the external injection, the FP-LD selectively amplifies one of the modes, and high-Q frequency selection is ensured. The frequency tuning is realized by either changing the wavelength of the incident light wave or the longitudinal modes of the FP-LD. The major limitation of the technique is the mode hoping in the FP-LD, which may deteriorate the frequency stability of the generated microwave signal. In [142, 145], a high-Q microwave photonic bandpass filter is formed based on phase-modulation to intensity-modulation (PM-IM) conversion by jointly using a phase modulator and a linearly chirped FBG. The frequency tuning is realized by tuning the dispersion of the linearly chirped FBG [146, 147]. To ensure a large frequency tunable range, the dispersion must be tuned in a large range, which is hard to realize for a practical system. In [144], a high-Q spectrum-sliced photonic microwave transversal filter is proposed and demonstrated. The high-Q photonic microwave transversal filter is implemented using a sliced broadband optical source and a dispersive element, to perform a frequency-tunable microwave filter. The central frequency of the microwave filter is a function of the wavelength spacing of the sliced optical source and the chromatic dispersion of the dispersive element. Therefore, the oscillation frequency can be tuned by changing either the channel spacing of the sliced broadband optical source or the chromatic dispersion of the dispersive element.

Second, the frequency of the generated microwave signal is relatively low. Due to the fact that the central frequency of an electrical bandpass filter with a 3-dB bandwidth of a few MHz or less is usually low, and the bandwidth of an EO modulator and a PA is usually a few tens of

GHz [148-150], the frequency of the generated microwave signal is low. To increase the frequency of the generated microwave or mm-wave signal, a solution is to use frequency multiplication in an OEO [139, 151-154]. For example, in [151], two CW lasers at 1550 and 1310 nm are used. Thanks to the wavelength dependence of the half-wave voltage of an EO modulator, the modulator is biased at the quadrature transmission point (QTP) for the wavelength at 1310 nm to produce a low-frequency oscillation signal, and at the MITP for the wavelength at 1550 nm to generate a frequency-doubled signal. In [152], a special phase modulator that can support both TE and TM modes with opposite phase modulation indices [155] is employed to realize frequency doubling. The special phase modulator is also known as a polarization modulator, whose bias status is dependent on the polarization status of the light wave. Therefore, by controlling the polarization statuses of two light waves from the same laser source, two bias statuses of the modulator can be achieved. One light wave travels in the OEO loop where the modulator is biased at the QTP to generate a low-frequency microwave signal, while the other goes through the modulator which is biased at the MITP for realizing frequency doubling.

Although many solutions have been proposed to either increase the frequency of the generated microwave signal or improve the frequency-tunable range, no methods have been proposed before to solve both problems simultaneously.

1.2.6. Comparison of approaches to photonic microwave generation

All the methods introduced above for generating microwave and mm-wave signals are summarized in Table 1.1. The methods are compared in terms of frequency, frequency tunability, frequency stability, and system complexity.

TABLE 1.1 COMPARISON OF DIFFERENT METHODS TO GENERATE MICROWAVE OR MM-WAVE SIGNALS IN THE OPTICAL DOMAIN

Method		Frequency	Tunability	Stability	Complexity
OIL		<100 GHz	Fair	Fair	Medium
OPLL		< 100 GHz	Fair	Fair	Medium
Dual-wavelength SLM laser	Semiconductor laser	~ THz	Fair	Good	Low
	Fiber laser (using EDFA or SOA as gain)	~THz	Poor	Poor	High
	Fiber laser (SBS-gain)	~ THz	Good	Fair	Medium
External modulation		< 100 GHz (no optical nonlinear effects)	Good	Excellent	Low
		< 1THz (assisted with optical nonlinear effects)	Fair	Excellent	High
OEO		< 100 GHz	Fair	Good	Low

From Table 1.1, we can see that different methods have their own advantages and disadvantages. As far as frequency tunability and stability are concerned, microwave

generation based on external modulation or optoelectronic oscillation is a better and more suitable solution for practical applications.

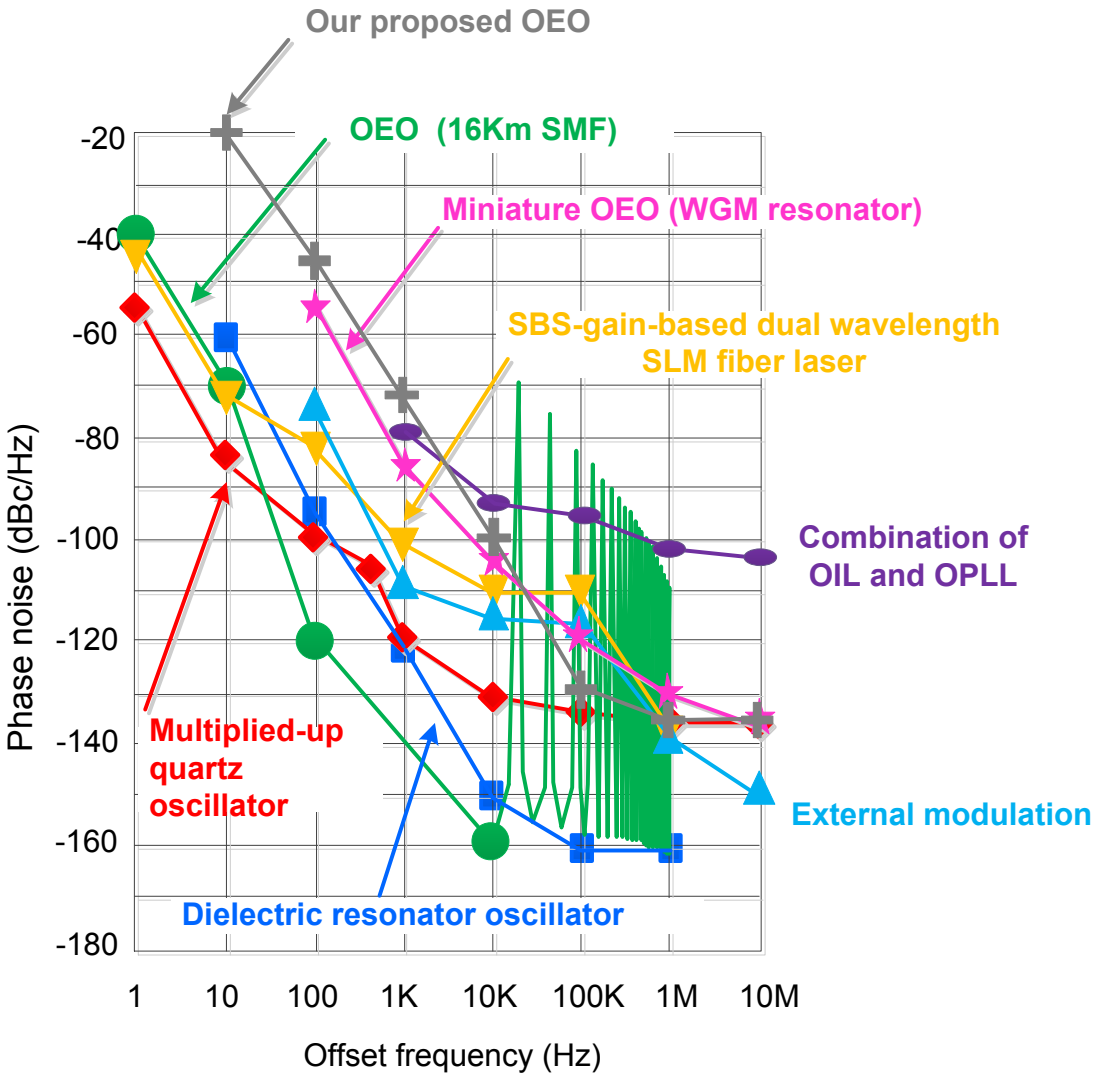

Fig. 1.11 Phase noise comparison of different photonic and electrical techniques to generate X-band microwave signals. All methods operate at 10 GHz except the combination of OIL and OPLL that operates at 36 GHz, and the miniature OEO at 30 GHz.

The comparison of the phase noise performance of approaches to photonic microwave generation is shown in Fig. 1.11 [21, 54, 67, 134, 156]. The phase noise curves of a

conventional dielectric resonator oscillator and a multiplied-up quartz oscillator are also plotted for comparison.

The phase noise performance of the generated microwave signal using an EDFA-based and SOA-based dual-wavelength SLM fiber laser is not included, since the generated microwave is so unstable that the phase noise measurement is hard to be realized. From Fig. 1.11, the combination of OIL and OPLL has the highest noise, and the OEO employing 16 km SMF provide the best phase noise performance except many undesired frequency peaks at offset frequencies higher than 10 kHz, which are the densely-spaced oscillation modes due to the long SMF. The state of art electrical techniques still beat most photonic approaches, but at the cost of small tunability.

The phase noise performance of a generated microwave or mm-wave signal can be further improved by tens of dBc/Hz using a solution called all-optical frequency division [157, 158]. Such a frequency division is accomplished by phase-locking a passively-locked femtosecond laser to an ultra-stable continuous wave optical reference. The phase locking could transfer the phase noise of the ultra-stable optical reference to the timing between the femtosecond laser pulses, and hence to a microwave signal acquired by beating two adjacent comb lines from the phase-locked femtosecond at a PD. Due to the phase locking, the phase noise of the generated microwave could be reduced by a factor of a ratio of the frequency of the optical reference to that of the microwave. Detailed description can be found in [159-163]. However, such a method is extremely complicated and cannot be widely used in practical applications.

In short, it has been demonstrated that photonic techniques are promising solutions to generate microwave or mm-wave signals with a high frequency, large frequency tunability, and ultra-low phase noise.

1.3. Major contributions of this thesis

Photonic techniques to generate microwave or mm-wave signals with improved phase noise performance and increased frequency tunability are proposed and experimentally demonstrated in this thesis.

First, techniques to generate microwave and mm-wave signals based on photonic microwave frequency multiplication are studied. Photonic microwave frequency multiplication can be realized based on external modulation using a MZM, but with limited multiplication factor. Although external modulation using two cascaded MZMs to realize microwave frequency multiplication has been proposed, the multiplication factor is still small and no generalized approach has been developed. In this thesis, a generalized approach to achieving microwave frequency multiplication using two cascaded MZMs is presented. A theoretical analysis leading to the operating conditions to achieve frequency multiplication with a larger multiplication factor, including frequency sextupling and octupling, is developed. The system performance in terms of remote generation of the microwave signals, phase noise, tunability and stability is investigated. Then external modulation assisted by optical nonlinear effects to achieve a higher frequency multiplication factor is also investigated. A technique to generate microwave generation with a frequency multiplication factor of 12 based on a joint operation of polarization modulation, four-wave mixing and stimulated-Brillouin-scattering-assisted filtering is proposed and experimentally demonstrated. The generation of a frequency-tunable

mm-wave signal from 48 to 132 GHz is achieved. The proposed architecture can even potentially boost the FMF up to 24.

Second, techniques to generate ultra-low phase noise and frequency-tunable microwave and mm-wave signals based on an optoelectronic oscillator (OEO) without using any electrical filter are investigated. In the thesis, we first develop and demonstrate a microwave photonic filter (MPF) with an ultra-narrow passband and large tunability based on a phase-shifted fiber Bragg grating (PS-FBG). Then, an OEO incorporating such an MPF is tested. The performance including the tunable range and phase noise is evaluated. To further increase the frequency tunable range, a technique to achieve microwave frequency multiplication in an OEO is proposed. An mm-wave signal with a tunable range more than 40 GHz is demonstrated.

1.4. Organization of this thesis

The thesis consists of eight chapters.

In Chapter 1, a brief review of the techniques for photonic generation of microwave and mm-wave signals is introduced. The major contributions of the work in the thesis are presented.

In Chapter 2, fundamentals about external modulation and OEO for microwave generation are presented.

In Chapter 3, external modulation using two cascaded MZMs is studied. A theoretical analysis leading to the operating conditions to achieve frequency quadrupling, sextupling or octupling is developed. Frequency sextupling and octupling are experimentally demonstrated, and the

performances of the techniques in terms of phase noise, tunability and stability are also evaluated.

In Chapter 4, photonically assisted microwave frequency twelvetupling with a large tuning range by a joint operation of external modulation, four wave mixing (FWM), and SBS-assisted filtering, is proposed and demonstrated. An mm-wave signal of a frequency up to 132 GHz is generated.

In Chapter 5, an approach to implementing a narrow-passband and frequency-tunable microwave photonic filter based on phase-modulation to intensity-modulation (PM-IM) conversion is proposed and experimentally demonstrated. Then two modified microwave photonic filter setups with an improved spurious free dynamic range (SFDR) are proposed, one of which is then experimentally demonstrated.

In Chapter 6, the incorporating the tunable microwave photonic filter in an OEO to form a frequency-tunable OEO is experimentally presented.

In Chapter 7, the implementation of an optically tunable frequency-multiplying OEO by employing external modulation in the frequency-tunable OEO achieved in Chapter 6 is investigated and experimentally demonstrated.

Finally, a conclusion is drawn in Chapter 8 with recommendations for future work.

CHAPTER 2 THEORETICAL FUNDAMENTALS

The work in the thesis is implemented based on two techniques: external modulation and optoelectronic oscillation. Thus, the fundamentals of external modulation and optoelectronic oscillation are introduced here.

2.1. External modulation using a Mach-Zehnder modulator

External modulation (see Fig. 1.5) is capable of generating two phase-correlated wavelengths for heterodyning at a photodetector (PD) to produce a microwave or mm-wave signal. It was first proposed and experimentally demonstrated by O'Reilly et al. [57] to use external modulation to generate a frequency-doubled signal. In the experiment, a Mach-Zehnder modulator (MZM) was biased at the minimum transmission point (MITP) to keep only two dominant first-order sidebands [57] for frequency doubling. To achieve a higher frequency multiplication factor (FMF) of four, O'Reilly et al. biased the MZM at the maximum transmission point (MATP) to only keep the two dominant second-order sidebands and the optical carrier. Then a Mach-Zehnder interferometer was used to remove the optical carrier for realizing the frequency quadrupling [58]. However, the frequency tunability of the generated microwave signal is limited due to the fixed free spectral range (FSR) of the Mach-Zehnder interferometer. To avoid using an Mach-Zehnder interferometer, Qi et al. proposed to use a narrow-bandwidth fiber Bragg grating (FBG) to remove the optical carrier [59]. Since the FBG has a narrow bandwidth and its central wavelength is not required to be tuned, the system provides good frequency tunability. The use of a phase modulator (PM) has also been

proposed to achieve microwave frequency doubling [60]. The key advantage of using a PM is the better long-term stability, since a phase modulator is not biased, which makes the system immune to the dc bias drifting problem. However, due to the existence of high order sidebands when operating at a large phase modulation index (PMI), undesired electrical harmonics can be observed and the power penalty due to fiber chromatic dispersion would occur when optical distribution of microwave signals over fibers are required. On the other hand, the low optical extinction ratio of the MZM caused by the imperfect optical divide ratio would cause an imperfect elimination of unwanted optical sidebands, which would degrade the optical sideband suppression ratio (OSSR) and the electrical spurious suppression ratio (ESSR). In order to realize a higher optical extinction ratio, Kawanishi et al. proposed a specially designed MZM whose optical extinction ratio can be as high as 70 dB [164-166]. Two dc-driven sub-MZMs as two active optical intensity trimmers are incorporated in the two arms of the main MZM to perfectly balance the light intensity travelling through the arms to improve the extinction ratio. However, since this special modulator requires the control of three dc bias voltages, an extra care is needed to avoid the bias fluctuations which would cause the appearance of the undesired sidebands and the degradation of the phase noise of the generated microwave signal. An alternative solution is to use an AlGaAs/GaAs-waveguide-based polarization modulator (PolM) [155]. A PolM is a special phase modulator that supports both transverse electric (TE) and transverse magnetic (TM) modes with opposite phase modulation indices (PMIs). By connecting the PolM with a polarizer, an equivalent MZM is achieved. Since no dc bias is needed, the PolM-based system is free from bias drifting problem which guarantees a more stable operation.

2.1.1. Mathematical description of external modulation

The experimental schematic of a conventional external modulation is shown in Fig. 2.1, it consists of a continuous wave (CW) laser source, an MZM, a polarization controller (PC), an erbium doped fiber amplifier (EDFA), a microwave source, a microwave power amplifier (PA) and a PD. A low-frequency microwave drive signal from a microwave source is amplified by the PA, and applied to the MZM. The PC is used to minimize the polarization-dependent insertion loss of the MZM. The EDFA is used to compensate the loss in the system. A wavelength-fixed FBG notch filter would be also incorporated if the optical carrier has to be removed.

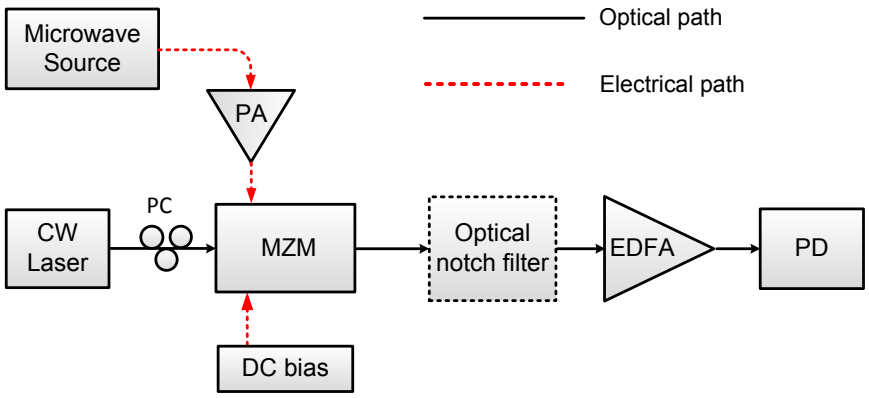

Fig. 2.1 Experimental schematic of the conventional external modulation system.

We start our analysis from a general expression of the electrical field at the output of the MZM driven by a low frequency microwave signal with a small phase modulation index (PMI). The optical extinction ratio of the MZM is assumed to be infinite. When the incident light wave is $E_0\cos(\omega_o t)$, the microwave signal is $V\cos(\omega_m t+\varphi)$, the electrical field $E(t)$ at the output of the MZM can be expressed as

$$
\begin{aligned}
E(t) \propto E_0 \left\{ \cos\left[\omega_o t + \beta\cos(\omega_m t + \varphi) + \Phi\right] + \cos\left[\omega_o t - \beta\cos(\omega_m t + \varphi)\right] \right\} \\
= E_0 \cos(\Phi/2) \times \\
\left\{ \cos(\omega_o t + \Phi/2) J_0(\beta) \right. \\
+ \sum_{n=1}^{\infty} (-1)^n J_{2n}(\beta) \left[\cos(\omega_o t + 2n(\omega_m t + \varphi) + \Phi/2) \right. \\
\left. \left. + \cos(\omega_o t - 2n(\omega_m t + \varphi) + \Phi/2) \right] \right\} \\
+ E_0 \sin(\Phi/2) \times \\
\sum_{n=1}^{\infty} (-1)^n J_{2n-1}(\beta) \left\{ \left[\cos\left[\omega_o t + (2n-1)(\omega_m t + \varphi) + \Phi/2\right] \right. \right. \\
\left. \left. + \cos\left[\omega_o t - (2n-1)(\omega_m t + \varphi) + \Phi/2\right] \right\} \right.
\end{aligned}
\tag{2-1}
$$

where E_0 is the electrical amplitude of the incident lightwave, V is the amplitude of the drive signal, ω_o and ω_m are respectively the angular frequencies of the light wave and the microwave drive signal, J_i is the i^{th}-order Bessel function of the first kind, φ is the phase of the microwave drive signal applied to the MZM, Φ is an additional phase difference between the two optical signals from the two arms of the MZM which is introduced by the bias voltage. And β is the PMI, equal to $\pi V/2V_\pi$ where V_π is the half-wave voltage of the MZM.

From (2-1), we can see that if Φ is 0, which means the MZM is biased at the MATP, all the odd-order sidebands would be suppressed; if Φ is π, which means the MZM is biased at the MITP, all the even-order sidebands would be suppressed. As long as the PMI is small, the high-order sidebands are negligible. Therefore, when the MZM is biased at the MATP and the optical notch filter is used to remove the residual optical carrier, only the two dominant second-order sidebands would be considered. By beating the two second-order sidebands at the PD, a frequency-quadrupled microwave signal can be generated; when the MZM is biased at the MITP, only the two dominant first-order sidebands would be considered. By beating the two first-order sidebands at the PD, a frequency-doubling microwave signal can be generated.

Thanks to the frequency multiplication, the generated frequency-multiplied microwave signal can be expressed as $V'\cos[N\omega_m t+N\varphi]$, where V' is the amplitude of the generated signal, and N is the frequency multiplication factor (FMF), which is two and four for frequency doubling and quadrupling. By tuning the frequency of the microwave source, ω_m, the frequency of the frequency-doubled or quadrupled microwave signal, $N\omega_m$, can also be changed. Practically, the lower limit of the frequency tunable range is determined by the bandwidth of the notch of the optical notch filter, while the upper limit of the frequency tunable range is determined by the bandwidth of the MZM and the PA.

For the signal from the microwave source, $V\cos(\omega_m t+\varphi)$, φ also is the phase deviation from the nominal phase $2\omega_m t$. In the frequency domain, we define $\tilde{\varphi}$, the Fourier transform of the phase deviation φ. Then the power spectral density $S_\varphi(f)$ of the phase fluctuations is given by

$$10\log_{10}\left[S_\varphi(f)\right]=10\log_{10}\left[\left(\tilde{\varphi}\right.\right. \qquad \left.\left.\tilde{\varphi}\right)\right] \tag{2-2}$$

Similarly, the power spectral density of the phase fluctuations $S'_{\tilde{\varphi}}(f)$ of the frequency-multiplied microwave signal is given by

$$\begin{aligned} 10\log_{10}\left[S'_{\tilde{\varphi}}(f)\right] &= 10\log_{10}\left[\left(N\tilde{\varphi}\right.\right. \\ &= 20\log_{10}\left(N\tilde{\varphi}\right. \\ &= 20\log_{10}\left(\tilde{\varphi}\right. \qquad {}_{10}(N) \\ &= 10\log_{10}\left[S_\varphi(f)\right]+20\log_{10}(N) \end{aligned} \tag{2-3}$$

From (2-3), we can see that due to the frequency multiplication, the phase noise of the frequency-multiplied microwave signal is theoretically degraded, causing an increase of $20\log_{10}(N)$ from the original phase noise of the signal applied to the MZM.

2.2. Optoelectronic oscillator

An OEO (see Fig. 1.10), which is a ring oscillator with both electrical and optical paths, was first proposed by Yao et al [115, 116]. In the OEO, the light wave is modulated by the input electrical signal $V_{in}(t)$ via the EO modulator. Note that at first the input electrical signal is the internal noise from the electrical devices in the loop. The modulated light wave is then delayed by the single mode fiber (SMF) and recovered at the output of the PD. The signal at the output of the PD is filtered by the bandpass filter and fed back into the input of the PA to be recombined with the input signal. If the net round trip gain is greater than or equal to unity, and the phase increments of certain frequencies of the input signal after each loop are some multiples of 2π, those frequency components will add resonantly and build up faster to start oscillating. The narrow bandpass filter in the loop is used to select one oscillation frequency, ensuring that the OEO operates at a single stable frequency oscillation.

2.2.1. Mathematical description of the optoelectronic oscillator

In order to determine the output signal $V_{out}(t)$ of the OEO, we need to study the signal evolution of the OEO over a single loop first. Assume the loss of the OEO is L, and the gain is G, the delay of the OEO loop is τ, the frequency response of the bandpass filter is $\tilde{H}(\omega)$, and its inverse Fourier transform is $F(t)$, the output signal after circulating the loop once becomes

$$V_{out}(t+\tau) = \int_{-\infty}^{\infty} GLV_{out}(t)F(t-s)ds \tag{2-4}$$

Then the input signal $V_{in}(t)$ is added to (2-4) to obtain the oscillator signal after one round trip

$$V_{out}(t+\tau) = \int_{-\infty}^{\infty} GLV_{out}(t)F(t-s)ds + V_{in}(t) \tag{2-5}$$

For convenience, we can apply the time shift t to t-τ to (2-5) to obtain

$$V_{out}(t) = \int_{-\infty}^{\infty} GLV_{out}(t-\tau)F(t-\tau-s)ds + V_{in}(t-\tau) \tag{2-6}$$

Practically, G is a decreasing function of $V_{out}(t)$. As the oscillating signal increases, the round trip gain decreases until, at equilibrium, the gain saturates and the oscillating signal remains constant with each round trip. In this stable equilibrium condition, the round trip gain becomes a constant value $G(V_s)$, where V_s is the amplitude of the oscillator signal at equilibrium. Replacing G with $G(V_s)$ in (2-6) gives

$$V_{out}(t) = G(V_s)L\int_{-\infty}^{\infty} V_{out}(t-\tau)F(t-\tau-s)ds + V_{in}(t-\tau) \tag{2-7}$$

The Fourier transform of (2-7) is

$$\tilde{V}_{out}(\omega) = G(V_s)L\tilde{V}_{out}(\omega)\tilde{F}(\omega)\exp(-j\omega\tau) + \tilde{V}_{in}(\omega)\exp(-j\omega\tau), \tag{2-8}$$

where $\tilde{V}_{in}(\omega)$ and $\tilde{V}_{out}(\omega)$ are the Fourier amplitudes of the oscillating input and output signals. It is noted that (2-8) is obtained by assuming that the oscillating signal remains unchanged from one round trip to the next at equilibrium.

Based on (2-8), at equilibrium, the output signal spectrum is

$$\tilde{I}_{out}(\omega) = \frac{\tilde{I}_{in}(\omega)\exp(-j\omega\tau)}{1-G(V_s)L\tilde{I}(\omega)\exp(-j\omega\tau)} \tag{2-9}$$

From, (2-9), we can see that the delayed feedback in the OEO loop acts as a first-order finite-impulse-response (FIR) filter.

The relative power spectral density of the oscillator's equilibrium output signal can be expressed as

$$\begin{aligned} P_{out}(\omega) &= \frac{\left|\tilde{I}_{out}(\omega)\right|^2}{R} \\ &= \left|\frac{\tilde{I}_{in}(\omega)}{1-G(V_s)L\tilde{I}(\omega)\exp(-j\omega\tau)}\right|^2 \frac{1}{R} \\ &= \frac{P_{in}(\omega)}{1+\left|G(V_s)L\tilde{I}(\omega)\right|^2 - 2\left|G(V_s)L\tilde{I}(\omega)\right|\cos(\omega\tau)} \end{aligned} \tag{2-10}$$

where R is the OEO's output impedance and

$$P_{in}(\omega) = \frac{\left|\tilde{I}_{in}(\omega)\right|^2}{R} \tag{2-11}$$

is the input signal power density. The relative power spectral density $S(\omega)$, as the power spectral density $P(\omega)$ divided by the total signal power $P_{osc}(\omega)$. The total signal power is

$$P_{osc} = \int_{-\infty}^{\infty} P(\omega)d\omega \tag{2-12}$$

The relative power spectral density can be written as

$$S(\omega)=\frac{\rho_{in}(\omega)}{1+\left|G(V_s)L\tilde{I}(\omega)\right|^2-2\left|G(V_s)L\tilde{I}(\omega)\right|\cos(\omega\tau)}, \tag{2-13}$$

where

$$\rho_{in}(\omega)=\frac{P_{in}(\omega)}{P_{osc}} \tag{2-14}$$

is the relative input power spectral density.

The input signal of the OEO comes from noise in the active devices in the OEO, including the laser, the PA and the PD. These noises are entirely additive noise, consisting of thermal noise, shot noise and laser noise [167-170]. Regardless of the noise sources, the input signal is treated as white noise. Then the relative input power spectral density of the OEO, $\rho_{in}(\omega)$, becomes a constant ρ_n, which is the relative white noise level.

In a typical OEO, the narrow bandpass filter ensures that the OEO's power spectrum lies in a narrow range (~MHz) around the filter's center frequency (~GHz). Since the filter's bandwidth is much smaller than its center frequency, we define an offset frequency $f'=(\omega-\omega_{osc})/2\pi$, where ω_{osc} is the central oscillating frequency of the OEO. Assume that the amplitude of the frequency response of the bandpass filter is constant over its bandwidth, the OEO's relative power spectral density becomes

$$S(f')=\frac{\rho_n}{1+\left|G_s\right|^2-2\left|G_s\right|\cos(2\pi f'\tau)} \tag{2-15}$$

within the filter's bandwidth, where $G_s=G(V_s)L\tilde{I}(\omega)$.

Eq. (2-15) is capable of providing qualitative analysis of the power spectral density of the OEO. Obviously, the denominator of (2-15) is periodic in offset frequency f'. The peak value of the power spectral density of the oscillating OEO is

$$S_{\max} = \frac{\rho_n}{\left(1-|G_s|\right)^2} \tag{2-16}$$

when $f' = n/\tau$, where n is an integer.

In a typical OEO, $\left(1-G_s\right) << 1$ so that $S_{\max} >> \rho_n$. Therefore, at equilibrium, the peak power density of the oscillating signal of the OEO is much larger than the white noise level. The offset frequencies that satisfy $f' = n/\tau$ are the resonant modes of the OEOs. Obviously, the mode-spacing of the OEO is simply 1/τ. And the bandwidth of the passband filter should be narrow enough to ensure single mode oscillation of the OEO.

If we do Taylor expanding to the denominator in (2-15) around $f' = 0$ and keep terms up to second order in f', we will have

$$\begin{aligned} S(f') &= \frac{\rho_n}{1+|G_s|^2 - 2|G_s|\left[1-2\left(\pi f'\tau\right)^2\right]} \\ &= \frac{\rho_n}{\left(1-|G_s|\right)^2 + |G_s|\left(2\pi f'\tau\right)^2} \end{aligned} \tag{2-17}$$

which is a Lorentzian with a full width at half-maximum (FWHM) given by

$$\Delta f_{FWHM} = \frac{1-|G_s|}{\pi\tau\sqrt{|G_s|}} \tag{2-18}$$

Then, (2-17) can be rewritten as

$$S(f') = \begin{cases} S_{\max} & , \quad |f'| << \Delta f_{FWHM}/2 \\ \dfrac{S_{\max}}{|G_s|(2\pi f'\tau)^2}, & |f'| >> \Delta f_{FWHM}/2 \end{cases} \tag{2-19}$$

For (2-17), by using the normalization condition

$$\int_{-\infty}^{\infty} S(f')df' \approx \int_{-1/2\tau}^{1/2\tau} S(f')df' = 1, \tag{2-20}$$

we have

$$1-|G_s|^2 \approx 2\left[1-|G_s|\right] = \rho_n/\tau \tag{2-21}$$

We assume that the spectral width of the oscillating frequency is much smaller than the mode spacing $1/\tau$, which is true in the real world, so that the integration over one mode spacing is sufficiently accurate. In addition, in a typical OEO, $\rho_n << 1$ and $(1-G_s) << 1$. Substituting (2-21) in (2-17), the OEO's relative power spectral density can be rewritten as

$$S(f') = \frac{\rho_n}{(\rho_n/2\tau)^2 + (2\pi f'\tau)^2} \tag{2-22}$$

and (2-19) can also be expressed as

$$S(f') = \begin{cases} \dfrac{4\tau^2}{\rho_n} & , \quad |f'| << \Delta f_{FWHM}/2 \\ \dfrac{\rho_n}{(2\pi f'\tau)^2} & , \quad |f'| >> \Delta f_{FWHM}/2 \end{cases} \tag{2-23}$$

From (2-23), we can see that for the offset frequencies much less than the FWHM frequency, the power spectral density, namely, the phase noise, of the oscillating frequency of the OEO is approximately constant; for the offset frequencies much larger than the FWHM frequency, the phase noise of the oscillating frequency is inversely proportional to the square of the delay and the offset frequency. However, in practice, the FWHM frequency is extremely small (~mHz), leading to a offset frequency range corresponding to the constant phase noise is too small to be measured using even the most sensitive carrier suppression techniques [171-173]. Therefore the flat region of the phase noise predicted theoretically here is never observed practically.

In addition, it is obvious from (2-23) that for a fix offset frequency, the phase noise decreases quadratically with the loop delay time. However, the phase noise will not drop to zero no matter how large the delay becomes, because, at a large delay, assumptions for (2-21) will not be correct, and (2-22) and (2-23) are not valid anymore.

More importantly, from (2-22), we can also know that the phase noise of the OEO is frequency-independent, which is a significant advantage and different from the frequency-multiplying methods by which the phase noise of the generated signal approximately increases quadratically with the frequency.

CHAPTER 3 EXTERNAL MODULATION USING TWO CASCADED MACH-ZEHNDER MODULATORS

Microwave frequency multiplication based on external modulation using two cascaded Mach-Zehnder modulators (MZMs) has been considered an effective solution for high-frequency and frequency-tunable microwave signal generation. Different techniques have been demonstrated, but no generalized approach has been developed. In this chapter, a theoretical analysis leading to the operating conditions to achieve frequency quadrupling, sextupling or octupling is developed. Depending on the bias of the two MZMs, the maximum transmission point (MATP) or the minimum transmission point (MITP), there are four bias combinations: 1) MATP, MATP, 2) MITP, MITP, 3) MATP, MITP, and 4) MITP, MATP, with each combination leading to a different multiplication factor. Experimental verifications are then provided to validate the analysis.

3.1 Principle of the frequency multiplication based on external modulation using two cascaded Mach-Zehnder modulators

A system using two cascaded MZMs to achieve microwave multiplication is shown in Fig. 3.1. The system consists of a continuous wave (CW) laser source, two MZMs, a tunable optical phase shifter (TOPS), two polarization controllers (PCs), an erbium doped fiber amplifier (EDFA), and a photodetector (PD). A low-frequency microwave drive signal from a microwave source is divided into two paths by a power divider, amplified by two microwave power amplifiers (PAs), and applied to the two MZMs. A tunable electrical phase shifter

(TEPS) can be used between one PA and the corresponding MZM to replace the TOPS. The functions of the TOPS and the TEPS are the same, which will be explained further on in this section. The two PCs are used to minimize the polarization-dependent insert losses of the two MZMs. A wavelength-fixed fiber Bragg grating (FBG) notch filter would be also incorporated in some cases to remove the optical carrier, which will be explained later.

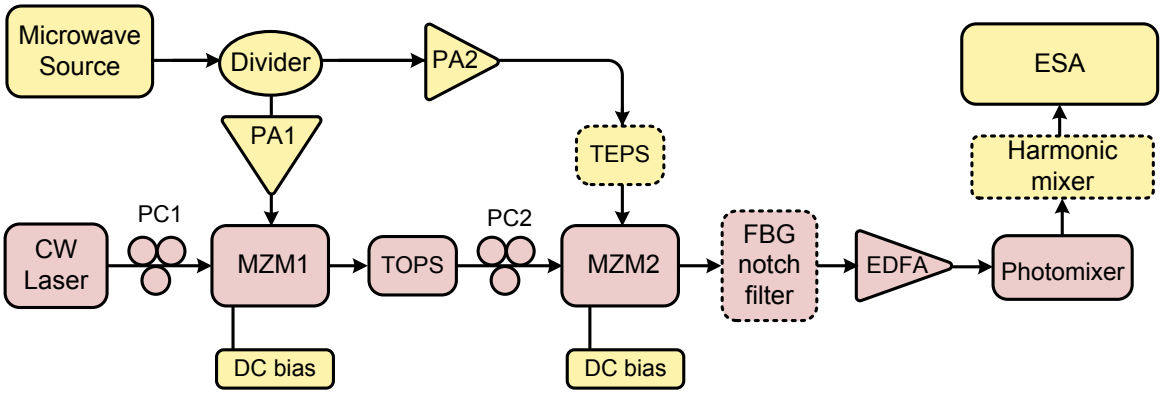

Fig. 3.1 Schematic diagram of the proposed microwave frequency multiplication system based on external modulation using two MZMs. ESA: electrical spectrum analyzer.

Each MZM is biased at the MATP or the MITP to suppress all the odd-order or the even-order sidebands. The cascade of two MZMs would lead to four bias combinations: 1) MATP, MATP, 2) MITP, MITP, 3) MATP, MITP, and 4) MITP, MATP. By properly controlling the power of the drive signals applied to the two MZMs and the phase shift introduced by the TOPS or the TEPS, only two dominant sidebands would remain at the output of the second MZM (MZM2). Depending on the different bias combinations, the frequency spacing of the two sidebands could be four, six, or eight times the frequency of the drive signal. By beating the two sidebands at the PD, a frequency quadrupled, sextupled or octupled microwave signal can be generated.

In the following, based on the theoretical analysis presented in Section 2.1, we will perform a theoretical analysis for the setup shown in Fig. 3.1 for four different bias point combinations.

3.1.1 MATP and MATP

The two MZMs are both biased at the MATP, that is, the additional phase difference between the two optical signals from the two arms of the i^{th} MZM Φ_i=0 for i=1, 2. According to (2-1), the signal $E_1(t)$ at the output of the first MZM (MZM1) can be written as

$$\begin{aligned} E_1(t) \propto\ & E_0 J_0(\beta_1)\cos(\omega_o t) \\ & - E_0 J_2(\beta_1)\cos\left((\omega_o - 2\omega_m)t - 2\varphi_1\right) \\ & - E_0 J_2(\beta_1)\cos\left((\omega_o + 2\omega_m)t + 2\varphi_1\right) \end{aligned} \tag{3-1}$$

where E_0 is the electrical amplitude of the incident light wave, ω_o and ω_m are respectively the angular frequencies of the light wave and the microwave drive signal, $J_i(\beta)$ is the i^{th}-order Bessel function of the first kind, β_1 is the phase modulation index (PMI) applied to MZM1 and φ_1 is the initial phase of the drive signal applied to MZM1. When the lightwave is traveling through the TOPS, a phase difference ϕ between the two adjacent even-order sidebands would be introduced and the electrical field $E_1'(t)$ at the output of the TOPS can be written as

$$\begin{aligned} E_1'(t) \propto\ & E_0 J_0(\beta_1)\cos(\omega_o t + 2\phi) \\ & - E_0 J_2(\beta_1)\cos\left((\omega_o - 2\omega_m)t - 2\varphi_1 + \phi\right) \\ & - E_0 J_2(\beta_1)\cos\left((\omega_o + 2\omega_m)t + 2\varphi_1 + 3\phi\right) \end{aligned} \tag{3-2}$$

$E_1'(t)$ is then sent to MZM2. The electrical field $E_2(t)$ at the output of MZM2 is given

$$
\begin{aligned}
E_2(t) \propto E_0 \{ & J_2(\beta_1) J_2(\beta_2) \cos((\omega_o - 4\omega_m)t + \phi - 2\varphi_1 - 2\varphi_2) \\
& - J_2(\beta_1) J_0(\beta_2) \cos((\omega_o - 2\omega_m)t + \phi - 2\varphi_1) \\
& - J_0(\beta_1) J_2(\beta_2) \cos((\omega_o - 2\omega_m)t + 2\phi - 2\varphi_2) \\
& + J_2(\beta_1) J_2(\beta_2) \cos(\omega_o t + \phi - 2\varphi_1 + 2\varphi_2) \\
& + J_0(\beta_1) J_0(\beta_2) \cos(\omega_o t + 2\phi) \\
& + J_2(\beta_1) J_2(\beta_2) \cos(\omega_o t + 3\phi + 2\varphi_1 - 2\varphi_2) \\
& - J_0(\beta_1) J_2(\beta_2) \cos((\omega_o + 2\omega_m)t + 2\phi + 2\varphi_2) \\
& - J_2(\beta_1) J_0(\beta_2) \cos((\omega_o + 2\omega_m)t + 3\phi + 2\varphi_1) \\
& + J_2(\beta_1) J_2(\beta_2) \cos((\omega_o + 4\omega_m)t + 3\phi + 2\varphi_1 + 2\varphi_2) \} \qquad (3\text{-}3)
\end{aligned}
$$

where β_2 is the PMI applied to MZM2 and φ_2 is the initial phase of the drive signal applied to MZM2. If two conditions, $\phi+2\varphi_1-2\varphi_2=(2k+1)\pi$, k is an integer, and $\beta_1=\beta_2=\beta$ are satisfied, we have $J_0(\beta_1)J_2(\beta_2)=J_0(\beta_2)J_2(\beta_1)$ and (3-3) can be simplified into

$$
\begin{aligned}
E_2(t) \propto E_0 \{ & J_2^2(\beta) \cos((\omega_o - 4\omega_m)t + \phi - 2\varphi_1 - 2\varphi_2) \\
& + \left[J_0^2(\beta) - 2J_2^{\,2}(\beta) \right] \cos(\omega_o t + 2\phi) \\
& + J_2^2(\beta) \cos((\omega_o + 4\omega_m)t + 3\phi + 2\varphi_1 + 2\varphi_2) \} \qquad (3\text{-}4)
\end{aligned}
$$

As can be seen only the carrier and the fourth-order sidebands are present. In addition, if $J_0^2(\beta) = 2J_2^2(\beta)$, that is $\beta \approx 1.6995$, is satisfied, then the optical carrier will be suppressed and only the fourth-order sidebands will remain. By beating the two fourth-order sidebands at the PD, a signal with a frequency that is eight times the frequency of the drive signal can be generated, which is called frequency-octupled signal. The FMF is eight.

If the condition $J_0^2(\beta) = 2J_2^2(\beta)$ is not satisfied, the optical carrier will appear which will become dominant as β is decreasing. An alternative solution to remove the optical carrier is to use a FBG wavelength-fixed notch filter, which is shown in Fig. 3.1.

In addition to the dominant fourth-order sidebands, if $\beta_1=\beta_2=\beta\approx1.6995$ and there is no optical carrier signal, there would also exit sixth-order sidebands. In the optical domain, the optical sideband suppression ratio (OSSR) in this case, $OSSR_{MATP,MATP}$ can be given by

$$OSSR_{MATP,MATP}=20\log_{10}\frac{J_2(\beta)J_2(\beta)}{J_4(\beta)J_2(\beta)}=23.5240 \tag{3-5}$$

Otherwise, a FBG notch filter with a notch depth of D dB can be used to remove residual optical carrier, correspondingly the $OSSR_{MATP,MATP}$ would be given by

$$\begin{aligned} OSSR_{MATP,MATP}=&\,20\log_{10}[J_2(\beta_2)J_2(\beta_1)] \\ &-\mathrm{Max}\left\{20\log_{10}[J_4(\beta)J_2(\beta)],\,20\log_{10}[J_0^2(\beta)-2J_2^2(\beta)]-D\right\} \end{aligned} \tag{3-6}$$

where Max() denotes the maximum value in the parentheses.

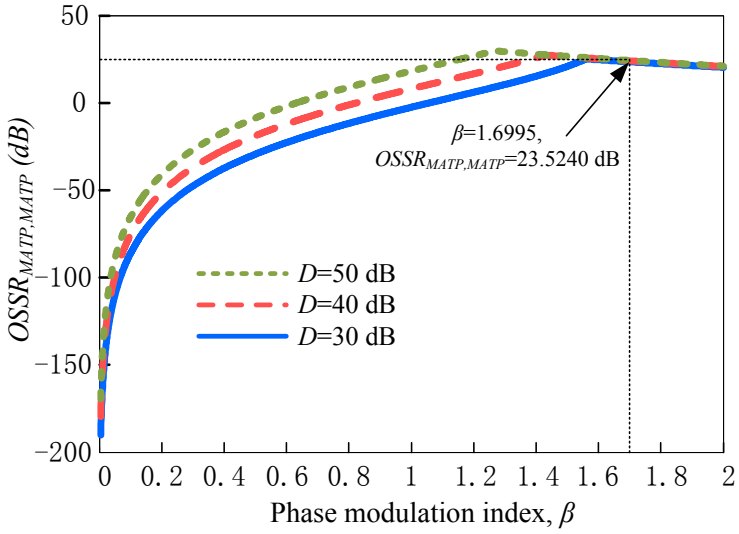

Fig. 3.2 Theoretical relationship between OSSRMATP, MATP and the phase modulation index β when a FBG notch filter with a notch depth of D.

According to (3-6), the theoretical relationship between the $OSSR_{MATP,MATP}$ and the PMI β is shown in Fig. 3.2 given three different values of D. The $OSSR_{MATP,MATP}$ will increase first and then decrease as the PMI β increases. As the values of D increase, the value of β needed to achieve a maximum $OSSR_{MATP,MATP}$ decrease. In the electrical domain, undesired harmonics would be generated by beating two fourth-order sidebands and the optical carrier or the two sixth-order sidebands. Thus, the $ESSR_{MATP,MATP}$ would be no less than $OSSR_{MATP,MATP}-10\log_{10}(2)$.

3.1.2 MITP and MITP

The MZMs are both biased at the MITP, that is, $\Phi_i=\pi$ for i=1, 2. According to (2-1), the signal at the output of MZM1 can be written as

$$E_1(t) \propto E_0 J_1(\beta_1)\sin\left((\omega_o-\omega_m)t-\varphi_1\right)+E_0 J_1(\beta_1)\sin\left((\omega_o+\omega_m)t+\varphi_1\right) \tag{3-7}$$

If a phase difference ϕ between the two sidebands is introduced by the TOPS, we have

$$E_1'(t) \propto E_0 J_1(\beta_1)\sin\left((\omega_o-\omega_m)t-\varphi_1+\phi\right)+E_0 J_1(\beta_1)\sin\left((\omega_o+\omega_m)t+\varphi_1+2\phi\right) \tag{3-8}$$

The optical signal is then sent to MZM2. The electrical field at the output of MZM2 is

$$\begin{aligned} E_2(t) \propto E_0 J_1(\beta_1) J_1(\beta_2)\{&\cos\left((\omega_o-2\omega_m)t+\phi-\varphi_1-\varphi_2\right)\\ &+\cos\left(\omega_o t+\phi-\varphi_1+\varphi_2\right)\\ &+\cos\left(\omega_o t+2\phi+\varphi_1-\varphi_2\right)\\ &+\cos\left((\omega_o+2\omega_m)t+2\phi+\varphi_1+\varphi_2\right)\} \end{aligned} \tag{3-9}$$

If the phase condition $\phi+2\varphi_1-2\varphi_2=(2k+1)\pi$ is satisfied, Eq. (3-9) can be simplified into

$$E_2(t) \propto E_0 J_1(\beta_1) J_1(\beta_2) \{\cos((\omega_o - 2\omega_m)t + \phi - \varphi_1 - \varphi_2) + \cos((\omega_o + 2\omega_m)t + 2\phi + \varphi_1 + \varphi_2)\} \quad (3\text{-}10)$$

By beating the maintained second-order sidebands at the PD, a frequency-quadrupled signal would be generated and the FMF is four. If the condition is not fully satisfied, the optical carrier would appear which can be removed by the FBG notch filter.

In addition to the dominant second-order sidebands, there could also exist the fourth-order sidebands, the $OSSR_{MITP,MITP}$ can be given by

$$OSSR_{MITP,MITP} = 20\log_{10}\frac{J_1(\beta_1)J_1(\beta_2)}{J_1(\beta_1)J_3(\beta_2)} = 20\log_{10}\frac{J_1(\beta_2)}{J_3(\beta_2)} \quad (3\text{-}11)$$

3.1.3 MATP and MITP

MZM1 is biased at the MATP with Φ_1=0, and MZM2 is biased at the MITP with Φ_2=π. The electrical fields at the outputs of MZM1 and the TOPS are identical to (3-1) and (3-2). The electrical field at the output of MZM2 can be expressed as

$$\begin{aligned} E_2(t) \propto E_0 J_1(\beta_2) \{ & J_2(\beta_1)\sin((\omega_o - 3\omega_m)t + \phi - 2\varphi_1 - \varphi_2) \\ & + J_2(\beta_1)\sin((\omega_o - \omega_m)t + \phi - 2\varphi_1 + \varphi_2) \\ & - J_0(\beta_1)\sin((\omega_o - \omega_m)t + 2\phi - \varphi_2) \\ & - J_0(\beta_1)\sin((\omega_o + \omega_m)t + 2\phi + \varphi_2) \\ & + J_2(\beta_1)\sin((\omega_o + \omega_m)t + 3\phi + 2\varphi_1 - \varphi_2) \\ & + J_2(\beta_1)\sin((\omega_o + 3\omega_m)t + 3\phi + 2\varphi_1 + \varphi_2) \} \end{aligned} \quad (3\text{-}12)$$

If the PMI condition $J_0(\beta_1)=J_2(\beta_1)$, that is $\beta_1 \approx 1.8412$ and phase condition $\phi - 2\varphi_1 + \varphi_2 + 2k\pi = 2\phi - \varphi_2$, $3\phi + 2\varphi_1 - \varphi_2 = 2\phi + \varphi_2 + 2k\pi$, that is $\phi + 2\varphi_1 - 2\varphi_2 = 2k\pi$ are satisfied, (3-12) can be simplified into

$$E_2(t) \propto E_0 \{ J_2(\beta_1) J_1(\beta_2) \sin((\omega_o - 3\omega_m)t + \phi - 2\varphi_1 - \varphi_2) + J_2(\beta_1) J_1(\beta_2) \sin((\omega_o + 3\omega_m)t + 3\phi + 2\varphi_1 + \varphi_2) \} \quad (3\text{-}13)$$

As can be seen only the third-order sidebands remain. By beating the third-order sidebands at the PD, a frequency-sextupled signal would be generated. The FMF is six. Considering the fact that $\beta_1 \approx 1.8412$ is relatively large, the neglected fourth order sidebands at the output of MZM1 would generate the fifth-order sidebands at the output of MZM2, which would contribute to the generation of the frequency-doubled and the frequency-octupled signals at the output of the PD. It is theoretically calculated that the $OSSR_{MATP,MITP}$ and the $ESSR_{MATP,MITP}$ would be given approximately by

$$OSSR_{MATP,MITP} = 20\log_{10} \frac{J_2(\beta_1)}{J_4(\beta_1)} \approx 21.9669 \text{ dB} \quad (3\text{-}14)$$

and

$$ESSR_{MATP,MITP} = OSSR_{MATP,MITP} - 10\log_{10} 2 \approx 18.9566 \text{ dB} \quad (3\text{-}15)$$

3.1.4 MITP and MATP

MZM1 is biased at the MITP with $\Phi_1 = \pi$, and MZM2 is biased at the MATP with $\Phi_2 = 0$. The electrical fields at the outputs of MZM1 and the TOPS are identical to (3-7) and (3-8). The electrical field at the output of MZM2 can expressed as

$$
\begin{aligned}
E_2(t) \propto E_0 J_1(\beta_1)\{ & J_2(\beta_2)\sin((\omega_o - 3\omega_m)t + \phi - \varphi_1 - 2\varphi_2) \\
& - J_0(\beta_2)\sin((\omega_o - \omega_m)t + \phi - \varphi_1) \\
& + J_2(\beta_2)\sin((\omega_o - \omega_m)t + 2\phi + \varphi_1 - 2\varphi_2) \\
& - J_2(\beta_2)\sin((\omega_o + \omega_m)t + \phi - \varphi_1 + 2\varphi_2) \\
& + J_0(\beta_2)\sin((\omega_o + \omega_m)t + 2\phi + \varphi_1) \\
& + J_2(\beta_2)\sin((\omega_o + 3\omega_m)t + 2\phi + \varphi_1 + 2\varphi_2)\}
\end{aligned}
\tag{3-16}
$$

If the PMI condition $J_0(\beta_2)=J_2(\beta_2)$, that is $\beta_2 \approx 1.8412$ and phase condition $2\phi+\varphi_1-2\varphi_2=\phi-\varphi_1+2k\pi$, $\phi-\varphi_1+2\varphi_2+2k\pi=2\phi+\varphi_1$, that is $\phi+2\varphi_1-2\varphi_2=2k\pi$, are satisfied, Eq. (3-16) can be simplified into

$$
\begin{aligned}
E_2(t) \propto E_0 J_1(\beta_1)\{ & J_2(\beta_2)\sin((\omega_o - 3\omega_m)t + \phi - \varphi_1 - 2\varphi_2) \\
& + J_2(\beta_2)\sin((\omega_o + 3\omega_m)t + 2\phi + \varphi_1 + 2\varphi_2)\}
\end{aligned}
\tag{3-17}
$$

As can be seen only the third-order sidebands are kept and the other sidebands are suppressed. By beating the two third-order sidebands at the PD, a frequency-sextupled signal would be generated and the FMF is six.

Similar to the case in Section 3.1.3, the frequency-doubled and the frequency-octupled signals at the output of the PD would be also generated due to the existence of the fifth-order sidebands. The theoretical $OSSR_{MITP,MATP}$ and the $ESSR_{MITP,MATP}$ would also be as same as those in the previous case in Section 3.1.3.

The conditions required for generated only two dominant optical sidebands using two MZMs which are biased at different modes are summarized in Table 3.1.

For the four cases discussed above, the phase condition $\phi+2\varphi_1-2\varphi_2=(2k+1)\pi$ or $\phi+2\varphi_1-2\varphi_2=2k\pi$ can be realized by using a TOPS. As a matter of fact, it can also be satisfied by using

a tunable optical delay line to change ϕ or a TEPS mentioned before to change φ_1 or φ_2. Therefore, the functions of the TOPS and the TEPS are equivalent.

TABLE 3.1 CONDITIONS FOR GENERATING ONLY TWO OPTICAL SIDEBANDS USING TWO MZMS BIASED AT DIFFERENT MODES.

Conditions / Bias modes	PMI	Phase	FMF
MATP+MATP	$\beta_1=\beta_2=\beta\approx1.6995$	$\phi+2\varphi_1-2\varphi_2=(2k+1)\pi$	8
MITP+MITP	NONE	$\phi+2\varphi_1-2\varphi_2=(2k+1)\pi$	4
MATP+MITP	$J_0(\beta_1)=J_2(\beta_1)$, $\beta_1\approx1.8412$	$\phi+2\varphi_1-2\varphi_2=2k\pi$	6
MITP+MATP	$J_0(\beta_2)=J_2(\beta_2)$, $\beta_2\approx1.8412$	$\phi+2\varphi_1-2\varphi_2=2k\pi$	6

3.2 Performance evaluation of the generated frequency-multiplied microwave signals

Experiments based on the setup shown in Fig. 3.1 are performed, and the generation of photonic frequency-sextupled and frequency-octupled signals is conducted. The frequency of the drive signal is set to be 4.25 GHz. Both the optical spectra at the output of MZM2 and the electrical spectra of the generated signals at the output of the PD are recorded. We also transmit the optical signals at the output of MZM2 through a 20 km SMF and compare the corresponding optical and electrical spectra of the remote signals to evaluate the transmission

performance of the system. To evaluate the phase noise performance, the single-side-band phase noise of the generated local and remote signals is measured. In addition, the frequency tunability and the system stability are also investigated. Furthermore, based on the frequency octupling and the high speed PD, we generate a 0.1 THz signal.

3.2.1 Transmission evaluation

In the experiments of the generation of the frequency-sextupled signals, one MZM is biased at the MITP, and the other MZM at the MATP. Fig. 3.3(a) shows the measured optical spectra of the generated third-order sidebands at the output of MZM2 and after 20 km fiber transmission in the case in Section 3.1.3. During the measurement, the EDFA is used to compensate the fiber loss after 20 km fiber transmission. We can clearly see that the two third-order sidebands are dominant in the optical spectra and experience no significant degradation after 20 Km fiber transmission. The electrical spectra of the generated 25.5 GHz local and remote signals are shown in Fig. 3.3(b) and Fig. 3.3(c) respectively, whose spectral spans are 40 GHz and 100 Hz. A conclusion can be reached that using this system a remote frequency-sextupled signal can be generated and exhibits as good spectral purity and narrow linewidth as a local signal does. The power of the 25.5 GHz signal is approximately 18.9 dB (Fig. 3.3(b)) greater than that of the next largest component, which are close to the theoretical value of 18.9566 dB. The linewidth of the generated signal is only a few Hz (Fig. 3.3(c)). Fig. 3.3(d)-(f) are the results in the case in Section 3.1.4 and also confirm the same conclusions mentioned above.

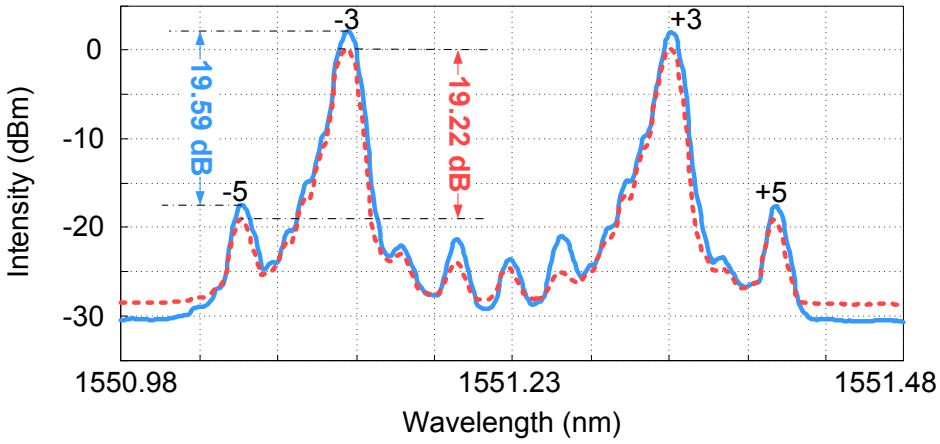
Intensity (dBm)
0
-10
-20
-30
-3
+3
-5
+5
19.59 dB
19.22 dB
1550.98
1551.23
1551.48
Wavelength (nm)

(a)

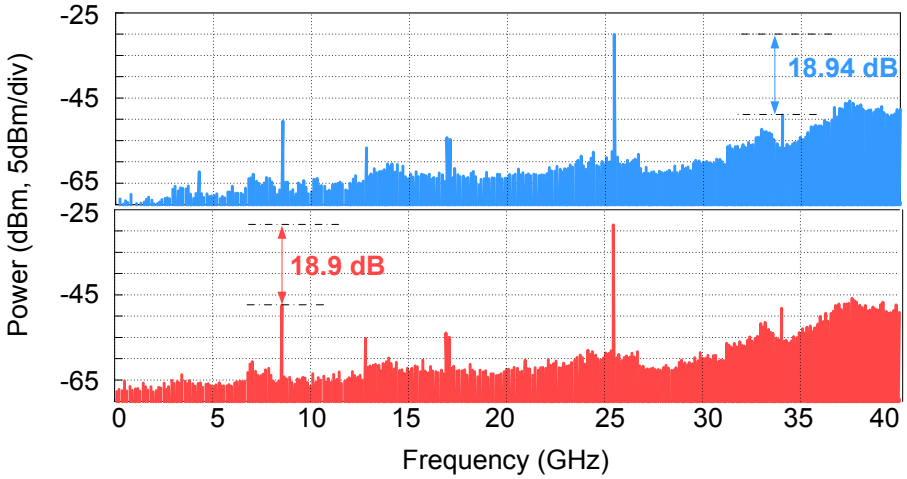
Power (dBm, 5dBm/div)
-25
-45
-65
18.94 dB
18.9 dB
0
5
10
15
20
25
30
35
40
Frequency (GHz)

(b)

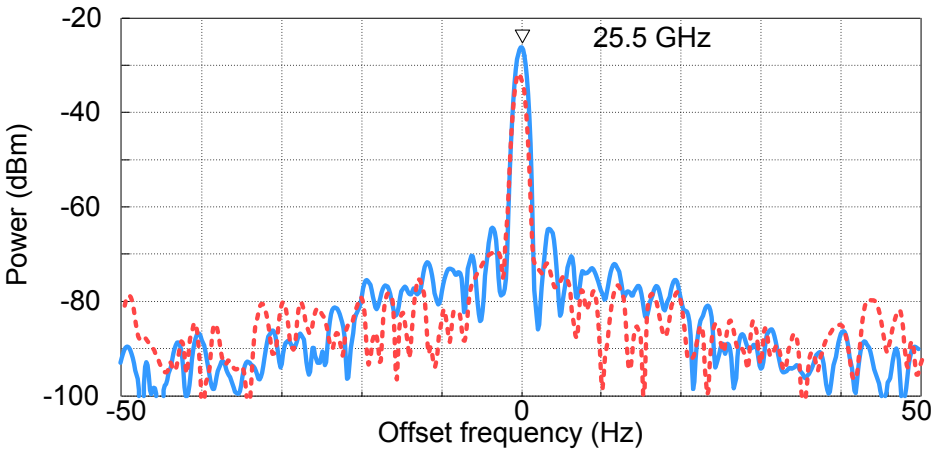
Power (dBm)
-20
-40
-60
-80
-100
25.5 GHz
-50
0
50
Offset frequency (Hz)

(c)

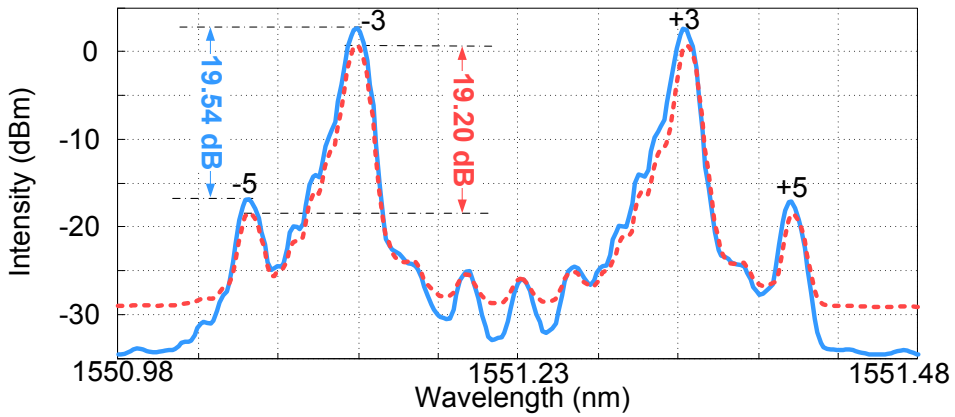

(d)

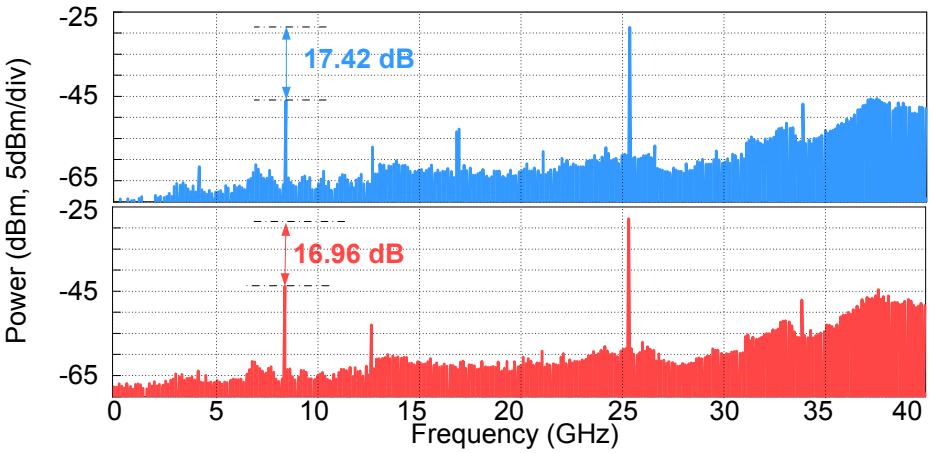

(e)

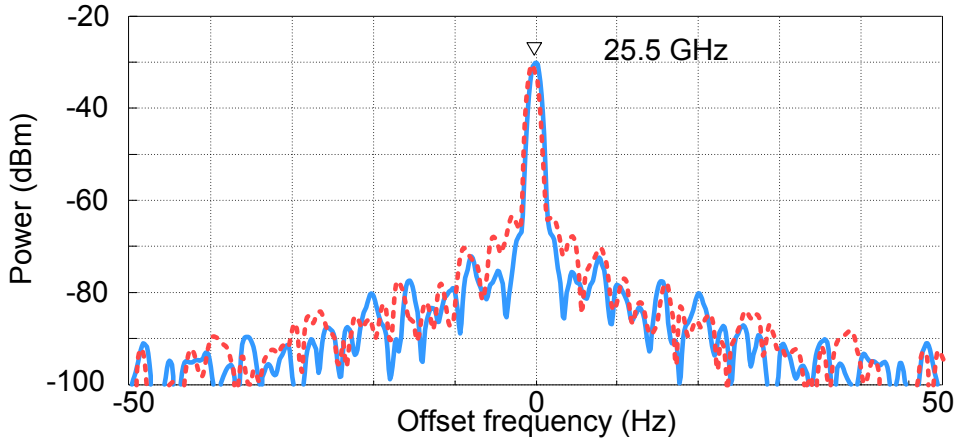

(f)

Fig. 3.3 (a), (d) Measured optical spectra of the third-order sidebands; (b), (e) Measured 40 GHz-span electrical spectra of the generated 25.5 GHz signals. The resolution bandwidth (RBW) is 3 MHz; (c) (f) Measured 100 Hz-span electrical spectra of the generated 25.5 GHz signals. The resolution bandwidth (RBW) is 1Hz ((a)-(c) and (d)-(f)) refer to the cases of Section 3.1.3 and 3.1.4 respectively. The blue and red lines refer to the local and remote signals, respectively).

In the experiment of the frequency octupling, both MZMs are biased at the MATP to suppress all the odd-order sidebands. Although theoretically no optical filters are need, in our experiment to avoid using a high-power microwave amplifier to realize $J_0^2(\beta) = 2J_2^2(\beta)$ and the optical carrier suppression, a FBG notch filter will facilitate the suppression of the residual optical carrier. The notch depth D of the FBG notch filter is about 40 dB, the PMI $\beta \approx 1.43$. According to (3-6), the maximum $OSSR_{MATP,MATP}$ is approximately equal to 26.7940 dB, and the $ESSR_{MATP,MATP}$ is approximately equal to 23.7837 dB when the PMI $\beta \approx 1.43$. From Fig. 3.4(a), we can clearly see that at the output of MZM2 there are dominant fourth-order sidebands, as well as the residual optical carrier that is then removed by the FBG notch filter. After 20 Km fiber transmission, the optical spectrum barely experiences degradation. The electrical spectra of the generated 34 GHz signal are shown in Fig. 3.4(b) and Fig. 3.4(c), with 45 GHz and 100 Hz spectral span respectively. The power of the frequency-octupled local signal is respectively 23.51 dB greater than that of the next largest component, which agrees well with the theoretical value of the $ESSR_{MATP,MATP}$, 23.7837 dB.

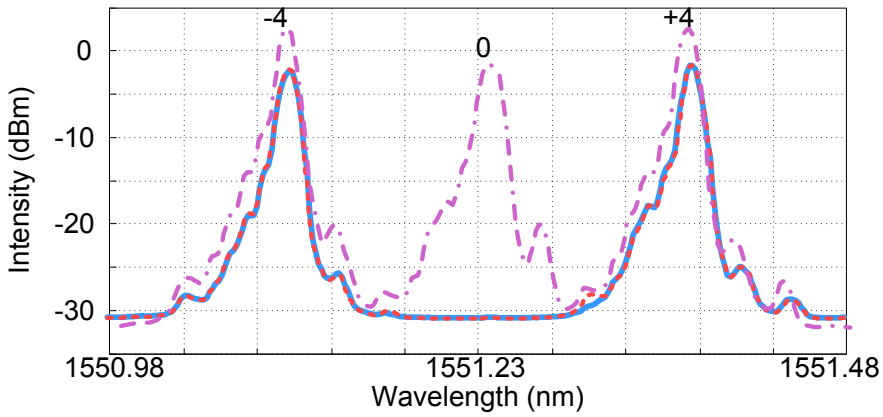

(a)

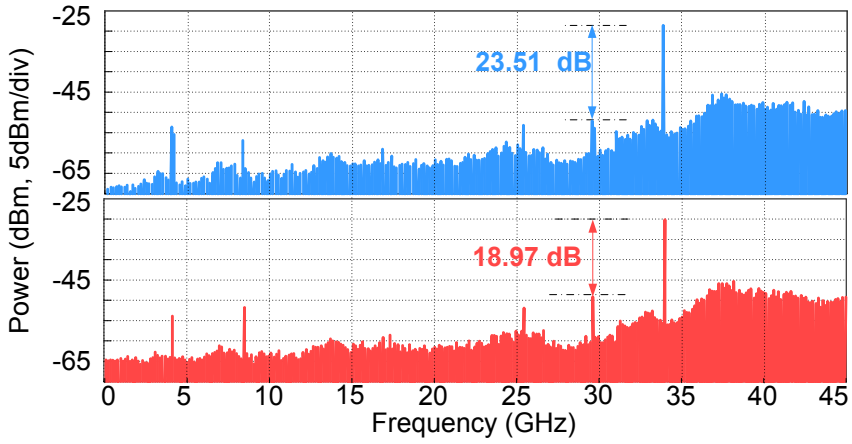

(b)

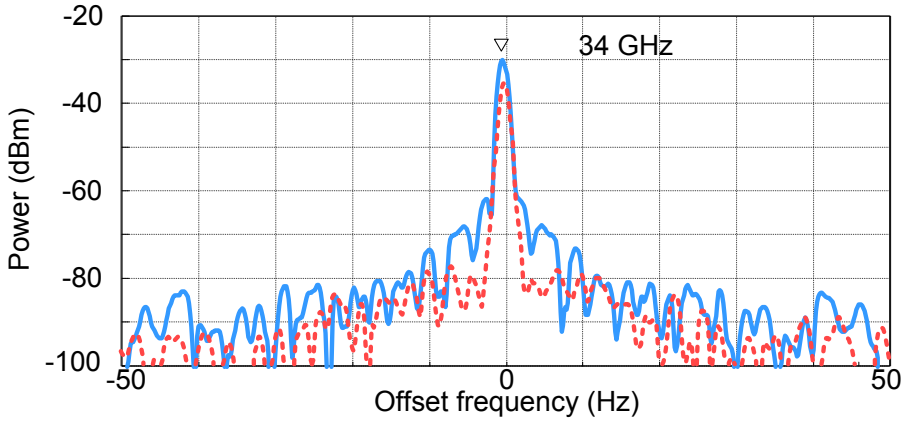

(c)

Fig. 3.4 (a) Measured optical spectra at the output of MZM2 (dash-dotted purple line) and the notch filter (solid blue and red dotted lines); (b) Measured 45 GHz-span electrical spectra of the generated 34 GHz signals. The resolution bandwidth (RBW) is 3 MHz; (c) Measured 100 Hz-span electrical spectra of the generated 34 GHz signals. The resolution bandwidth (RBW) is 1Hz. (The blue and red lines refer to the local and remote signals, respectively)

3.2.2 Phase noise evaluation

The phase noise power spectrum density of the generated frequency-multiplied signal based on the external modulation can be given theoretically by (2-3), in practical, it should also include some residual noise of the system. Thus, the phase noise power spectrum density, $S(f)$, of the generated microwave signal can be written as,

$$10\log_{10}\left[S(f)\right]=10\log_{10}\left[S_{\mathrm{e}}(f)\right]+20\log_{10}(N)+10\log_{10}\left[S_{\mathrm{res}}(f)\right] \tag{3-18}$$

where $S_{\mathrm{e}}(f)$ and $S_{\mathrm{res}}(f)$ are the power spectrum density of the drive signal and the residual noise of the system, respectively. Therefore, the multiplied phase noise of the drive signal and the residual phase noise of the system both contribute to the phase noise of the generated signal. If condition

$$S_{\mathrm{res}}(f) << N^2 S_{\mathrm{e}}(f) \tag{3-19}$$

is satisfied, the third term in the right-hand side of (3-18) can be neglected and the phase noise of the generated signal is approximately equal to that of the drive source plus $20\log_{10}(N)$; if

$$S_{\mathrm{res}}(f) >> N^2 S_{\mathrm{e}}(f) \tag{3-20}$$

is satisfied, the first two terms in the right-hand side of (3-18) can be neglected and the phase noise of the generated signal is approximately determined by the residual noise of the system.

To evaluate the phase noise performance of the generated frequency-multiplied signal, we measure the single-side-band phase noise of the 34 GHz frequency-octupled local and remote signals using an Agilent E5052B signal source analyzer incorporating an Agilent E5053A downconverter. As a comparison, the phase noise of the drive signal at 4.25 GHz and the phase noise of the drive signal including residual noise of the system are also measured and plotted in Fig. 3.5.

Observing the phase noise curves in Fig. 3.5, we can clearly see that when the offset frequency is lower than 1 MHz, Eq. (3-19) is satisfied and the phase noise of the 34 GHz signal is approximately increased by $20\log_{10}(10)\approx 18$ dB from that of the drive signal; when the offset

frequency is higher than 1 MHz, Eq. (3-20) is satisfied and the phase noise of the 34 GHz signal is approximately equal to that of the residual noise of the system. In addition, the generated 34 GHz signal has a phase noise of as low as -89.35 dBc/Hz at the offset frequency of 1 KHz. Furthermore, it is obvious that after 20 km fiber transmission, the phase noise of the generated signal is still as good as that before the transmission.

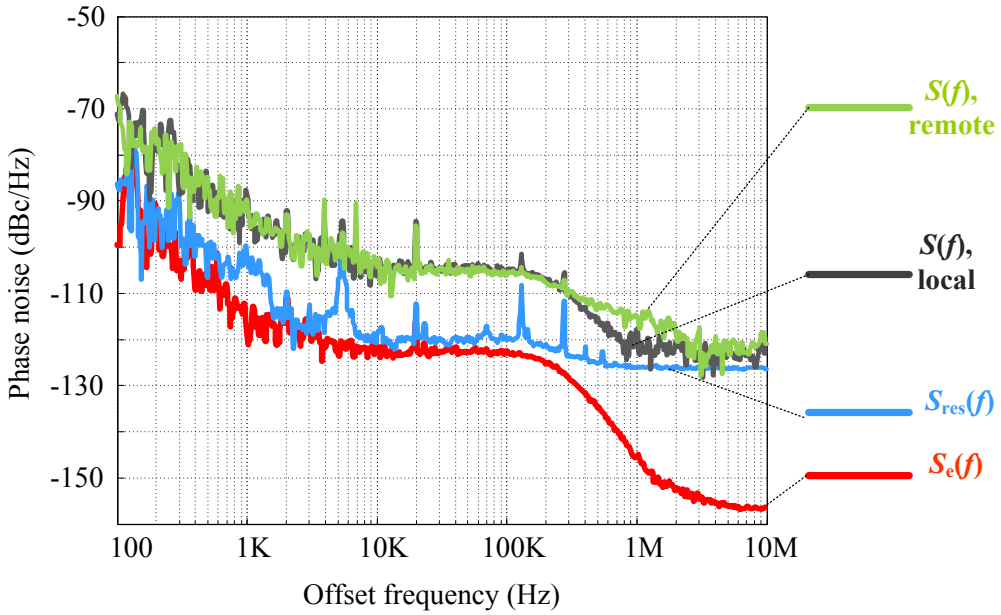

Fig. 3.5 Measured phase noise of the generated 34 GHz signal (green line: local; gray line: remote), and the phase noise of the drive signal with (blue line) and without (red line) including the residual noise of the system.

According to (3-18), the phase noise of the frequency-multiplied signal can be decreased by reducing either the phase noise of the drive signal source or the residual noise of the system. The residual noise of the system is mainly introduced in our experiments by the output instability of the dc power suppliers. An improvement is to replace each MZM as well as each dc power supplier with a PolM, a polarization analyzer and two PCs forming an equivalent MZM. Because the bias of each equivalent MZM can be controlled by adjusting the PC which is a passive device and more stable than a dc power supplier, the residual noise of the system

would be significantly reduced. Therefore, the phase noise performance of the generated signal would be also enhanced.

3.2.3 Tunability and stability

One important feature of the proposed technique is its excellent tunability. The frequency of the frequency-multiplied signal can be continuously tuned by changing the frequency of the drive signal and adjusting the TOPS or the TEPS. To evaluate the tunability, in the frequency sextupling experiment, the frequency of the drive signal is tuned from 2 to 4 GHz with an interval of 0.5 GHz, a frequency-sextupled signal from 12 to 24 GHz is thus generated, as shown in Fig. 3.6(a); in the frequency octupling experiment, the frequency of the drive signal is tuned from 3.4 to 3.8 GHz with an interval of 0.1 GHz, a frequency-octupled signal from 27.2 to 30.4 GHz is thus observed, as shown in Fig. 3.6(b). The spectral span is set to be 100 Hz. In such system, the tunable range is only limited by the operation bandwidth of the MZMs, the microwave amplifiers and the PD.

Another important feature is the stability. External modulation method can provide good short-term stability; however, its long-term stability is undermined by the bias drift the two MZMs, which is mainly caused by the output drift of the dc power suppliers. Using a PolM, a polarization analyzer and two PCs is still an alternative. Due to the same reason mentioned in Section 3.3.2, the stability of the system can be improved. In addition, such equivalent MZM can provide better even/odd-order suppression thanks to the better optical intensity balance in the two modes of the PolM introduced by adjusting the PC.

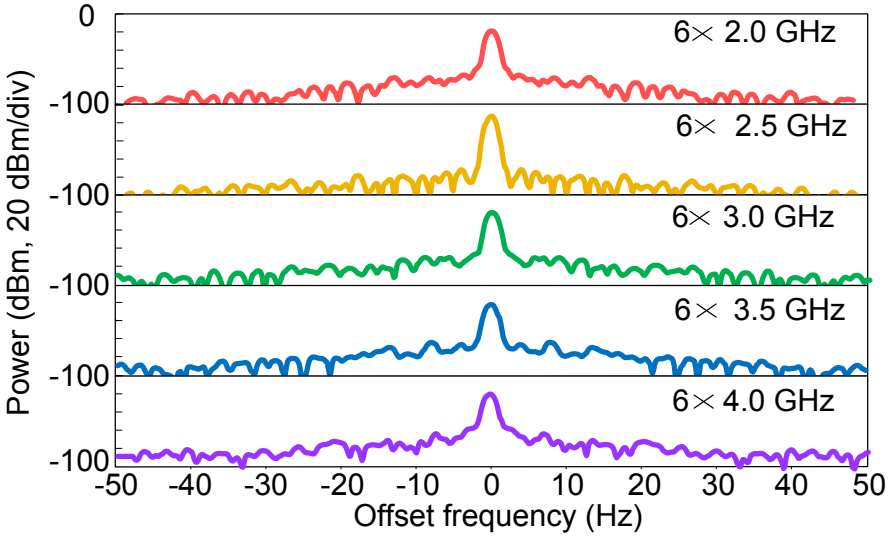

(a)

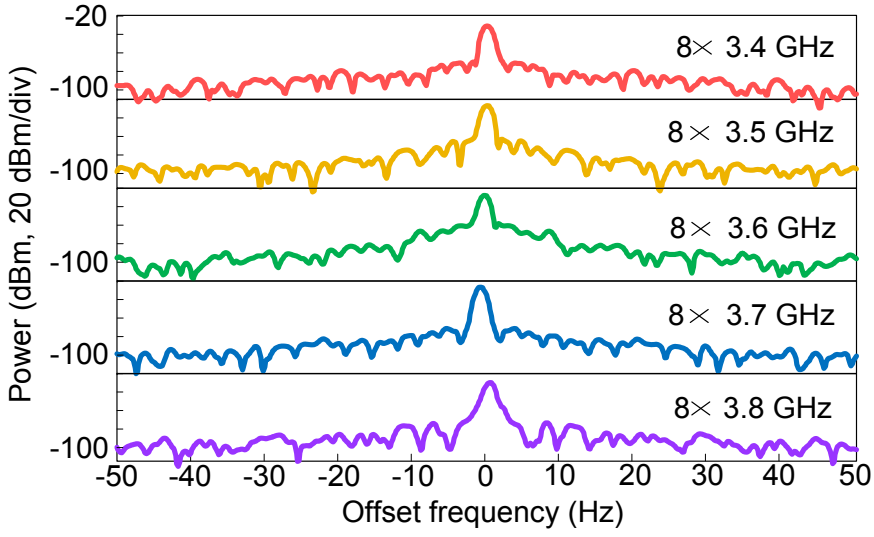

(b)

Fig. 3.6 (a) Measured electrical spectra of the generated frequency-sextupled signals; (b) measured electrical spectra of the frequency-octupled signals. The resolution bandwidth (RBW) is 1Hz

3.2.4 Terahertz generation

Frequency multiplication based on the external modulation is even capable of facilitating the generation of mm-wave even terahertz wave using relatively low frequency microwave components. To investigate the terahertz generation, the frequency octupling method is used to generate a 0.1 THz signal. The frequency of the drive signal is increased to 12.5 GHz and a

high speed 0.1THz U^2T photomixer is used for beating the two fourth-order sidebands. The measured optical spectrum of the two fourth-order sidebands and the electrical spectrum of the generated 0.1 THz signal are shown in Fig. 3.7. To measure the electrical spectrum of the generated 0.1 THz signal, an external harmonic mixer is used by mixing the 0.1 THz with a RF signal from a local oscillator to down-convert the 0.1 THz to a much lower frequency falling in the measurement range of the electrical spectrum.

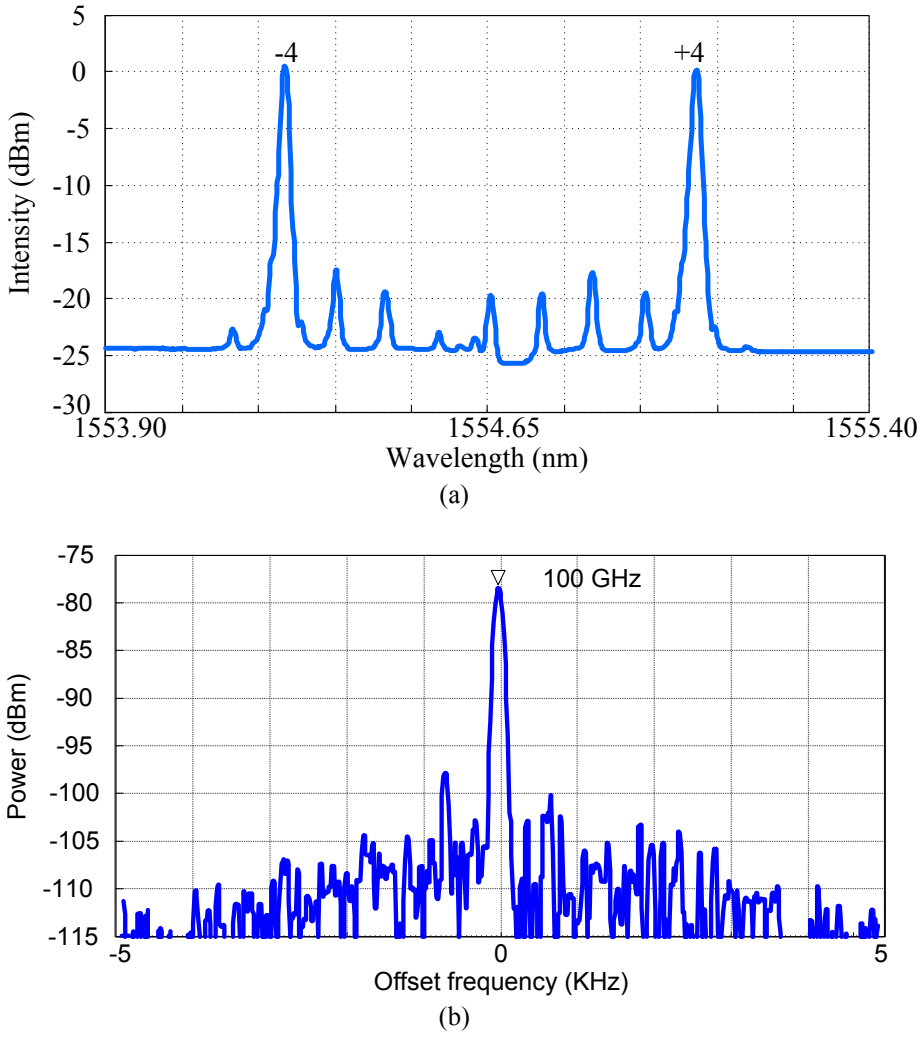

Fig. 3.7 (a) Measured optical spectrum (a) of the two forth-order sidebands; (b) measured electrical spectrum of the generated 0.1 THz signal with a spectral span of 10 KHz and a resolution bandwidth (RBW) of 91 Hz.

From Fig. 3.7(a), we can clearly see that two fourth-order sidebands spacing approximately 0.8 nm (0.1 THz) are dominant in the optical spectrum and other sidebands and optical carrier are significantly suppressed. The appearance of the residual sidebands and carrier is caused by the following reasons: 1) the PMI which is approximately 1.3 at 12.5 GHz is not large enough; 2) the extinction ratio of the MZMs we used is not large enough to effectively suppress all the odd-order sidebands, and using the PolMs can eliminate such drawbacks.

Considering that 40-GHz MZMs, 40-GHz PAs, and 0.3-THz uni-traveling carrier PD (UTC-PD) [82] are already available, the frequency-octupling is capable of generating a frequency-tunable mm-wave or terahertz wave signal with a frequency up to 0.3 THz.

3.3 Conclusion

A comprehensive investigation on microwave frequency multiplication based on the external modulation using two MZMs was presented. Based on two cascaded MZMs and a TOPS/TEPS, a comprehensive theoretical analysis was performed to prove that the frequency octupling, sextupling other than frequency quadrupling can be achieved as long as the corresponding bias condition, PMI condition and phase condition are satisfied. The theoretical results were also verified by the experiments. In the experiments, the frequency sextupling and octupling were successfully demonstrated. In addition, the system features excellent transmission performance, tunability and stability which were also confirmed by the experiments. The generated signals exhibit as low phase noise as that of the drive signal source, which were confirmed by a signal source analyzer. Furthermore, using the proposed frequency octupling, a frequency up to 0.3 THz can be potentially generated. In our experiment, a 0.1 THz terahertz wave was successfully generated using a 0.1-THz photomixer.

CHAPTER 4 EXTERNAL MODULATION ASSISTED BY OPTICAL NONLINEAR EFFECTS

Although external modulation based on two MZMs is capable of achieving frequency octupling, obtaining a higher frequency multiplication factor (FMF) is still important and necessary for generating a microwave or mm-wave signal of a higher frequency. Using optical nonlinear effects could effectively increase the FMF by increasing the number of sidebands; however, too many sidebands cause the optical filtering system to be complicated and be lack of tunability, which would usually limit the frequency tuning range of the system, and deteriorate the stability of the generated frequency-multiplied microwave signal.

In this chapter, we propose and demonstrate a approach to achieving frequency-twelvetupling for microwave and mm-wave generation by a combined use of a polarization modulator (PolM) for frequency quadrupling, a semiconductor optical amplifier (SOA) for frequency tripling, and stimulated-Brillouin-scattering-assisted (SBS-assisted) filter for adaptive filtering to remove unwanted spectral components**.** The PolM in conjunction with two PCs is operating as an equivalent Mach-Zehnder modulator (MZM) that is biased at the maximum transmission point (MATP), to generate only even-order sidebands. By removing the optical carrier using a fixed fiber Bragg grating (FBG), two second-order sidebands with a wavelength spacing corresponding to four times the microwave drive frequency are dominant. The introduction of the two second-order sidebands as two pump waves to the SOA would generate two idler waves due to four wave mixing (FWM). The two pump waves are then removed by the SBS-assisted filter. The key significance of this approach is that the SBS-assisted filtering is

adaptive which would simplify significantly the frequency tuning. In addition, the use of the wavelength-independent SBS-assisted filter would improve the frequency tunable range. Furthermore, the PolM is not dc biased; the system is free from bias drifts. An experiment is performed. The generation of a microwave or terahertz signal that is tunable from 48 to 132 GHz with excellent spectral quality and high stability is demonstrated.

4.1 Principle of the frequency twelvetupling based on optical-nonlinear-effect-assisted external modulation

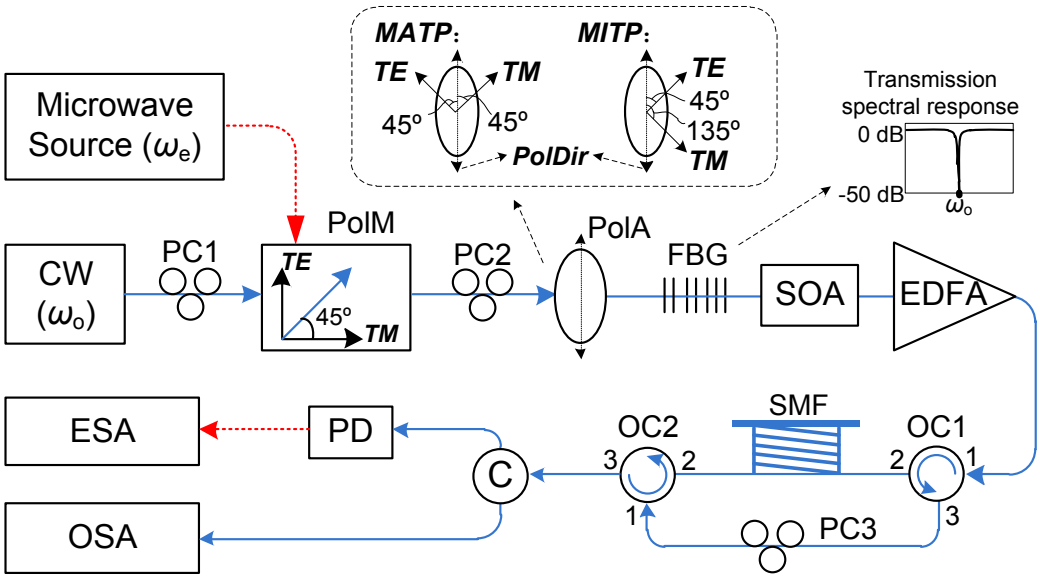

Fig. 4.1 Schematic of the proposed photonically assisted microwave frequency twelvetupling system. C: optical coupler; OSA: optical spectrum analyzer; PolA: polarization analyzer; PolDir: polarization direction.

The proposed system is shown in Fig. 4.1. The configuration includes a continuous wave (CW) laser source, a PolM, two polarization controllers (PC1 and PC2) before and after the PolM, a microwave power amplifier (PA), a FBG notch filter, an SOA, an erbium doped fiber amplifier (EDFA), an SBS-assisted filter and a photodetector (PD). The key module in the system is the

SBS-assisted filter, which consists of a spool of single mode fiber (SMF), a PC (PC3) and two optical circulators (OC1 and OC2), and operates as a wavelength-independent narrow band notch filter.

As can be seen a CW light wave from the laser source is directed into the PolM via PC1, and a microwave drive signal from a microwave source is applied to the PolM via the RF port. The PolM is a special phase modulator that supports both transverse-electric (TE) and transverse-magnetic (TM) modes with however opposite phase modulation indices (PMIs). The polarization direction of the incident light wave to the PolM is adjusted by tuning PC1 to have an angle of 45^{o} with respect to the two orthogonal principal axes, referring to the orthogonal TE and TM modes of the PolM, as shown in Fig. 4.1. The two light waves along the two principal axes of the PolM are then sent to the PA via PC2. By tuning PC2, the polarization directions of the phase-modulated light waves along the two principal axes of the PolM can be aligned, either both with an angle of 45^{o} with respect to the polarization direction of the PA or one with an angle of 45^{o} and another with an angle of 135^{o} with respect to the polarization direction of the PA. Therefore, an intensity-modulated signal would be generated at the output of the PA, which is equivalent to the operation of an MZM that is biased at either the MATP or the minimum transmission point (MITP).

Based on the analysis in Section 2.1, the electrical field at the output of the polarization analyzer (PolA) can be given by (2-1). When Φ, which here is a static phase term introduced by PC2, is equal to 0, the PolM-based equivalent MZM is biased at the MATP, and when Φ is equal to π, the PolM-based equivalent MZM is biased at the MITP. When the PolM-based MZM operates at the MATP, all the odd-order sidebands would be suppressed. Under small

signal modulation condition, the higher even-order sidebands are too small and can be ignored. The electrical field at the output of the PolA can be given by (3-1).

After passing through the FBG notch filter, the optical carrier is filtered out and only the two second-order sidebands, $\omega_o+2\omega_m$ and $\omega_o-2\omega_m$, remain, where ω_o and ω_m are respectively the angular frequencies of the light wave and the microwave drive signal.

The two second-order sidebands are then launched into the SOA as two pump waves. According to the theory of FWM, two sidebands will mix in the SOA to produce two new idler waves with the frequencies being $\omega_o+6\omega_m$ and $\omega_o-6\omega_m$ and a frequency spacing corresponding to twelve times the frequency of the microwave drive signal. In addition, the powers of the pump waves are usually larger than those of the idler waves.

The two pump waves and the two idler waves are amplified by the EDFA and then routed, through OC1, to the SBS-assisted filter. It is well know that the SBS is resulted from a physical phenomenon called electrostriction, change of the medium's density by action of light wave. Due to the effect of electrostriction, the incident light wave interferes with the backscattered Stokes light wave caused by the incident light wave and generates an acoustic. As the intensity of the incident light wave increases, both intensity of the Stokes wave and the interference pattern becomes more enhanced, and the acoustic wave also increases in amplitude, which effectively acts as a Bragg grating, scattering even more light in the backward direction, namely Stokes waves. Therefore, if intentionally increasing the backward Stokes wave in the fiber, we can reduce the forward incident light wave at the output of the fiber.

In the experiment, the powers of the pump waves are controlled to be above the threshold of the SBS. Thus Stokes waves would only be generated by the pump waves. Then the Stokes

waves are intentionally re-injected into the SMF via OC2 in a direction opposite to the pump waves, which could enhance the intensity distribution of the Stokes wave along the fiber. Therefore, the interaction of the re-injected Stokes waves with the pump waves would greatly enhance the induced acoustic grating, causing more backscattering of the pump waves into the Stokes waves and thus significantly suppress the pump waves [174-177]. Such a suppression procedure is illustrated in Fig. 4.2. The suppression ratio is determined by the power of the input light wave regardless of the wavelength, and the suppression ratio would increase significantly as the power of the light wave increases. The SBS-assisted filter can remove the two pump waves while keeping the two idler waves. Since the output from OC2 consists of only the two idler waves, $\omega_o+6\omega_m$ and $\omega_o-6\omega_m$, the beating of the two idler waves at the PD would generate a frequency-twelvetupled microwave signal.

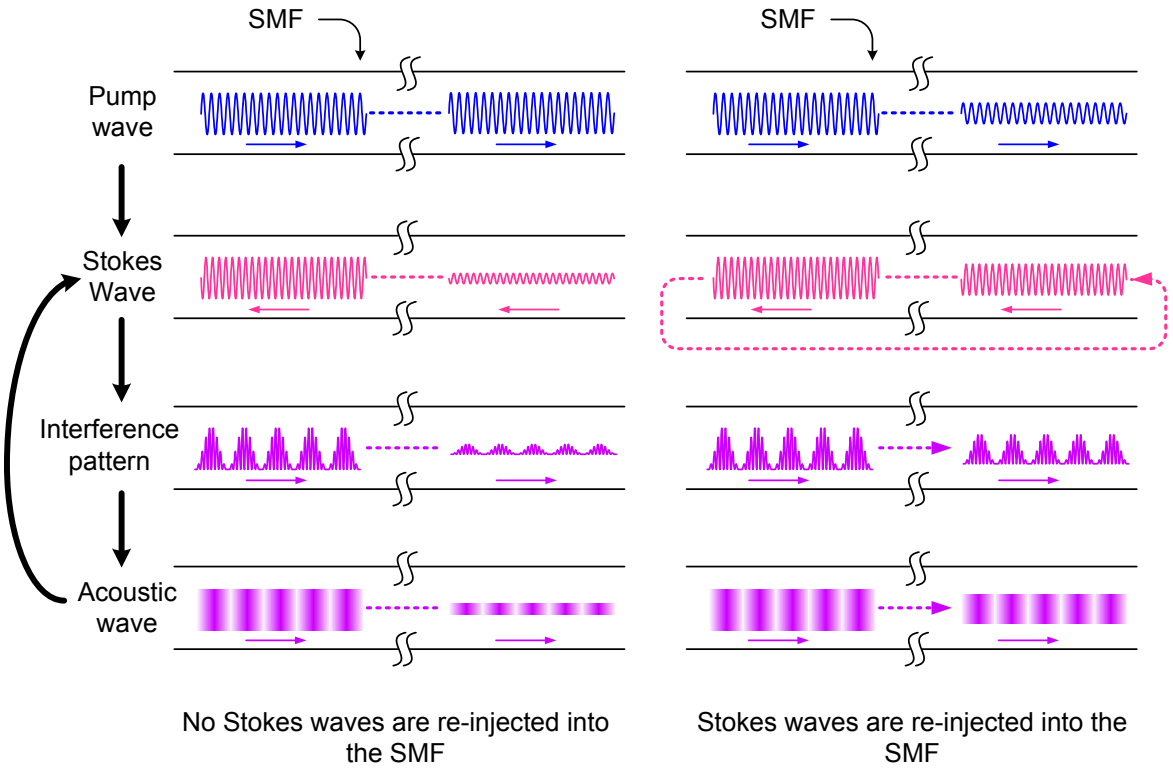

Fig. 4.2 Illustration of the pump wave suppression using an SBS-assisted filter.

The same adaptive wavelength-independent SBS-assisted filter can also replace the FBG notch filter to suppress the optical carrier, which would enable the system to become filterless and wavelength-independent.

Compared with the approaches where two cascaded MZMs are employed for frequency multiplication [57-62], the proposed approach here could be much simpler for continuous frequency tuning, since only the microwave drive frequency needs to be tuned, while in other approaches, the phase and phase modulation index (PMI) conditions must be simultaneously met.

Since the FMF is 12, theoretically, the resolution of the frequency tuning step and the tuning range of the system are both 12 times those of the microwave source; the phase noise of the frequency-multiplied microwave would be increased by $20\log10(12)\approx21$ dB from that of the microwave drive signal. In addition, since no dc bias is actually needed, the PolM-based system is free from bias drifting problem.

4.2 Experimental results and discussion

An experiment based on the setup shown in Fig. 4.1 is performed. In the experiment, the wavelength of the CW laser source is set at 1556 nm to make it coincide with the central wavelength of the FBG notch filter. The power of the microwave drive signal is about 20 dBm. Considering the half-wave voltage of the PolM is 6.5 V, the PMI is calculated to be about 1.5. The powers of the light waves sent to the SOA and the SBS-assisted filter are about 6 and 16 dBm, respectively. The length of the SMF is about 24 km with a loss of about 7 dB. The estimated SBS threshold of the SMF is about 10 dBm. First, we adjust PC1 and PC2 to make

the PolM operate as an equivalent MZM that is biased at the MATP. We also adjust PC3 to maximize the suppression ratio of the pump waves by the SBS-assisted filtering.

The optical spectra at the outputs of the FBG, the SOA and the SBS-assisted filter, and the electrical spectrum of the beat note at the output of the PD are shown in Fig. 4.3, for which the frequency of the microwave drive signal is set at 4 GHz. From Fig. 4.3(a) we can clearly see that a symmetric optical spectrum consisting of only the two second-order sidebands is generated, and the optical carrier and other sidebands are significantly suppressed. Fig. 4.3(b) shows the optical spectrum of the signal after the SOA. Thanks to FWM, two idler waves are generated. Due to the non-flat gain spectrum of the SOA, the spectral symmetry becomes poor. The spectral symmetry is critical to ensure an efficient SBS-assisted filtering to suppress simultaneously the two pump waves since its suppression ratio is power-dependent. Fig. 4.3(c) shows the spectrum at the output of the SBS-assisted filter. As can be seen the pump waves are suppressed and only the idler waves are kept. The small peaks between the two idler waves are: 1) the residual first- and forth-order sidebands, which can be reduced by decreasing the PMI or by increasing the extinction ratio of the PolM and the notch depth of the FBG; 2) the residual pump waves, which can be further suppressed by increasing their powers before being injected into the SMF; 3) the Stokes waves, which can be removed by reducing the end face reflections between the OCs and the SMF. In Fig. 4.3(d), a frequency-twelvetupled microwave signal by beating the two idler waves at the PD is generated.

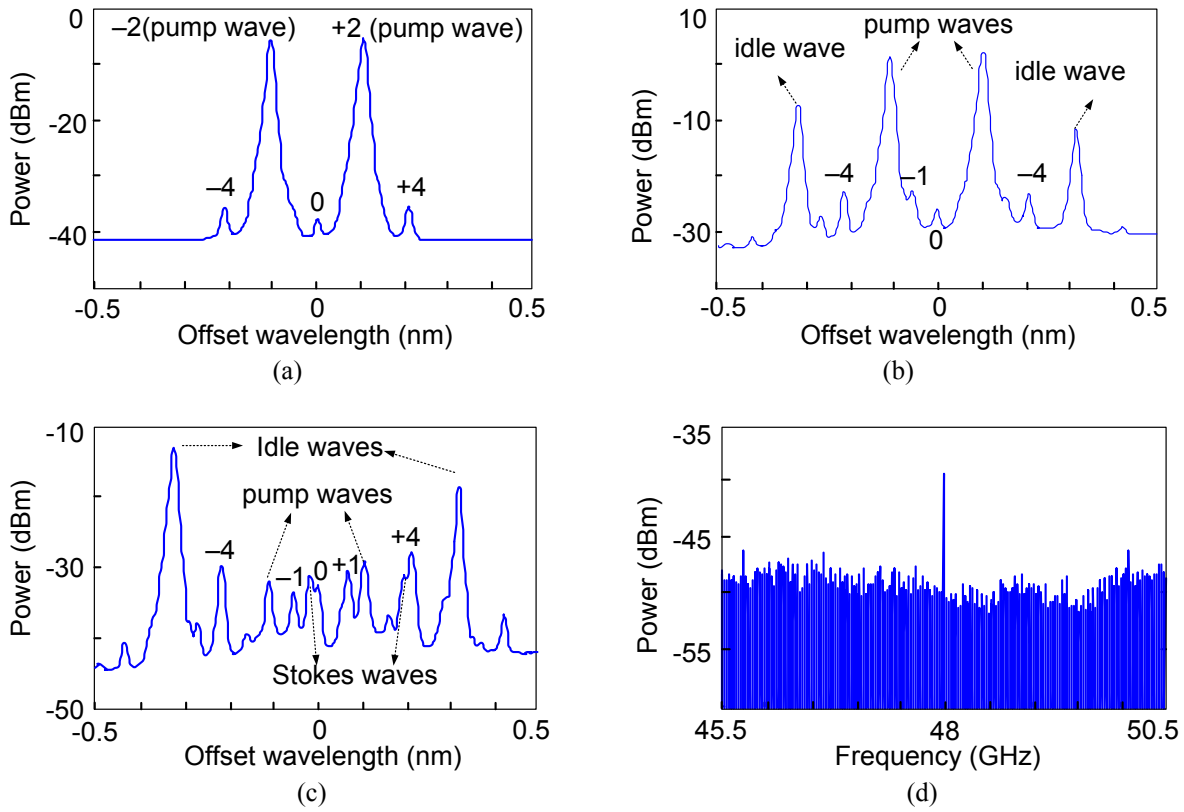

Fig. 4.3 Measured optical spectra at the outputs of (a) the FBG notch filter, (b) the SOA, and (c) the second OC; (d) measured electrical spectrum of the generated frequency twelvetupled microwave signal with a frequency span of 5 GHz and a resolution bandwidth (RBW) of 3 MHz.

The frequency tuning capability of the technique is also evaluated. In the experiment, we tune the frequency of the microwave drive signal with two different tuning steps and record the electrical spectra of the generated frequency-twelvetupled microwave signals, which are shown in Fig. 4.4 and Fig. 4.5. When the frequency of the microwave drive signal is tuned from 4 GHz to 4.000008 GHz with a tuning step of 1 KHz, a frequency twelvetupled signal from 48 GHz to 48.000096 GHz is generated, as shown in Fig. 4.4. When the frequency of the microwave drive signal is tuned from 4 GHz to 11 GHz with a tuning step of 1 GHz, a frequency twelvetupled signal from 48 GHz to 132 GHz is generated.

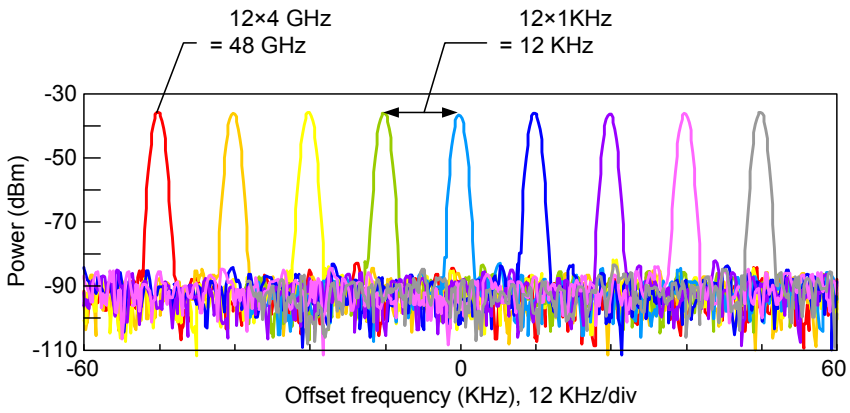

Fig. 4.4 The superimposed spectra of the generated frequency twelvetupled microwave signals with a 120 KHz spectral span when the frequency of the microwave drive signal is tuned from 4 to 4.000008 GHz with a 1 KHz interval. The RBW is 1.1 KHz.

In the experiment, the notch width of the FBG and the bandwidth of the PD used are two factors that limit respectively the minimum (48 GHz) and maximum (132 GHz) frequencies of the generated microwave signals. The notch width of the FBG is about 10 GHz, if the frequency of the drive signal applied to the PolM is too low (< ~4 GHz), not only the optical carrier but also the two second-order sidebands will be suppressed greatly. Therefore, the minimum frequency of the generated signal is about 48 GHz; however, if we can replace the FBG notch filter with another adaptive wavelength-independent SBS-assisted filter, then, the limit on the minimum frequency would be eliminated.

The bandwidth of the PD is about 100 GHz in the experiment, when the frequency spacing between the two idler waves is larger than 100 GHz, the PD will not response efficiently and the power of the generated microwave signal is extremely low. In the experiment, we can only detect a signal with a frequency up to 132 GHz. However, the bandwidth of a uni-travelling carrier PD (UTC-PD) up to about 300 GHz is now available, which would enable our scheme to generate a signal with the highest frequency up to 300 GHz.

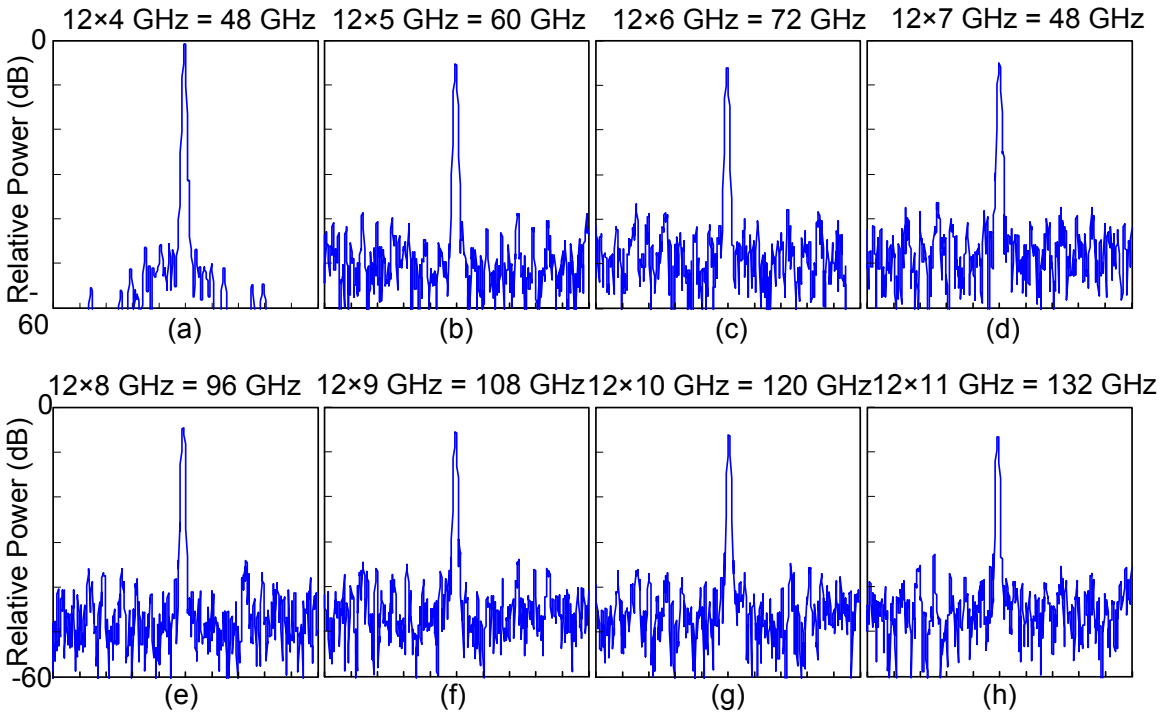

Fig. 4.5 The spectra of the generated frequency twelvetupled signals with a 1 kHz spectral span when the frequency of the microwave drive signal is tuned from 4 GHz to 11 GHz with a 1 GHz interval. The RBW is 9.1 Hz.

The spectral purity of the generated microwave signals is also evaluated, which is done by observing the electrical spectra of the generated signals. As can be seen from Fig. 4.5, the generated signals demonstrate an excellent spectral purity; very narrow spectral peaks with a frequency span of only 1 KHz are observed.

The phase noise performance of the generated microwave signals is also evaluated, which is done by observing the electrical spectra of the generated signals. As can be seen from Fig. 4.5, the generated signals demonstrate an excellent phase noise performance; very narrow spectral peaks with a frequency span of only 1 KHz are observed.

4.3 Higher frequency multiplication factor

It is evident that the joint use of FWM and SBS-assisted filtering is capable of tripling the FMF of a conventional external modulation method and effectively suppressing undesired sidebands. In our experiment, a FMF of 12 is obtained by tripling a smaller FMF of 4 which is achieved using one PolM-based MZM. Therefore, if the frequency octupling replaces the frequency quadrupling in Fig. 4.1, a higher FMF as large as 24 can be achieved, which would greatly facilitate the generation of an mm-wave or terahertz wave signal using a much lower frequency components in the system. For example, using the commercially available 40-GHz PolM and the PA could enable the generation of a 0.96-THz signal. In such a case, a terahertz photomixer would become the key component in the system [81, 83].

4.4 Conclusion

An approach to achieving frequency-twelvetupling with large tunability in the optical domain was proposed and experimentally demonstrated. By a joint use of a PolM, an SOA and an SBS-assisted filter, a frequency-twelvetupled microwave signal with high spectral purity was generated. The key significance of the proposed approach is the simplicity of the frequency tuning and large tunable range, which was enabled by the adaptive nature of the SBS-assisted filtering. The proposed system could be used for high-frequency electrical signal generation up to terahertz if a photomixer with a bandwidth extending to terahertz range is employed.

CHAPTER 5 NARROW-PASSBAND AND FREQUENCY-TUNABLE MICROWAVE PHOTONIC FILTER

In the chapter, a novel approach to implementing a narrow-passband and frequency-tunable microwave photonic filter (MPF) is proposed and experimentally demonstrated. The proposed MPF will be incorporated in an OEO to generate microwave and mm-wave signals, which will be discussed in Chapter 6 and 7. The proposed MPF is based on phase-modulation to intensity-modulation (PM-IM) conversion in a phase-shifted fiber Bragg grating (PS-FBG). In the proposed MPF, a phase-modulated signal is sent to a PS-FBG. If one of the sidebands falls in the notch of the PS-FBG, the phase-modulated signal is converted to an intensity-modulated signal. Due to the ultra-narrow notch of the PS-FBG, a microwave filter with an ultra-narrow passband is realized. The tunability of the microwave filter is achieved by tuning the wavelength of the optical carrier. A theoretical analysis is performed in which the value of the phase shift and the location of the phase shift in the PS-FBG on the frequency response of the MPF are studied. Two PS-FBGs with different reflection bandwidths and different phase-shift values introduced at the center of the gratings are fabricated and incorporated into the proposed MPF. For the two PS-FBGs we used, the 3-dB bandwidths are 120 MHz and 60 MHz and the tunable ranges are 5.5 GHz and 15 GHz.

5.1 Microwave photonic filter

Microwave filters implemented in the optical domain have been intensively studied in the past few years. Compared with microwave filters implemented in the electrical domain, MPFs exhibit unique properties such as high frequency, large tunability, light weight and immunity to electromagnetic interference, which can find numerous applications, such as in modern radar and warfare systems [178-181]. An MPF usually has a delay-line structure with a finite impulse response (FIR). The bandpass selectivity of an MPF is mainly determined by the number of taps [179]. To avoid optical interference, the multiple taps are usually realized by using a multi-wavelength light source, such as a laser array [182-184], a broadband spectrum-sliced source [185-188] or an optical comb source [189-191]. To improve the selectivity, the number of the taps should be large, but at the cost of increased complexity. An MPF can also be implemented with an infinite impulse response (IIR). Compared with a FIR filter, an IIR filter usually has a simpler structure and better selectivity [192-195]. However, due to the use of resonators [194] or feedback loops [195] in an IIR filter, the stability is poor and the tunability is limited. To implement a large tunability, various MPFs based on stimulated Brillouin scattering (SBS) have been proposed [196-200]. For example, in [197] SBS gain is used to selectively amplify the sideband of the single-sideband modulated light wave. However, double-sideband with suppressed carrier modulation and single-sideband modulation are needed which significantly increase the complexity and cost of the system. In [198], such a complicated modulation technique is replaced by using an optical filter, and an SBS-based tunable true time delay line has been proposed to implement a dynamically reconfigurable MPF. The time delay can be tuned by changing the SBS pump power. The major limitation of the approach is that multiple modulators are employed, making the system complicated. An

MPF can also be achieved based on phase-modulation to intensity-modulation conversion. By selecting the optical carrier and one sideband of a phase-modulated light wave using two uniform FBGs [201], a phase-modulated signal is converted to an intensity-modulated signal. The major limitation of the approach is that the passband is wide, which is determined by the bandwidth of the uniform FBG used to select the sideband. The use of a ring resonator to filter out one sideband of a phase-modulated light wave can also achieve an MPF with potentially large tunability [202]. Since the bandwidth of the ring resonator is wide, the width of the passband is wide, in the range of several GHz. For many applications, an MPF with a narrow passband is needed.

Therefore, we propose and experimentally demonstrate a narrow-passband and frequency-tunable MPF based on phase-modulation to intensity-modulation (PM-IM) conversion employing a PS-FBG that serves as a reflection filter with an ultra-narrow notch in the reflection band [203]. In the proposed MPF, a microwave signal is modulated on an optical carrier at a phase modulator. The phase-modulated signal is then sent to the PS-FBG. When one of the first-order sidebands falls in the notch of the PS-FBG, the magnitude and the phase of the sideband are modified, and the magnitude and phase relationship for the phase-modulated signal is no longer maintained; thus the phase-modulated signal is converted to an intensity-modulated signal, and the detection of the intensity-modulated signal at a photodetector (PD) would lead to the generation of an electrical signal. Due to the ultra-narrow notch of the PS-FBG, an MPF with an ultra-narrow passband is implemented. The tunability of the MPF can be easily achieved by tuning the wavelength of the optical carrier, and the frequency tuning range can be as wide as tens of GHz, which is determined by the reflection bandwidth of the PS-FBG and the notch location within the reflection band. A theoretical

analysis is performed in which the value of the phase shift and the location of the phase shift in the PS-FBG on the frequency response of the MPF were studied. Two PS-FBGs with different reflection bandwidths and different phase-shift values introduced at the center of the gratings are fabricated and are incorporated into the proposed MPF. For the two PS-FBGs, the 3-dB bandwidths are 120 MHz and 60 MHz and the tunable ranges are 5.5 GHz and 15 GHz. To the best of our knowledge, the 15-GHz frequency tuning range is the widest frequency-tunable range ever demonstrated for single bandpass MPF.

5.2 Principle of the narrow-passband and frequency-tunable microwave photonic filter

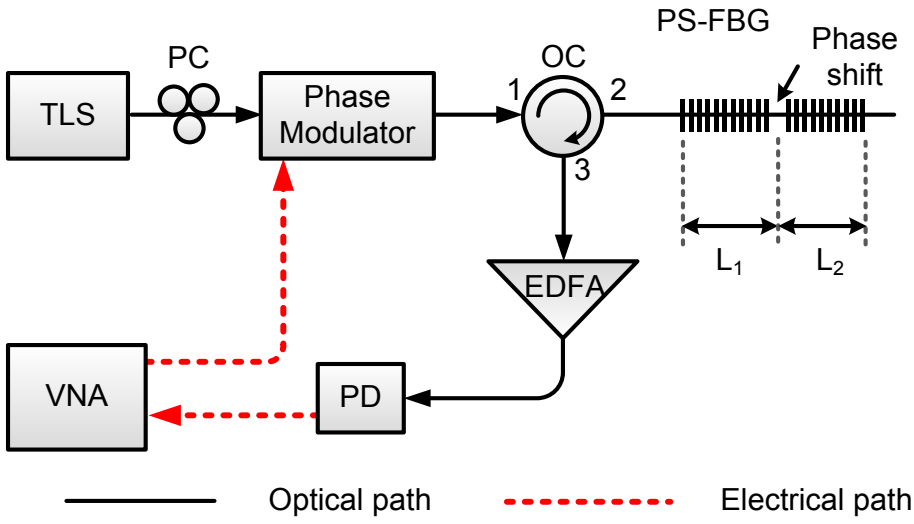

Fig. 5.1 Schematic of the proposed MPF. L1 and L2 are respectively the lengths of the left and right sub-FBGs separated by the phase shift.

The configuration of the proposed MPF is shown in Fig. 5.1. It consists of a tunable laser source (TLS), a polarization controller (PC), a phase modulator (PM), an optical circulator (OC), a PS-FBG, an erbium doped fiber amplifier (EDFA) and a PD. In the proposed MPF, a continuous wave (CW) light wave with a tunable angular frequency of ω_o from the TLS is sent to the phase modulator via the PC. The polarization state of the light wave to the phase modulator is adjusted by the PC to minimize the polarization-dependent loss. The phase modulator is driven by a sinusoidal microwave signal with a tunable angular frequency ω_e generated by a vector network analyzer (VNA).

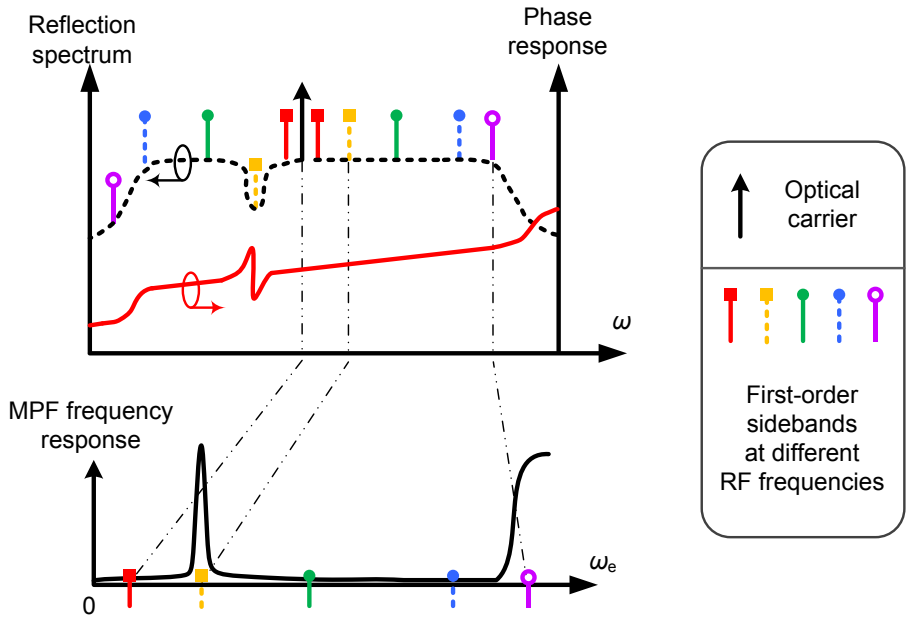

Fig. 5.2 Illustration of the operation of the MPF. (a) The reflection spectrum (dashed line) and phase response (solid line) of the PS-FBG. (b) The frequency response of the MPF.

If the phase-modulated signal is applied directly to the PD, no signal would be detected except a dc since the beating between the optical carrier and the upper sideband will cancel completely the beating between the optical carrier and the lower sideband, due to the fact that the two beat signals are out of phase. However, it is well known that a phase-modulated signal

can be converted to an intensity-modulated signal if the magnitude or phase relationship among the two sidebands and the optical carrier is changed, and such PM-IM conversion has a transfer function corresponding to a bandpass filter [204, 205]. It is also well known for a uniform FBG, if a phase shift is introduced to the FBG, an ultra-narrow notch with a phase jump in the notch would be generated in the reflection band [206, 207]. Thus, in our system, the phase-modulated light wave is injected into the PS-FBG that is employed to modify the magnitude and the phase of either the upper or the lower sideband falling in the ultra-narrow notch of the PS-FBG, to achieve PM-IM conversion, leading to the implementation of an ultra-narrow passband, as shown in Fig. 5.2.

Note that if ω_e is too large such that one sideband of the phase-modulated light wave is located outside the reflection spectrum, as shown in Fig. 5.2(a), PM-IM conversion would also happen and another passband at much higher frequencies would appear, as shown in Fig. 5.2(b). Practically, the reflection bandwidth of the PS-FBG could be large enough such that the second passband would be beyond the bandwidth of the PD. Thus, the proposed MPF will have a single bandpass. The central frequency of the achieved bandpass filter is equal to the frequency difference between the frequency of the optical carrier and that of the notch. Therefore, by simply tuning the wavelength of the optical carrier, the center frequency of the MPF can be tuned. The tuning range is determined by the total reflection bandwidth of the PS-FBG and the location of the notch within the reflection band.

Mathematically, the electrical field $E_{PM}(t)$ at the output of the phase modulator can be expressed as

$$
\begin{aligned}
E_{\mathrm{PM}}(t) &= E_{\mathrm{o}} \exp\left[j\omega_{\mathrm{o}} t + j\beta \cos\left(\omega_{\mathrm{e}} t + \varphi_{\mathrm{e}}\right)\right] \\
&= E_{\mathrm{o}} \sum_{n=-\infty}^{\infty} i^n J_n(\beta) \exp\left\{ j\left[\omega_{\mathrm{o}} t + n\left(\omega_{\mathrm{e}} t + \varphi_{\mathrm{e}}\right)\right]\right\} \\
&\approx E_{\mathrm{o}} J_0(\beta) \exp\left(j\omega_{\mathrm{o}} t\right) \\
&+ E_{\mathrm{o}} J_1(\beta) \exp\left[j\left(\omega_{\mathrm{o}} t + \omega_{\mathrm{e}} t + \varphi_{\mathrm{e}} + \pi/2\right)\right] \\
&- E_{\mathrm{o}} J_1(\beta) \exp\left[j\left(\omega_{\mathrm{o}} t - \omega_{\mathrm{e}} t - \varphi_{\mathrm{e}} - \pi/2\right)\right]
\end{aligned}
\tag{5-1}
$$

where E_{o} is the electrical amplitude of the incident light wave, $J_n(\cdot)$ is the n^{th}-order Bessel function of the first kind, φ_{e} is the initial phase of the microwave drive signal applied to the PM, and $\beta = \pi V/\mathrm{V}_\pi$ is the phase modulation index (PMI), where V is the amplitude of the signal applied to the phase modulator, and V_π is the half-wave voltage of the PM. The value of the PMI is set small, so that the power of the second- and higher-order sidebands is much smaller than that of the carrier and the first-order sidebands. Therefore, only the optical carrier and the two first-order sidebands are to be considered.

Since the amplitude and the phase of the optical carrier and the sidebands will be modified by the PS-FBG, in the following, we will give the amplitude response and the phase response of the PS-FBG first. The PS-FBG can be described by a 2 × 2 matrix $\boldsymbol{F}$ through [208]

$$
\boldsymbol{F} = {}^{2}F \cdot {}^{\mathrm{PS}}F \cdot {}^{1}F \tag{5-2}
$$

where ${}^{\mathrm{PS}}F$ is a 2 × 2 diagonal phase-shifted matrix with elements $\exp\left(\mp \quad\right)$, where φ_{PS} is the phase shift; the ${}^{i}F$ is a matrix describing each sub-FBG at each side of the phase shift section, where i = 1, 2 identifies respectively the left and right sub-FBGs separated by the phase shift. Its elements are given by

$$
{}^{i}F_{11} = {}^{i}F_{22}^{*} = \cosh\left(\gamma L_i\right) - j\left(\hat{\sigma} / \gamma\right) \cdot \sinh\left(\gamma L_i\right) \tag{5-3}
$$

$$ {}^{i}F_{12} = {}^{i}F_{21}^{*} = -j\left(\kappa / \gamma\right) \cdot \sinh\left(\gamma L_i\right) \tag{5-4} $$

where * denotes complex conjugation, L_i is the corresponding sub-grating length (see Fig. 5.1), $\gamma^2 = \kappa^2 - \hat{\sigma}$, κ is the "AC" coupling coefficient defined as $\kappa = \omega \cdot \Delta n / (2c)$ and Δn is the refractive index change, $\hat{\sigma}$ is the general "DC" self-coupling coefficient defined as $\hat{\sigma} = n_{eff} \cdot (\omega - \omega_{\mathrm{D}}) / c$, n_{eff} is the effective refractive index, c is the velocity of light in vacuum, ω is the angular frequency of the incident light wave, and ω_{D} is the angular frequency corresponding to the Bragg wavelength of the sub-FBGs.

Based on the coupled-mode theory and the transmission-matrix approach [208], the amplitude reflection coefficient $\rho(\omega)$, the power reflection coefficient $r(\omega)$, and the phase response $\theta(\omega)$ of the PS-FBG can be expressed respectively as

$$ \rho(\omega) = \frac{{}^{1}F_{11} / {}^{1}F_{21} - \left({}^{2}F_{11} / {}^{2}F_{21}\right)^{*} \cdot \exp\left(j\varphi_{\mathrm{PS}}\right)}{{}^{1}F_{11} \cdot {}^{2}F_{11} / \left({}^{1}F_{21} \cdot {}^{1}F_{21}\right) - \exp\left(j\varphi_{\mathrm{PS}}\right)} \tag{5-5} $$

$$ r(\omega) = \left|\rho(\omega)\right|^2 \tag{5-6} $$

$$ \theta(\omega) = phase\left[\rho(\omega)\right] \tag{5-7} $$

Then, after reflection at the PS-FBG, the modified electrical field $E_{\mathrm{IM}}(t)$ of the phase-modulated light wave can be expressed as

$$
\begin{aligned}
E_{\mathrm{IM}}(t) = & \sqrt{r(\omega_{\mathrm{o}})}E_{\mathrm{o}}J_0(\beta)\exp\left[j\omega_{\mathrm{o}}t + j\theta(\omega_{\mathrm{o}})\right] \\
& + \sqrt{r(\omega_{\mathrm{o}}+\omega_{\mathrm{e}})}E_{\mathrm{o}}J_1(\beta)\times \\
& \quad \exp\left\{j(\omega_{\mathrm{o}}t + \omega_{\mathrm{e}}t + \varphi_{\mathrm{e}} + \pi/2) + j\theta(\omega_{\mathrm{o}}+\omega_{\mathrm{e}})\right\} \\
& - \sqrt{r(\omega_{\mathrm{o}}-\omega_{\mathrm{e}})}E_{\mathrm{o}}J_1(\beta)\times \\
& \quad \exp\left\{j(\omega_{\mathrm{o}}t - \omega_{\mathrm{e}}t - \varphi_{\mathrm{e}} - \pi/2) + j\theta(\omega_{\mathrm{o}}-\omega_{\mathrm{e}})\right\}
\end{aligned}
\tag{5-8}
$$

Due to PM-IM conversion, we could have an intensity-modulated signal at the output of the PD. The recovered microwave signal $V(\omega_{\mathrm{e}})$ and its power $P(\omega_{\mathrm{e}})$ are given by

$$
\begin{aligned}
V(\omega_{\mathrm{e}}) \propto ac\left\{\left|E_{\mathrm{IM}}(t)\right|^2\right\} \approx A\times\Big\{ & \sqrt{r(\omega_{\mathrm{o}}+\omega_{\mathrm{e}})}\cdot\cos(\omega_{\mathrm{e}}t+\theta_1) \\
& - \sqrt{r(\omega_{\mathrm{o}}-\omega_{\mathrm{e}})}\cdot\cos(\omega_{\mathrm{e}}t+\theta_2)\Big\}
\end{aligned}
\tag{5-9}
$$

$$
\begin{aligned}
P(\omega_{\mathrm{e}}) & \propto \left|V(\omega_{\mathrm{e}})\right|^2 \\
& \approx A^2\cdot\Big\{r(\omega_{\mathrm{o}}+\omega_{\mathrm{e}}) + r(\omega_{\mathrm{o}}-\omega_{\mathrm{e}}) \\
& \quad - 2\sqrt{r(\omega_{\mathrm{o}}+\omega_{\mathrm{e}})r(\omega_{\mathrm{o}}-\omega_{\mathrm{e}})}\cdot\cos(\theta_1-\theta_2)\Big\}
\end{aligned}
\tag{5-10}
$$

where

$$
A = 2E_{\mathrm{o}}{}^2J_0(\beta)J_1(\beta)\sqrt{r(\omega_{\mathrm{o}})} \tag{5-11}
$$

$$
\theta_1 = \varphi_{\mathrm{e}} + \pi/2 + \theta(\omega_{\mathrm{o}}+\omega_{\mathrm{e}}) - \theta(\omega_{\mathrm{o}}) \tag{5-12}
$$

$$
\theta_2 = \varphi_{\mathrm{e}} + \pi/2 + \theta(\omega_{\mathrm{o}}) - \theta(\omega_{\mathrm{o}}-\omega_{\mathrm{e}}) \tag{5-13}
$$

and $ac(\cdot)$ denotes the ac term of the output electrical signal. If no first-order sidebands fall in the notch or the phase jump, we have

$$\sqrt{r(\omega_o+\omega_e)}=\sqrt{r(\omega_o-\omega_e)} \tag{5-14}$$

$$\theta_1-\theta_2=\theta(\omega_o+\omega_e)+\theta(\omega_o-\omega_e)-2\theta(\omega_o)=0 \tag{5-15}$$

which are obtained assuming the top of the reflection spectrum is flat and the phase response within the reflection spectrum except the phase jump is linear. Substituting (5-14) and (5-15) into (5-10), we have $P(\omega_e)=0$. This explains that the detection of a phase-modulated signal at a PD would generate no microwave signals except a dc. If one sideband falls in the notch of the PS-FBG, neither (5-14) nor (5-15) is satisfied and we have $P(\omega_e)>0$, which indicates that the phase-modulated signal is converted to an intensity-modulated signal and the detection of the intensity-modulated signal at a PD will generate a microwave signal. Therefore, due to PM-IM conversion at the PS-FBG, a narrow passband corresponding to the ultra-narrow notch in the reflection spectrum of the PS-FBG is resulted, an MPF with a narrow passband is thus realized.

The frequency response of the MPF can be calculated using (5-9) after incorporating $r(\omega)$ and $\theta(\omega)$ of the PS-FBG. Since L_i, which indicates the position where the phase shift is introduced, and the phase shift φ_{PS} are two important parameters in $r(\omega)$ and $\theta(\omega)$, we calculate the $r(\omega)$, $\theta(\omega)$ and $P(\omega_e)$ for different values of L_i and φ_{PS}.

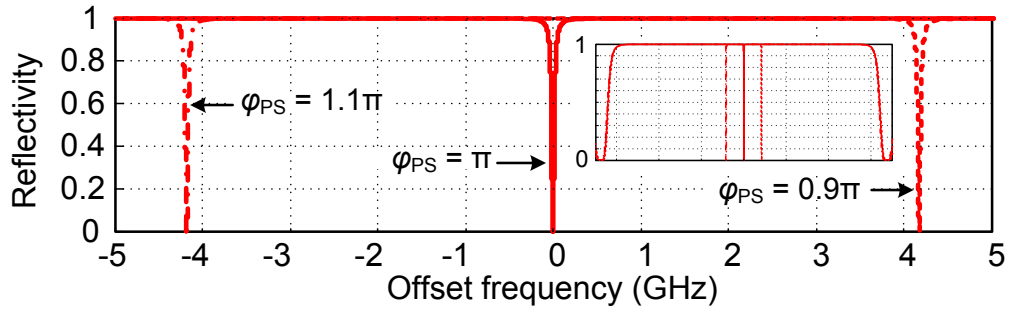

(a)

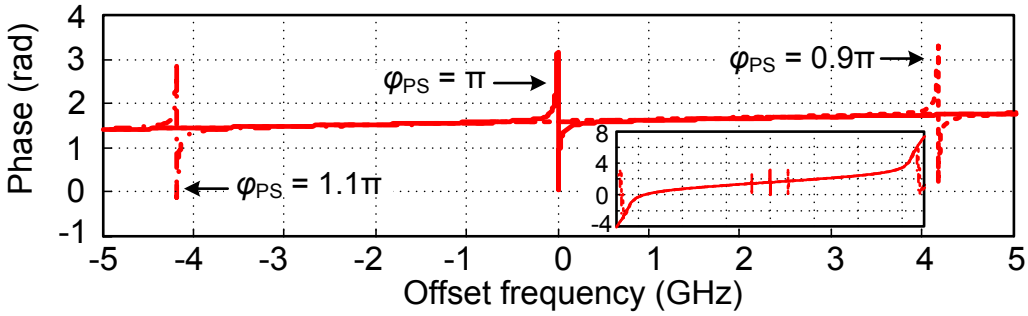

(b)

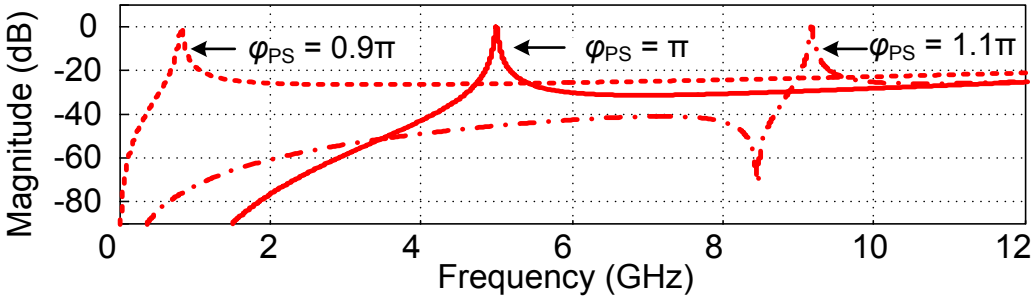

(c)

Fig. 5.3 A PS-FBG with different phase shifts. (a) Theoretical reflection spectra of the PS-FBG. (b) Theoretical phase responses of the PS-FBG (The insets in (a) and (b) show the corresponding reflection spectra and phase responses with a much larger frequency span of 70 GHz.) (c) Theoretical frequency responses of the MPF for different phase shifts.

Fig. 5.3(a) and (b) shows the theoretically calculated $r(\omega)$ and $\theta(\omega)$ for φ_{PS} at three different values, 0.9π, π and 1.1π, where $L_1 = L_2$. The total length of the PS-FBG is 10 mm with an n_{eff} of 1.45 and a Δn of 4×10^{-4}. Fig. 5.3(c) shows the corresponding frequency responses $P(\omega_e)$.

From Fig. 5.3, we can see when φ_{PS} is π, a notch is observed at the center of the reflection spectrum with a phase jump corresponding to a single phase cycle. We assume here that the optical carrier frequency is larger than the notch frequency. The center frequency of the passband of the MPF is equal to the frequency difference between the optical carrier frequency and the center frequency of the notch. If φ_{PS} is greater or smaller than π, the center frequency of the notch is shifted to a smaller or a greater frequency, and the center frequency of the passband of the MPF is also accordingly increased or decreased. Therefore, we can see that the phase shift φ_{PS} only determines the location of the notch and the phase jump within the notch, and would further determine the center frequency of the MPF for a given optical carrier frequency.

The length difference between L_1 and L_2 will have an impact on the notch and the phase jump of the PS-FBG and thus the passband of the MPF. Fig. 5.4(a) and (b) shows the theoretically calculated $r(\omega)$ and $\theta(\omega)$ for $L_1 = L_2$, $L_1 > L_2$ and $L_1 < L_2$, given φ_{PS} is equal to π. As can be seen for $L_1 = L_2$, the PS-FBG has the deepest notch with a single phase cycle corresponding to the notch, and the 3-dB bandwidth of the passband of the corresponding MPF, as shown in Fig. 5.4(c), is the smallest, which is equal to the 3-dB bandwidth of the notch. If $L_1 < L_2$, (say $L_1 : L_2 = 2:3$), both the notch depth and the phase jump become smaller. The small notch depth and phase jump would lead to an inefficient PM-IM conversion, thus a very weak passband in the MPF frequency response would be observed. If L_1 is larger than L_2 (say $L_1 : L_2 = 3:2$), despite that the notch depth becomes smaller, a fast 2π-phase jump corresponding to the notch is generated. Because of the fast and large phase jump, an efficient PM-IM conversion is obtained, leading to a strong passband in the MPF response. However,

since the frequency range corresponding to the 2π-phase jump is wider than that for $L_1 = L_2$ where the phase response has a single phase cycle, the 3-dB bandwidth of the passband is also increased, which leads to a smaller Q-factor of the MPF.

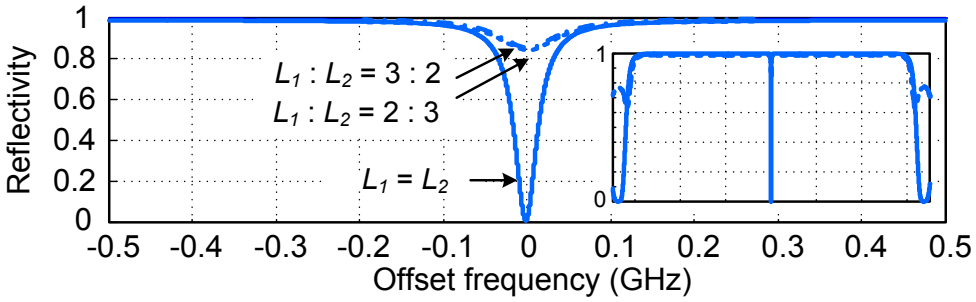

(a)

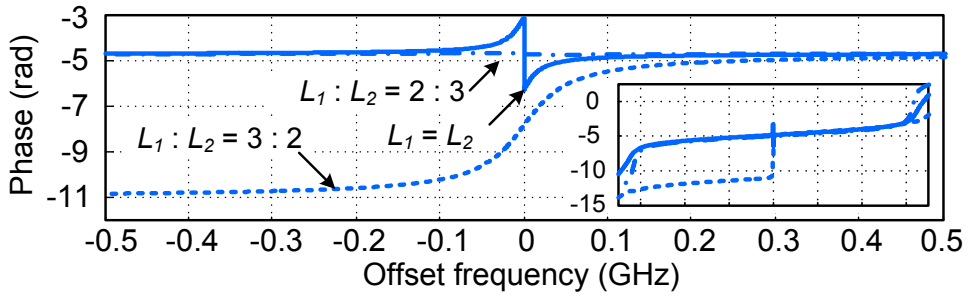

(b)

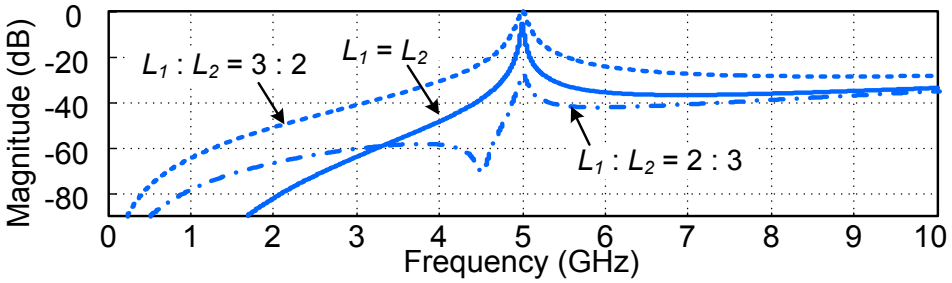

(c)

Fig. 5.4 The impact of the length difference between L1 and L2 on the reflection magnitude and phase responses of the PS-FBG. (a) Theoretical reflection spectra of the PS-FBG. (b) Theoretical phase responses of the PS-FBG; (The insets in (a) and (b) show the corresponding reflection spectra and phase responses with a much larger frequency span of 70 GHz.) (c) Theoretical frequency response of the obtained MPF.

Therefore, to obtain a high-Q MPF, it is preferable to employ a symmetric PS-FBG where $L_1 = L_2$ to ensure a narrow notch with a fast phase jump. Since the notch and the phase jump can be controlled as narrow as a few MHz and the width of the MPF passband is equal to that of the notch, the bandwidth of the MPF can be as narrow as a few MHz, leading to a high-Q value. For example, if the 3-dB bandwidth of the notch of the symmetric PS-FBG is 10 MHz, the 3-dB bandwidth of the MPF would also be 10 MHz; assuming the center frequency of the MPF is 10 GHz, a Q-factor as large as 1000 is thus obtained. The key significance of the proposed MPF is that a large tunable range can be achieved by simply tuning the wavelength of the optical carrier while maintaining a narrow and fixed passband. In addition, the passband can be potentially designed to have a shape with flat top and sharp transitions by designing the magnitude and phase response of the PS-FBG.

5.3 Evaluation of the frequency tunable microwave photonic filter

5.3.1 Tunability of the proposed microwave photonic filter

An experiment based on the setup shown in Fig. 5.1 is performed. A vector network analyzer (VNA) is employed to measure the frequency response of the MPF. A microwave sinusoidal signal from the VNA is applied to the phase modulator with a frequency (ω_e) sweeping from 50 MHz to 10 GHz. The power of the signal is fixed at 5 dBm. The half-wave voltage of the phase modulator is 15 V. The PMI is about 0.12, so that small-signal modulation is guaranteed. The PS-FBG, which is about 30 mm long with a gaussian-apodized refractive index profile, is fabricated by Teraxion Inc. by using a uniform phase mask by scanning an UV beam along the axial direction of an optical fiber. The estimated refractive index modulation amplitude is about 4×10^{-4}. A π phase shift is introduced at the center of the grating by shifting the phase

mask by half the corrugation width to create an ultra-narrow notch at the middle of the reflection spectrum. The phase response in the notch has a phase jump corresponding to a single phase cycle. The reflection magnitude and phase responses of the PS-FBG are measured using an optical vector analyzer, and are shown in Fig. 5.5. There is an ultra-narrow notch at about 1550.055 nm in the middle of the reflection spectrum and a single phase cycle in the phase response. The total reflection bandwidth of the PS-FBG is about 37.5 GHz; but the bandwidth in which the phase response is linear is about 23.4 GHz. The 3-dB bandwidth of the notch is about 120 MHz

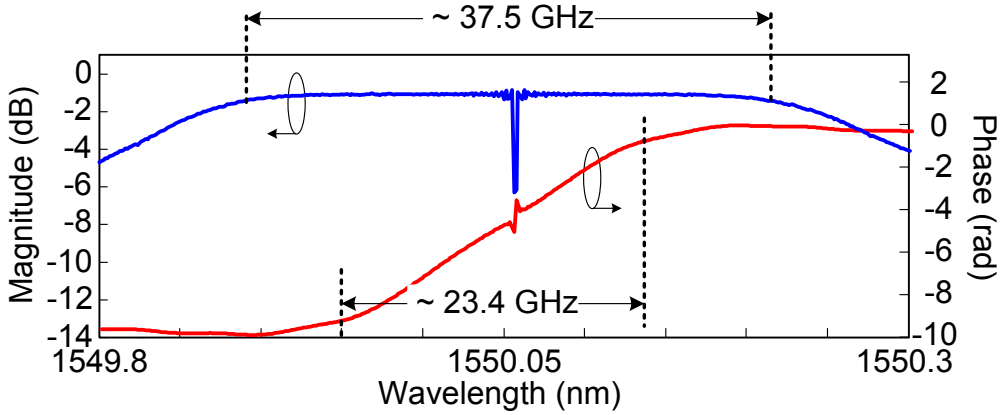

Fig. 5.5 Measured reflection magnitude and phase responses of the PS-FBG.

Then, the PS-FBG is incorporated into the proposed MPF to perform PM-IM conversion. The wavelength of the optical carrier is set at a wavelength that is less than the center wavelength of the notch; the upper sideband will fall in the notch of the PS-FBG when the microwave frequency is equal to the frequency difference between those of the optical carrier and the center frequency of the notch. To measure the spectral response of the MPF, a microwave sinusoidal signal generated by the VNA with a sweeping frequency from 50 MHz to 10 GHz is applied to the phase modulator. The output signal from the PS-FBG is then applied to the PD.

The tuning of the center frequency of the MPF is achieved by changing the wavelength of the optical carrier. Fig. 5.6(a) shows the superimposed frequency responses of the MPF with the central frequency tuned from about 1 GHz to about 6.5 GHz with a tuning step of about 700 MHz. The frequency tuning range here is about 5.5 GHz, which is limited by the reflection bandwidth of the PS-FBG. The tuning range could be further increased to tens of GHz by using a PS-FBG with a wider reflection bandwidth. The frequency tuning resolution is limited by the smallest wavelength tuning step of the TLS.

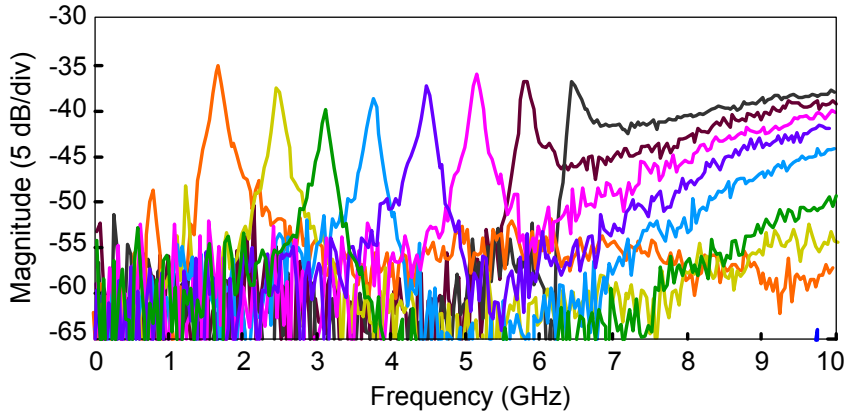

(a)

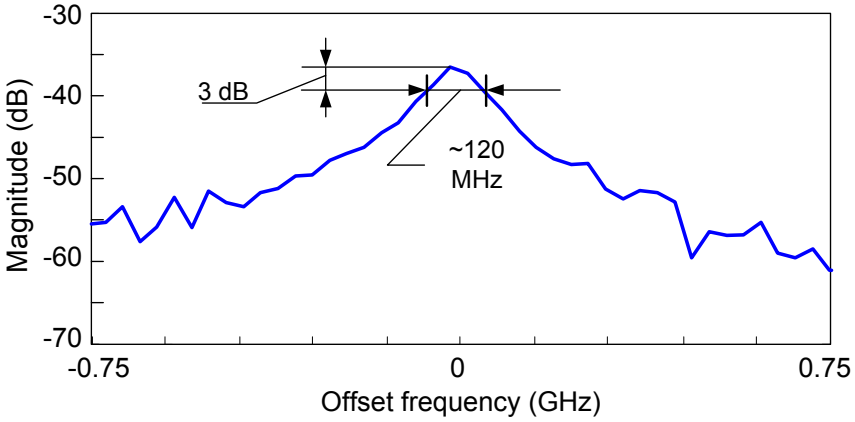

(b)

Fig. 5.6 Measured frequency responses of the MPF with the central frequency tuned from about 1 GHz to about 6.5 GHz with a tuning step of about 700 MHz. (b) The zoom-in view of the frequency response when the center frequency is tuned at about 4.9 GHz.

From Fig. 5.6(a), we can also see that the insertion loss of the MPF is more than 30 dB. Such a high insertion loss is mainly caused by the poor PD optical power handling. By using a high-power handling PD [209-211], the insertion loss can be greatly reduced. The ratio of the transmission peak to the sidelobe can be as large as 25 dB. When tuning the center frequency of the passband, the ratio would be smaller. The degradation in peak to the sidelobe ratio is resulted from the amplitude and phase response ripples of the PS-FBG. PM-IM conversion at the PS-FBG would convert the ripples to noise. In addition, given a certain modulation frequency, as the wavelength of the optical carrier is shifting away from the notch, one sideband of the phase-modulated light wave would be falling outside the reflection spectrum, PM-IM conversion would also happen and another passband starting at such a frequency would appear, as shown in Fig. 5.6(a). A solution to avoid the second passband is to use a PS-FBG with a wider reflection bandwidth.

The average 3-dB bandwidth of the MPF is about 135 MHz; the variation of the 3-dB bandwidth over the tuning range is about 15 MHz. Such a variation is also caused by the magnitude and phase response ripples of the PS-FBG.

Fig. 5.6(b) shows a zoom-in view of the measured frequency response of the MPF with a center frequency of 4.9 GHz. The 3-dB bandwidth is about 120 MHz, which is equal to the 3-dB bandwidth of the notch of the PS-FBG. The bandwidth of the MPF can be further reduced by using a PS-FBG with a narrower notch and a narrower phase jump within the notch.

Theoretically, the central frequency of the MPF can be as close to zero as the optical carrier is close to the notch. Thus, the frequency tunability range of the proposed MPF is from zero to the largest central frequency of the MPF. As the optical carrier is shifting away from the notch, the central frequency of the MPF and the lower cutoff frequency of the second passband are increasing and decreasing, respectively, and would be finally identical when the frequency spacing between the optical carrier and the notch is identical to the frequency spacing between the optical carrier and the closer edge of the reflection spectrum. Therefore, the largest central frequency is equal to the minimum lower cutoff frequency, and the frequency tunability range here is from zero to the largest central frequency.

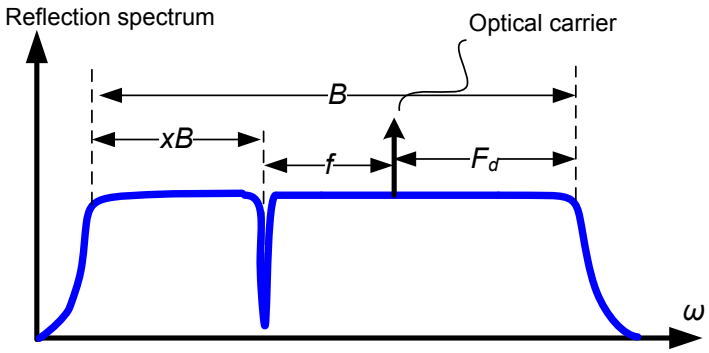

Fig. 5.7 Illustration of the parameters of the PS-FBG for the calculation of the frequency tunable range of the MPF.

For a given PS-FBG, assume that the total reflection bandwidth of the PS-FBG is B, and the reflection bandwidths of two sub-gratings are xB and $(1-x)B$. The value of x would be less than or equal to 0.5. The optical carrier is assumed to locate in the reflection band with a reflection bandwidth of $(1-x)B$ (see Fig. 5.7). So the lower cutoff frequency F_d, which is the frequency spacing between the optical carrier and the closer edge of the reflection spectrum, can be expressed as

$$F_{\mathrm{d}} = \min\left[xB + f \,, (1-x)B - f \right] = \begin{cases} xB + f, & 0 \le f \le (1-2x)B/2 \\ (1-x)B - f, & (1-2x)B/2 \le f \end{cases} \tag{5-16}$$

where f is the frequency difference between the frequency of the optical carrier and that of the notch, and also is the center frequency of the MPF. Considering the condition that the central frequency f should be less than the lower cutoff frequency F_{d}, we have $f < (1-x)B - f$. Then we can have the upper limit of f for (5-16), given by $f < \left[(1-x)B \right] / 2$.

Since the frequency tunable range of the MPF is the minimum lower cutoff frequency, it can be expressed as F_{T}

$$F_{\mathrm{T}} = \min\left(F_{\mathrm{d}}\right) = \min\left(xB \,, (1-x)B/2\right) = \begin{cases} xB, & 0 \le x \le 1/3 \\ (1-x)B/2, & 1/3 < x \le 1/2 \end{cases} \tag{5-17}$$

From (5-17), we can see that the frequency tunable range is a function of both the reflection bandwidth and the location of the notch, namely the value of x. For the PS-FBG employed in the experiment, the notch is located at the middle of the reflection spectrum, which means x is equal to 1/2. The tuning range F_{T} should be equal to one fourth of the reflection bandwidth, that is, 37.5/4 ≈ 9.4 GHz. However, the reflection bandwidth with a linear phase response is only about 23.4 GHz, in which the notch is not located at the middle, and the value of x is equal to about 0.42, as can be seen in Fig. 5.5. Therefore, a second passband would appear at a frequency smaller than 9.4 GHz, which is about 23.4×(1-0.42)/2 = 7.02 GHz. In Fig. 5.6(a), we can see that a second passband with a lower cutoff frequency of around 7 GHz exists, which limits the tunable range to be within 7 GHz.

Although the tuning range can be increased by using a PS-FBG with a wider reflection bandwidth, the maximum tuning range of the MPF for a given reflection bandwidth of B would be achieved when x is equal to 1/3, which is $B/3$. Based on (5-5), the value of x can be optimized by choosing a proper value of φ_{PS} in the design.

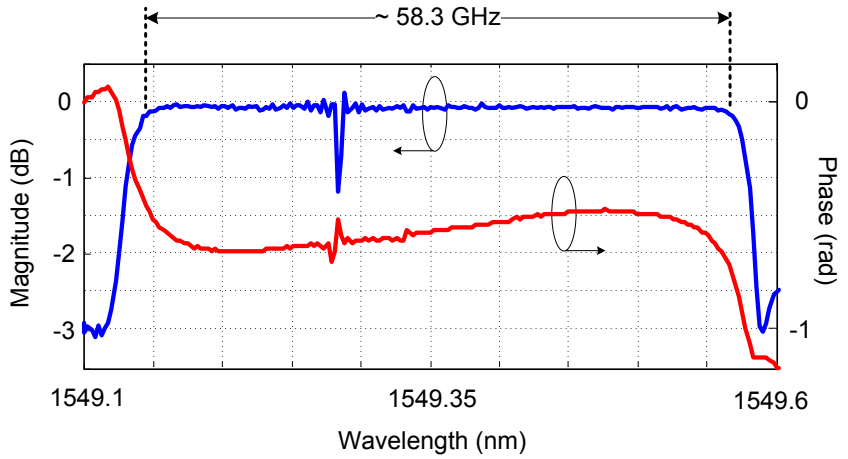

(a)

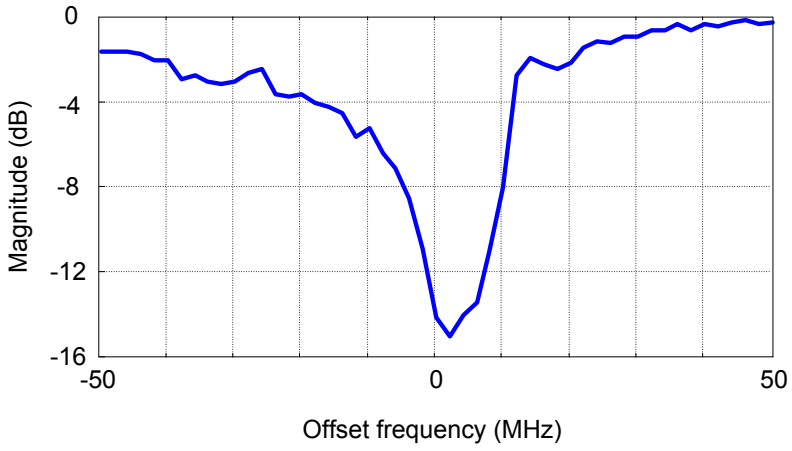

(b)

Fig. 5.8 (a) Measured reflection magnitude and phase response of the second PS-FBG; (b) Zoom-in view of the notch of the PS-FBG (resolution: 2 MHz).

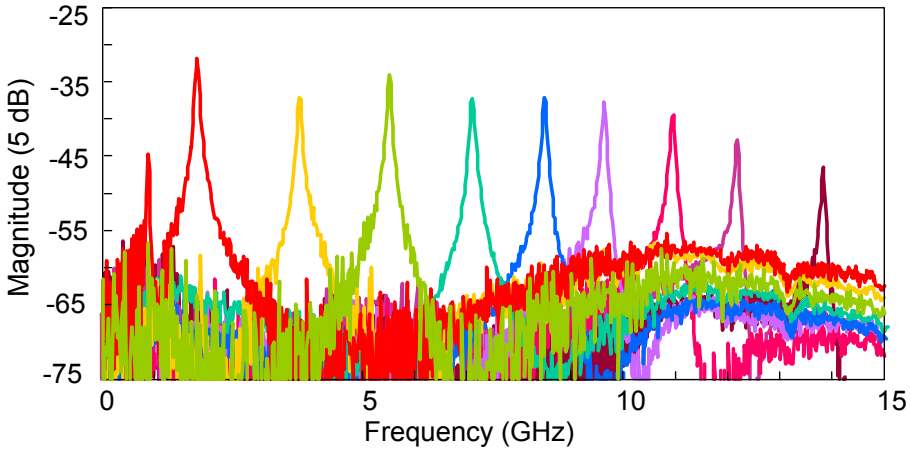

(a)

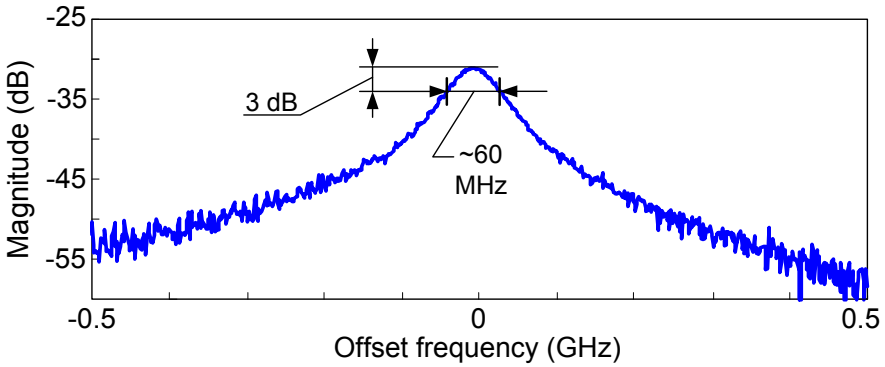

(b)

Fig. 5.9 (a) Measured frequency responses of the MPF when a second PS-FBG is employed. (b) The zoom-in view of the frequency response when the center frequency is tuned at 6.9 GHz.

Then, a second experiment is performed, in which the first PS-FBG is replaced by a second PS-FBG with a wider reflection bandwidth, and a narrower notch. The location of the notch is adjusted by adjusting the phase shift such that the value of x is 1/3. Thus, a maximum tuning range is obtained. The measured magnitude and phase responses of the new PS-FBG are shown in Fig. 5.8. As can be seen, the location of the notch is at 1549.275 nm, corresponding to an x of 1/3. The reflection bandwidth is about 0.46 nm or 58.5 GHz. Therefore, the tuning range could be as large as 19.5 GHz. To measure the zoom-in view of the notch of the PS-

FBG, we send a phase modulated light wave in the PS-FBG and only measure the power of one sideband using the optical spectrum analyzer. By changing the microwave modulation frequency, we can scan the notch with a very high resolution.

The wavelength of the optical carrier is set at 1549.275 nm, which is more than the center wavelength of the notch; therefore the lower sideband will fall in the notch of the PS-FBG when the microwave frequency is equal to the difference between the frequency of the optical carrier and the center frequency of the notch. By increasing the wavelength of the optical carrier, the center frequency of the MPF is accordingly increased. Fig. 5.9(a) shows the superimposed frequency responses of the MPF with a tunable central frequency covering a frequency range of about 15 GHz with a tuning step of 1.45 GHz. From Fig. 5.9(a), we can also see that the ratio of the transmission peak to the sidelobe can be as large as 40 dB. The frequency tuning range here is less than the theoretical result of 19.5 GHz, which is caused by the limited bandwidth of the 10-GHz PD. The second passband is not seen since it is eliminated by the PD due to its limited bandwidth. The central-frequency-dependency of the frequency response of the MPF is resulted from the frequency-dependent response of the 10-GHz PD. At the high frequency band (> 10 GHz), the electrical frequency response of the PD becomes small, which leads to the power reduction of the recovered microwave signal. In Fig. 5.9(b), a zoom-in view of the measured frequency response of one MPF at about 6.9 GHz is shown. The 3-dB bandwidth is about 60 MHz. The bandwidth can be further decreased by using a PS-FBG with a narrower notch.

In two cases using different PS-FBGs, there are power variations as a function of tuning. The origin of the variation is caused by the variations of the frequency response of the modulator, the PD and the nonlinearity of the phase response of the PS-FBGs.

The average 3-dB bandwidth of the second MPF is about 72 MHz. The variation of the 3-dB bandwidth over the tuning range is about 15 MHz, as shown in Fig. 5.10. Such a variation is also caused by the nonlinearity of the phase response of the PS-FBG, which leads to the frequency-dependency of PM-IM conversion.

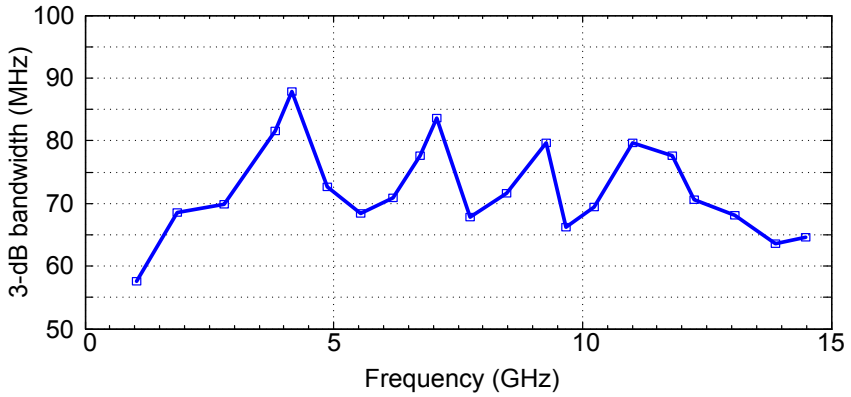

Fig. 5.10 The relationship between the 3-dB bandwidth of the MPF and the central frequency.

5.3.2 Dynamic range of the proposed microwave photonic filter

Another important performance measure for the MPF is the dynamic range (DR). In the earlier analysis, small signal modulation is considered. For small signal modulation, only the optical carrier and the first-order sidebands are considered. However, as the power of the input signal or equivalently the phase modulation index increases, the power of the higher-order sidebands would increase, thus nonlinear distortions start.

The DR here is defined as the range from the minimum discernable signal (lower limit) to the maximum allowable signal (upper limit). The lower limit is directly measured here by the VNA, which is -37 dBm. The upper limit determined by the nonlinearity of the phase modulator is quantified by the 1-dB compression point. Namely, in the analysis, the upper limit

is found when the transmission peak of the frequency response of the MPF drops by 1 dB from the maximum value.

For convenience and simplicity, we assume the reflectivity of the PS-FBG is one and the notch of the PS-FBG is deep enough to totally suppress the plus first-order sideband of the phase-modulated light wave. The optical carrier and the other sidebands are totally reflected by the PS-FBG. Therefore, the power of the recovered microwave signal can be expressed as the summation of the power of the beatings between any adjacent sidebands. Based on (5-1), the electrical field $E_{\mathrm{IM}}{}'(t)$ at the input of the PD can be expressed as

$$\begin{aligned} E_{\mathrm{IM}}{}'(t) &\approx E_{\mathrm{o}}\sum_{n=2}^{\infty} i^n J_n(\beta)\exp\left\{j\left[\omega_{\mathrm{o}}t+n\left(\omega_{\mathrm{e}}t+\varphi_{\mathrm{e}}\right)\right]\right\} \\ &+ E_{\mathrm{o}}\sum_{n=-\infty}^{0} i^n J_n(\beta)\exp\left\{j\left[\omega_{\mathrm{o}}t+n\left(\omega_{\mathrm{e}}t+\varphi_{\mathrm{e}}\right)\right]\right\} \\ &= E_{\mathrm{o}}\sum_{n=2}^{\infty} i^n J_n(\beta)\exp\left\{j\left[\omega_{\mathrm{o}}t+n\left(\omega_{\mathrm{e}}t+\varphi_{\mathrm{e}}\right)\right]\right\} \\ &+ E_{\mathrm{o}}\sum_{n=0}^{\infty} i^n J_n(\beta)\exp\left\{j\left[\omega_{\mathrm{o}}t-n\left(\omega_{\mathrm{e}}t+\varphi_{\mathrm{e}}\right)\right]\right\} \end{aligned} \tag{5-18}$$

From (5-18), if only consider the fundamental frequency, we can see that: 1) the fundamental frequency generated by beating the optical carrier and the minus first-order sideband is in phase with a beat signal between any two adjacent lower sidebands. All these beat signals are grouped in group A; 2) the beat signals between any two adjacent upper sidebands are in phase. All these beat signals are grouped in group B; 3) the two groups of beat signals are out of phase. Therefore, the power of the recovered microwave signal can be expressed as

$$P'(\omega_e) \propto \left| \sum_{n=0}^{\infty} J_n(\beta) J_{n+1}(\beta) - \sum_{n=2}^{\infty} J_n(\beta) J_{n+1}(\beta) \right|^2 = \left| \sum_{n=0}^{1} J_n(\beta) J_{n+1}(\beta) \right|^2 \quad (5\text{-}19)$$

Based on (5-19), the level at the transmission peak of the frequency response of the MPF as a function of the power of the input signal is shown in Fig. 5.11. From Fig. 5.11, we can see that the input power corresponding to the 1-dB compression point is about 20 dBm. Since the minimum measurable output power is -37 dBm, the 1-dB compression DR of the proposed MPF is 57 dB. When the power of the input signal increases, more and more power of the incident light wave will be distributed to high-order sidebands, which leads to the power reduction of the recovered signal and the fast decrease of the frequency response of the MPF at the transmission peak.

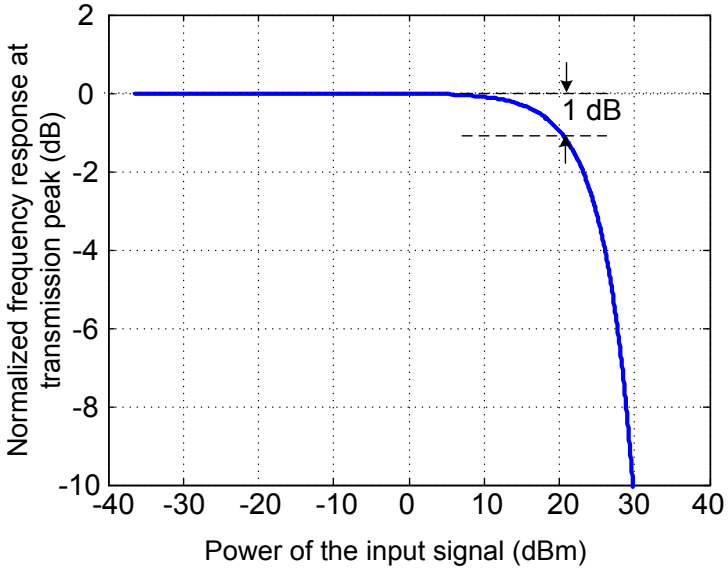

Fig. 5.11 Frequency response at the transmission peak versus the power of the input signal (Vπ = 10V).

Due to the fact that the frequency response of the MPF is determined by the PS-FBG, the change of the power of the input signal within the DR would not distort the profile of the transmission band of the MPF. Fig. 5.12 shows the frequency responses of the MPF using the second PS-FBG at different input signal power levels.

From Fig. 5.12, we can see that as the power of the input signal decreases, the profile of the transmission band of the MPF barely distorted. Thus, as the power of the input signal decreases, we can see that the power of the recovered signal decreases and the ratio of the transmission peak to the sidelobe also decreases.

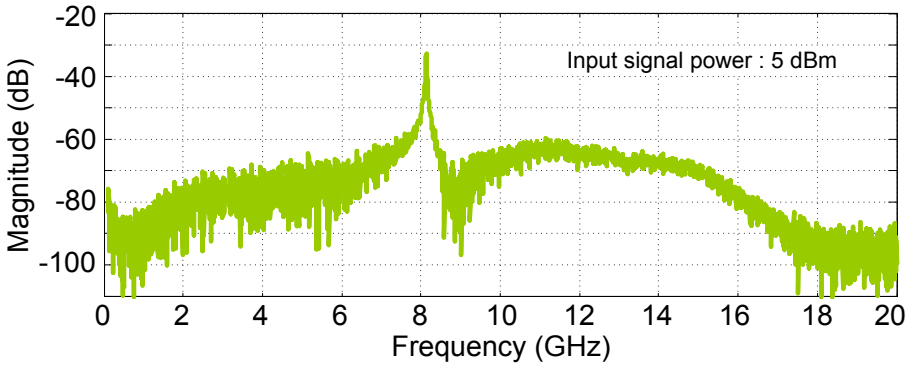

(a)

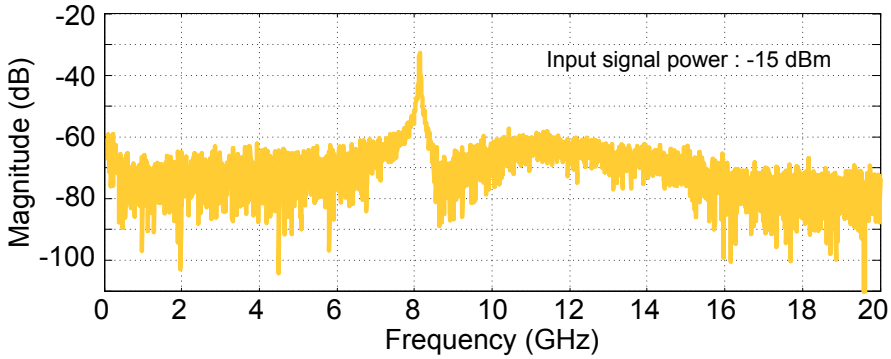

(b)

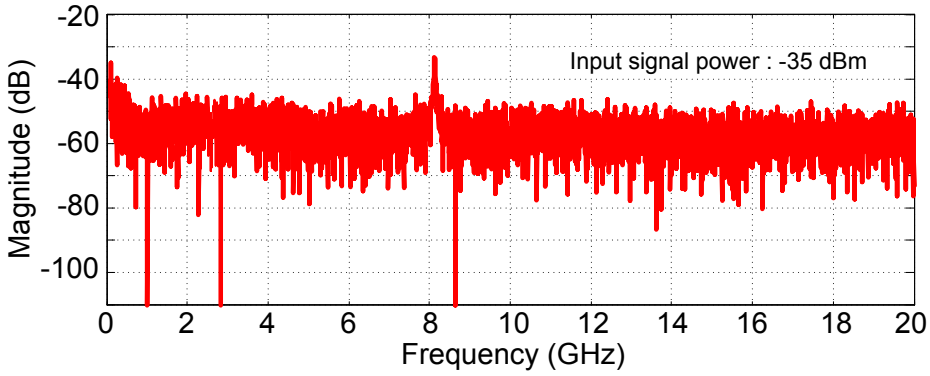

(c)

Fig. 5.12 Frequency response of the MPF using the second PS-FBG at different input signal power levels. (a) 5 dBm. (b) -15 dBm. (c) -35dBm.

The DR can also be characterized by the spurious free dynamic range (SFDR). Assume that two closely spaced microwave signals, $V\cos\left(\omega_{e1}t+\varphi_{e1}\right)$ and $V\cos\left(\omega_{e2}t+\varphi_{e2}\right)$, are applied to the input of the MPF, where ω_{e1} and ω_{e2} are angular frequencies, φ_{e1} and φ_{e2} are the initial phases of the two signals, and the two signals have identical amplitudes. The electrical field $E_{PM}{}'(t)$ at the output of the phase modulator can be expressed as

$$\begin{aligned} E_{PM}{}'(t) &= E_o \exp\left\{j\left[\omega_o t+\beta\left(\cos\left(\omega_{e1}t+\varphi_{e1}\right)+\cos\left(\omega_{e2}t+\varphi_{e2}\right)\right)\right]\right\} \\ &= E_o \exp\left(j\omega_o t\right)\sum_{n=-\infty}^{\infty}\sum_{m=-\infty}^{\infty}\left\{i^{n+m}\cdot\right. \\ &\quad \left. J_n(\beta)J_m(\beta)\exp\left[jn\left(\omega_{e1}t+\varphi_{e1}\right)+jm\left(\omega_{e2}t+\varphi_{e2}\right)\right]\right\} \\ &\approx E_o \exp\left(j\omega_o t\right)\sum_{n=-2}^{2}\sum_{m=-1}^{1}\left\{i^{n+m}\cdot\right. \\ &\quad \left. J_n(\beta)J_m(\beta)\exp\left[jn\left(\omega_{e1}t+\varphi_{e1}\right)+jm\left(\omega_{e2}t+\varphi_{e2}\right)\right]\right\} \end{aligned} \tag{5-20}$$

where the high order sidebands ($|n+m|\geq 4$) are ignored due to their relatively low power levels when the phase modulation index is small.

Assume that PS-FBG is used to suppress the plus first-order sideband of the phase-modulated light wave, which is $\omega_o+\omega_{e1}$. After heterodyning at the PD, two third-order intermodulation terms would occur at $2\omega_{e1}-\omega_{e2}$ and $2\omega_{e2}-\omega_{e1}$. In the following we will calculate the power of the third-order intermodulation term at $2\omega_{e1}-\omega_{e2}$.

To simplify the calculation, we consider the nature of the phase modulation: a phase-modulated signal will not generate any microwave signal except a dc if directly detected at a PD. Based on this property, if the sideband at $\omega_o+\omega_{e1}$ is not removed by the PS-FBG, the third-order intermodulation term at $2\omega_{e1}-\omega_{e2}$ generated by beating the sidebands at $\omega_o+\omega_{e1}$ and $\omega_o-\omega_{e1}+\omega_{e2}$ would have an equal amplitude but opposite phase with that generated by beating all other sidebands. Thus, the power of the third-order intermodulation term at $2\omega_{e1}-\omega_{e2}$ when the PS-FBG is used is equal to that generated by only beating the sidebands $\omega_o+\omega_{e1}$ and $\omega_o-\omega_{e1}+\omega_{e2}$ if the PS-FBG is not used to remove sidebands $\omega_o+\omega_{e1}$. Thus, the power of the third-order intermodulation term at $2\omega_{e1}-\omega_{e2}$ can be expressed as

$$\begin{aligned} P''(2\omega_{e1}-\omega_{e2}) &\propto \left| i\cdot J_1(\beta)J_0(\beta)\cdot i^{-1}iJ_{-1}(\beta)J_1(\beta)\right|^2 \\ &= \left|J_0(\beta)J_1^3(\beta)\right|^2 \end{aligned} \tag{5-21}$$

Based on (5-19) and (5-21), we can plot the theoretical output powers of the fundamental and the third-order intermodulation terms as a function of the input power, as shown in Fig. 5.13. The third-order intercept point is about 26 dBm. Given the minimum detectable signal level in the proposed system which is -160 dBm/Hz, the calculated SFDR is about 102 dB·Hz$^{2/3}$.

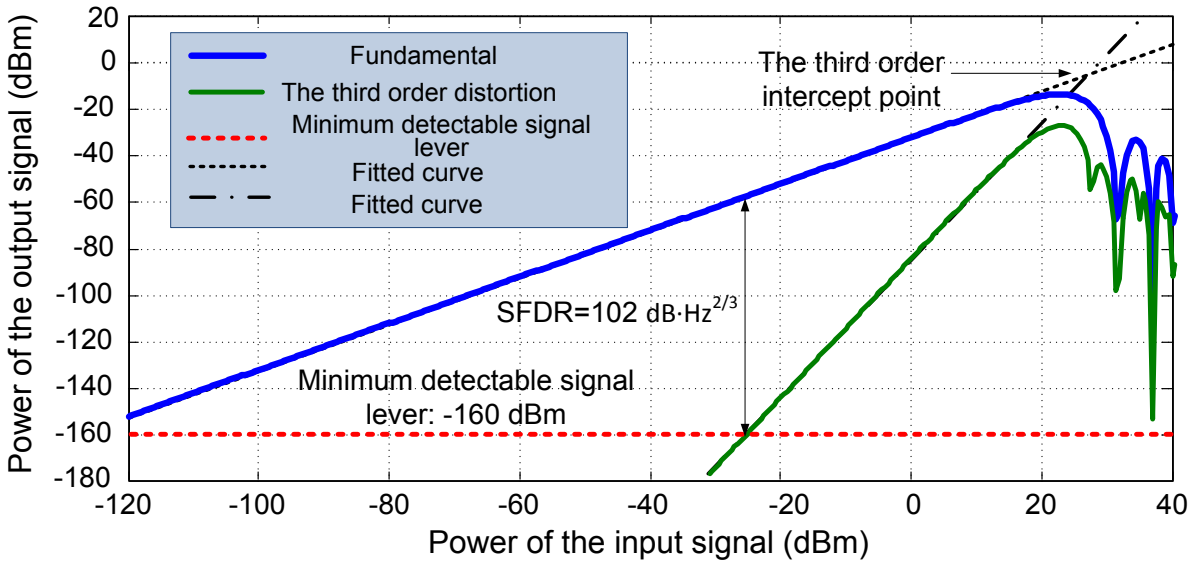

Fig. 5.13 The powers of the fundamental signal and the third order intermodulation terms, as a function of the input power of the input signal (Vπ = 10V).

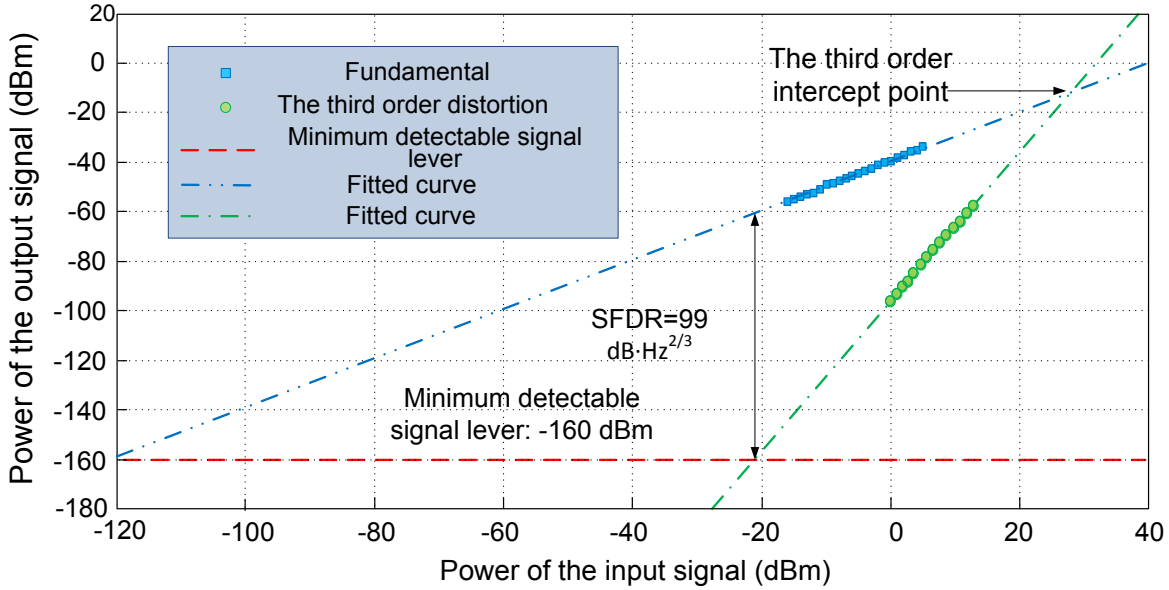

Fig. 5.14 Measured powers of the fundamental signal and the third order intermodulation terms, as a function of the input power of the input signal.

Then, the experimental output powers of the fundamental and the third-order intermodulation terms as a function of the input power are measured, as shown in Fig. 5.14. The experimental

SFDR is about 99 dB·Hz$^{2/3}$. The experimental results agree well with the theoretical calculation.

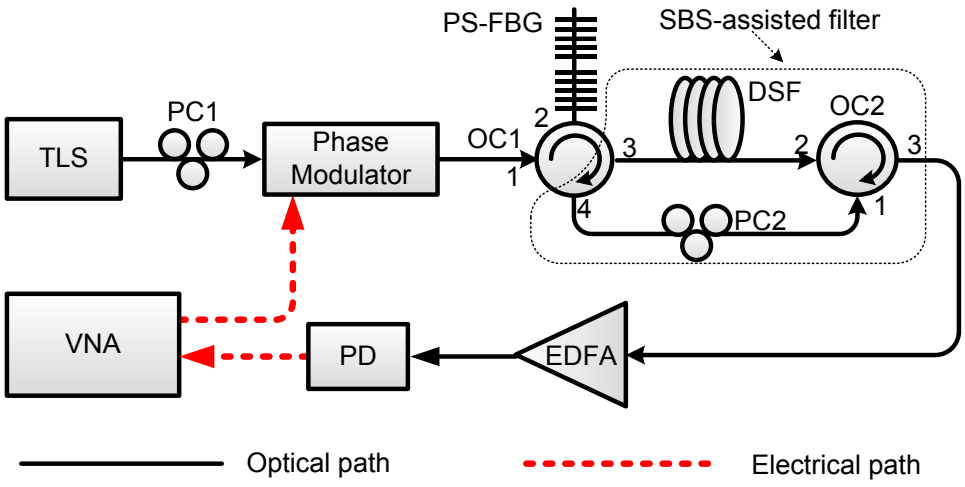

Fig. 5.15 Schematic of the proposed wideband SFDR-increased MPF.

To further improve the SFDR, SBS-assisted adaptive filtering in a dispersion-shifted fiber (DSF) can be employed in the previous MPF, as shown in Fig. 5.15. An SBS-assisted adaptive filter is capable of increasing the PMI equivalently by suppressing the relatively large optical carrier when the input microwave signal is small, which leads to the improvement of the SFDR of the MPF.

As can be seen from Fig. 5.15, a light wave from a TLS is sent through a PC (PC1) to a PM, which is driven by a microwave signal from a VNA. The phase-modulated light wave is sent to and reflected by a PS-FBG with an ultra-narrow notch in the reflection band via an OC (OC1). The reflected light wave is routed by OC1 to an SBS-assisted filter that consists of a DSF, a PC (PC2) and an OC (OC2). At the output of the SBS-assisted filter (port 3 of OC2), the light wave is boosted to a fixed power level by an erbium-doped fiber amplifier (EDFA) and then

sent to a photodetector (PD). The output from the PD is sent back to the VNA where the frequency response of the MPF is measured. At the output of the PM, under a small microwave signal modulation condition, the phase-modulated light wave only contain the optical carrier and the two 1st-order sidebands, which is then sent to the SBS-assisted filter.

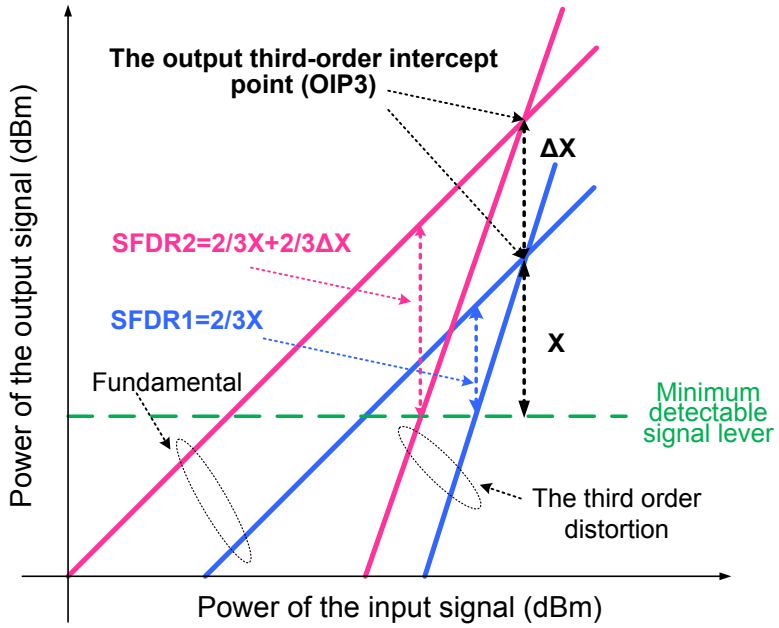

Fig. 5.16 Illustration of the increase of the SFDR when the output powers of the fundamental signal and the third order intermodulation terms are moved up.

The SBS-assisted filter located between OC1 and the EDFA is used to increase the SFDR of the MPF by moving up the output power measurements at the third-order distortion and the fundamental frequency. It is known that on a logarithmic scale the slopes of curve of the output power of the third-order distortion and that of the fundamental with respect to the input power are 3 and 1. Since the SFDR is the distance between the fundamental and the third-order distortion when the output power of the third-order distortion reaches the minimum detectable signal level (MDSL), and also is 2/3 the distance between the minimum detectable signal level and the output third-order intercept point (OIP3) which is the point of intersection when the

linear portions of these two curves are extended. Thus, when the two output curves, or, the OIP3 are moved up, the SFDR would be increased by 2/3 the shift, which is illustrated in Fig. 5.16. If both output curves are shifted up by ΔX, the SFDR will be increased by 2/3ΔX.

The moving up of the output power measurements at the third-order distortion and the fundamental frequency can be achieved by increasing the PMI, and the increase of the PMI can be equivalently achieved by increasing the power ratio of the sideband to the optical carrier given a certain power of the input microwave signal. In the MPF, the reflected optical carrier and the upper first-order sideband from the PS-FBG are routed through OC1 to the DSF in the SBS-assisted filter. The use of the DSF is to avoid introducing additional PM-IM conversion to the system due to the chromatic dispersion of the fiber. When the power of the microwave signal is low, the PMI is small, which gives a relatively high-power optical carrier and a relatively low-power sideband. If only the power of the optical carrier is above the threshold of the SBS, Stokes waves would be generated by the optical carrier and would go backward along the DSF. The Stokes waves are then re-injected into the DSF via OC1, PC2 and OC2 in a direction opposite to the optical carrier. As discussed in Section 4.1, the interaction between the optical carrier and the re-injected Stokes waves would significantly enhance the induced acoustic grating so that more backscattering of the optical carrier into the Stokes waves would occur, leading to a suppression of the optical carrier and thus an increase of the power ratio of the sideband and the optical carrier at the port 3 of OC2. The increase in the power ratio can be as large as 30 dB. Therefore, at the output of the PD the powers of the recovered fundamental signal and the third-order distortion are correspondingly increased and the power measurements of the third-order distortion and the fundamental should be shifted upward.

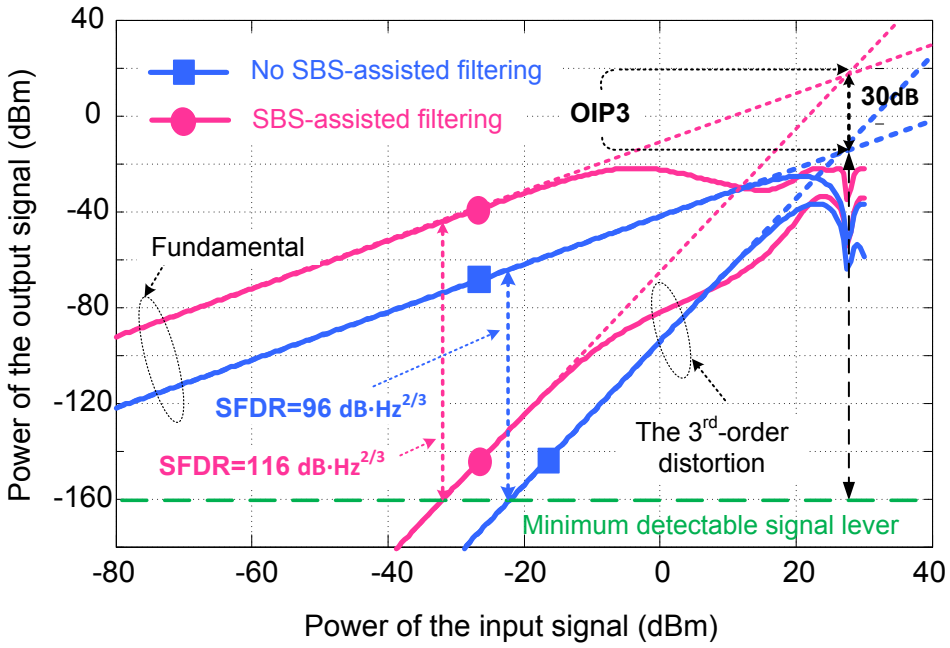

Fig. 5.17 Theoretical calculations of the SFDR of the MPF by comparing the output powers of the 3rd-order distortion and the fundamental with and without using SBS-assisted filtering.

The theoretical calculations are presented in Fig. 5.17. The optical carrier is assumed to be suppressed by 30 dB, correspondingly the output powers of the fundamental and the third-order distortion are both up-shifted by 30 dB. The SFDR is also increased by 20 dB.

An experiment based on the setup shown in Fig. 5.15 is then performed. The PS-FBG used in the SFDR-improved MPF is the same one shown in Fig. 5.8. The SBS-assisted filter employed consists of a DSF of 9 km. The frequency responses of the MPF are superimposed and shown in Fig. 5. 18(a). The central frequency is tuned by changing the wavelength of the incident light wave, covering a frequency range of about 14 GHz with a tuning step of 1 GHz. A zoom-in view of the measured frequency response of one MPF at about 10 GHz is shown in Fig. 5.18(b) with a 3-dB bandwidth of about 60 MHz. Due to the use of the DSF, some undesired PM-IM conversion caused by the small chromatic dispersion of the DSF reduces the ratio of the transmission peak to the sidelobe to as small as 10 dB.

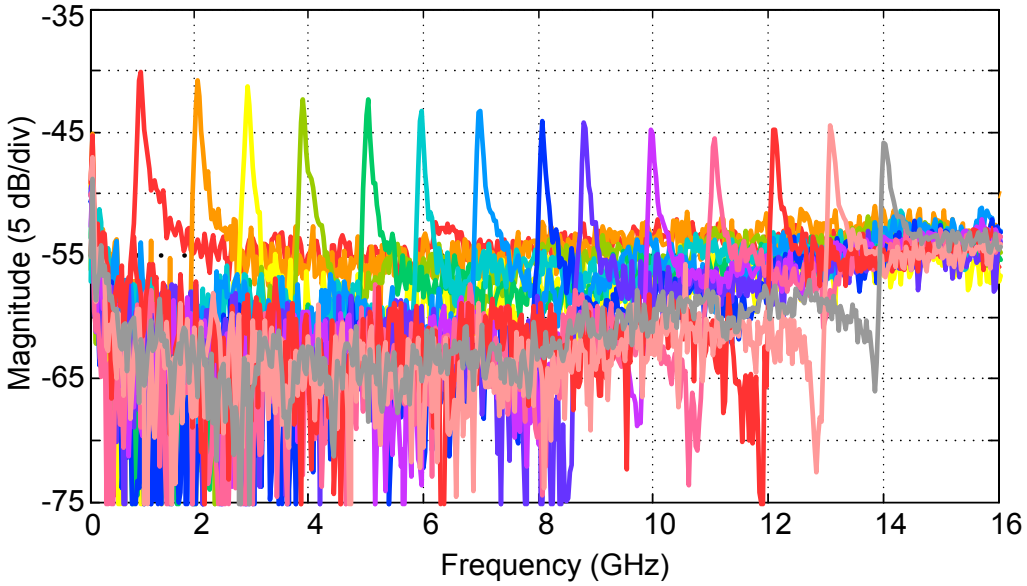

(a)

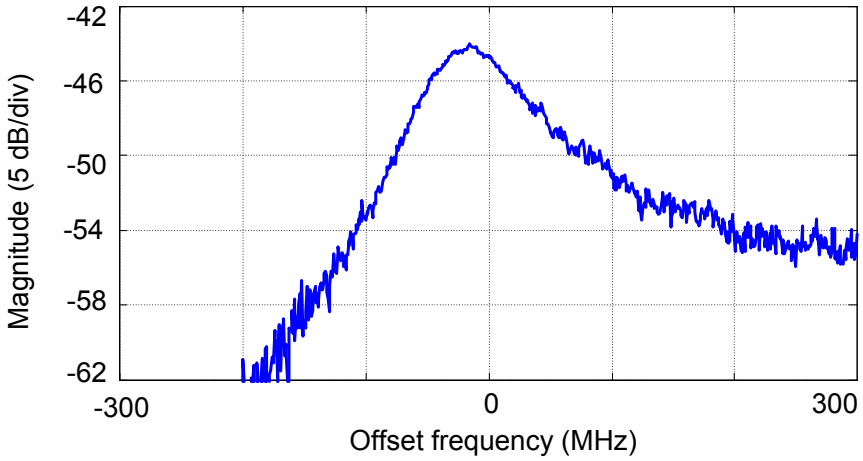

(b)

Fig. 5.18 (a) Measured frequency responses of the MPF with the central frequency tuned from 1 to 14 GHz. (b) a zoom-in view of the measured frequency response of the MPF when the center frequency is tuned at about 10 GHz.

To investigate the SFDR of the new MPF, the measurements of the output powers of the third-order distortion and the fundamental are performed in two cases where an SBS-assisted adaptive filter is and is not activated, as shown in Fig. 5.19. When SBS-assisted filtering is not activated (port 4 of OC1 and port 1 of OC2 are disconnected), an SFDR of 77 dB·Hz$^{2/3}$ is

achieved. Then, the SBS-assisted filtering is activated by connecting port 4 of OC1 and port 1 of OC2. Due to the low incident power of about 5 dBm to the DSF, the optical carrier is suppressed by about 10 dB, and an upward curve shift of about 10 dB is accordingly achieved, which gives a 6-dB increase in the SFDR, as shown in Fig. 5.19. To further improve the dynamic range, the SBS-assisted filter should be optimized with a further suppressed optical carrier up to 30 dB, the SFDR could then be increased by 20 dB.

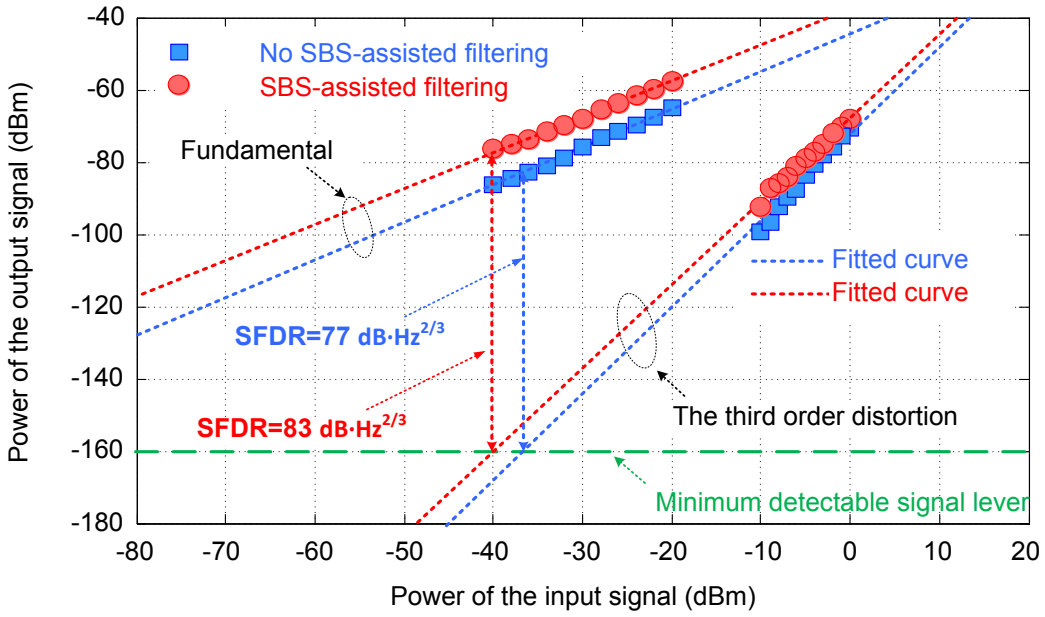

Fig. 5.19 Measured curves of the 3rd-order distortion response and the fundamental frequency response with and without using SBS-assisted filtering.

Obviously that suppression the optical carrier when the microwave signal applied to the PM is small is capable of increasing the SFDR of the MPF, however, as shown in Fig. 5.18(a), using a DSF-based SBS-assisted filter inevitably decreases the ratio of the transmission peak to the sidelobe due to the accumulated dispersion of the fiber. To significantly increase the SFDR, the optical carrier must be greatly removed in the DSF which requires a large power of the incident light wave. Such a large power could result in undesired nonlinear optical effects and

degrade the performance of the MPF. Thus, an alternative is apposed here to replace the DSF-based SBS-assisted filter for suppressing the optical carrier more easily.

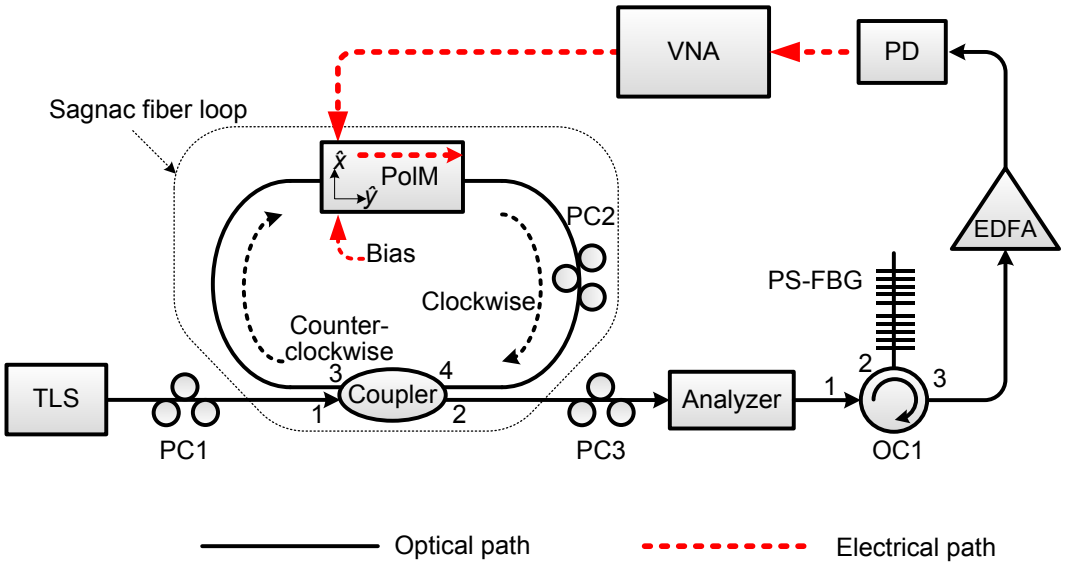

Fig. 5.20 Schematic of the proposed novel SFDR-increased MPF by jointly using of a polarization modulator (PolM) and a PS-FBG.

The schematic of the proposed set-up is shown in Fig. 5.20. A continuous-wave light wave as an optical carrier from a TLS is sent to a Sagnac fiber loop consisting of a 1:1 optical coupler, a polarization modulator (PolM) and a polarization controller (PC2). The PolM is driven by a microwave signal from a VNA and a bias voltage from a dc power supplier. Since the PolM is a special phase modulator that supports phase modulation with complementary modulation indices along the two principal axes (x and y in Fig. 5.20) of the PolM, by adjusting PC1 and PC2, the counterclockwise and clockwise propagating light waves inside the Sagnac loop can be made along the two principal axes (say x and the y axes) respectively when both light waves go through the PolM. Due to the fact that the PolM is a traveling wave modulator, when the clockwise propagating light wave goes through the PolM, the velocity mismatch would

make the microwave modulation have very low modulation index and thus can be ignored, and only the dc bias applied to the PolM would introduce a phase shift to the clockwise propagating light wave, therefore, at the output of the Sagnac loop (port 2 of the optical coupler), a phase-modulated light wave and a phase-shifted light wave with orthogonal polarization directions can be achieved.

Mathematically, the optical signals at the output of the Sagnac loop can be expressed as

$$E_{S\text{agnac}}(t) \approx e^{j\omega_o t}\left(xE_x e^{j\phi}, yE_y e^{-j\phi}\right)\begin{pmatrix} J_0(\beta) + J_1(\beta) i e^{j\omega_e t} + J_{-1}(\beta) i^{-1} e^{-j\omega_e t} \\ 1 \end{pmatrix} \quad (5\text{-}22)$$

where x and y denote the two orthogonal principle axes of the PolM, E_x and E_y are the amplitudes of the counterclockwise and clockwise propagating light waves respectively, and E_x is equal to E_y, ϕ is the phase shift introduced by the dc bias applied to the PolM, given by $\pi V_{\text{bias}}/V_\pi$, where V_{bias} is the voltage of the bias. Note that due to the small PMI, the higher order sidebands are also ignored here.

Then, the phase-modulated and the phase-shifted light waves along the x and y axes are sent to a polarization analyzer via a third PC (PC3). By adjusting PC3, the polarization directions of the two light waves along the x and y axes can be aligned at 45^o to the polarization direction of the polarization analyzer, namely, be polarized in the same direction. Thus, at the output of the polarization analyzer, the optical signals can be expressed as

$$
\begin{aligned}
E'_{S\text{agnac}}(t) &= \frac{\sqrt{2}}{2} e^{j\omega_o t}\left[\left(E_x e^{j\phi} + E_y e^{-j\phi}\right) J_0(\beta) + J_1(\beta) i e^{j\omega_e t} + J_{-1}(\beta) i^{-1} e^{-j\omega_e t}\right] \\
&= \frac{\sqrt{2}}{2} e^{j\omega_o t}\left[2E_x \cos(\phi) J_0(\beta) + J_1(\beta) i e^{j\omega_e t} + J_{-1}(\beta) i^{-1} e^{-j\omega_e t}\right] \\
&= \frac{\sqrt{2}}{2} e^{j\omega_o t}\left[2E_x \cos\left(\frac{V_{\text{bias}}}{V_\pi}\pi\right) J_0(\beta) + J_1(\beta) i e^{j\omega_e t} + J_{-1}(\beta) i^{-1} e^{-j\omega_e t}\right]
\end{aligned}
\tag{5-23}
$$

As can be seen from (5-23), by changing the voltage of the dc bias, the optical carrier can be easily suppressed and the light wave at the output of the polarization analyzer is only a phase-modulated light wave. Then similar to the case in the set-up in Fig. 5.1, such a phase-modulated light wave is sent to the PS-FBG to enable PM-IM conversion, leading to the implementation of the MPF.

Thanks to the electrically bias-controlled optical carrier suppression in the Sagnac loop, the SFDR of the proposed MPF could be easily improved using a simple configuration and avoid complicated nonlinear optical effects.

5.4 Conclusion

A simple and novel approach to implementing a narrow-passband and frequency-tunable MPF based on PM-IM conversion employing a phase modulator and a PS-FBG was proposed and experimentally demonstrated. A theoretical analysis was performed in which the value of the phase shift and the location of the phase shift in the PS-FBG on the frequency response of the MPF were studied. Two PS-FBGs with different reflection bandwidths and phase-shift values introduced at the center of the gratings were fabricated and incorporated into the proposed MPF. For the two PS-FBGs, the 3-dB bandwidths of the MPF were 120 MHz and 60 MHz and the tunable ranges were 5.5 GHz and 15 GHz. Both the width of the passband and the tunable

range could be further improved by using a PS-FBG with a narrower notch and a wider reflection bandwidth. The key advantage of the proposed technique is that the MPF can be tuned with a large tunable range which could be tens of GHz, and high tuning speed, which is difficult for a purely electronic microwave filter. In addition, the notch profile can be controlled, which enables the design and implementation of a MPF with a specific frequency response, such as a passband with a flat top and sharp transitions. However, due to the low output power of the PD, the insertion loss of the microwave photonic filter is as high as tens of dB.

Then an SFDR-improved wideband and frequency-tunable MPF was demonstrated based on PM-IM conversion using a PS-FBG and SBS-assisted adaptive filtering using a DSF. Thanks to the increase of the PMI caused by an SBS-assisted filter, the SFDR of the MPF was increased by 6 dB. A further improvement up to 20 dB could be achieved if the SBS-assisted filter is optimized to further increase the carrier suppression. Finally, to further simply the set-up of an SFDR-improved wideband and frequency-tunable MPF, a PolM-based Sagnac fiber loop was proposed to replace the SBS-assisted adaptive filter, which could potentially enable the increase of the SFDR by simply tuning the voltage of the dc bias applied to the PolM.

CHAPTER 6 WIDEBAND FREQUENCY TUNABLE OPTOELECTRONIC OSCILLATOR

In this chapter, by incorporating the frequency-tunable microwave photonic filter (MPF) demonstrated in Chapter 5, an optically tunable optoelectronic oscillator (OEO) with a wide frequency tunable range is proposed and experimentally demonstrated. The phase-shifted fiber Bragg grating (PS-FBG) in conjunction with two optical phase modulators (PMs) in the OEO loop form a high-Q, wideband and frequency-tunable microwave photonic bandpass filter, to achieve simultaneously single-frequency selection and frequency tuning. Since the tuning of the microwave filter is achieved by tuning the wavelength of the incident light wave, the tunability can be easily realized at a high speed. A theoretical analysis is performed, which is verified by an experiment. A microwave signal with a frequency tunable from 3 GHz to 28 GHz is generated. The phase noise performance of the OEO is also investigated, which is -102 dBc/Hz at a 10-kHz offset frequency.

6.1 Tunability of optoelectronic oscillators

Microwave signal generation using an OEO has been considered a promising solution for the generation of a high frequency and ultra-low phase noise microwave signal, and it can find important applications in optical and wireless communications, radar, modern instrumentation, microwave imaging and microwave spectroscopy. To reduce the phase noise, a simple solution is to design an OEO to have a long fiber loop, but an OEO with a long loop length will have a large number of densely-spaced oscillation modes. To ensure that the OEO operates at a single

oscillation mode, a high-Q electrical bandpass filter is required. However, the using of such an electrical bandpass filter leads to two limitations to the OEO. First, it is difficult to obtain a frequency-tunable single mode OEO for the implementation of frequency-tunable high-Q electrical bandpass filters is a challenge. In a conventional OEO, the frequency of the generated microwave can only be tuned within a small frequency range. Second, it is difficult to generate a high-frequency microwave or mm-wave signal for the central frequency of an electrical high-Q bandpass filter is usually low (~ GHz). To solve this problem, frequency-tunable MPFs have been proposed to replace the conventional electrical bandpass filters in the OEOs [140- 142]

In this chapter, a novel approach to realizing a wideband and frequency tunable OEO using a MPF is proposed and experimentally demonstrated [143]. The MPF has a high Q and a large frequency tunable range, which is implemented using two cascaded PMs and a PS-FBG. By tuning the wavelength of the laser source, the central frequency of the high-Q microwave photonic bandpass filter is tuned. The key significance of the proposed approach is that no electrical filters are employed, which ensures a simple tuning and a large frequency tunable range. In addition, the PMs are not dc biased, which would eliminate the bias drifting problem existing in an MZM. A theoretical analysis is performed, which is validated by an experiment. The generation of a microwave signal tunable from 3 to 28 GHz is demonstrated. The phase noise performance of the generated microwave signal is also investigated.

6.2 Principle of the wideband frequency-tunable OEO

The implementation of the wideband and frequency tunable OEO incorporating a tunable microwave photonic bandpass filter based on phase-modulation to intensity modulation (PM-

IM) conversion using a PS-FBG is presented in this section. Fig. 6.1 shows a schematic of the proposed frequency-tunable OEO. The OEO consists of a tunable laser source (TLS), two PMs, a single mode fiber (SMF) connecting the two PMs, an optical circulator (OC), a PS-FBG, a PD, a microwave power amplifier (PA), and a microwave power divider (Div). A light wave from the TLS is sent to the two cascaded PMs (PM1 and PM2) connected by the SMF. The phase-modulated light wave is sent to the PS-FBG via the OC, reflected by the PS-FBG and sent to the PD via again the OC. The signals at the output of PM2 and at the input of the PD are monitored by two optical spectrum analyzers (OSAs). After electrical amplification by the PA, the signal at the output of the PD is split into two parts by the power divider, and applied to the two PMs via the RF ports. The signal at the output of the PD is also monitored by an electrical spectrum analyzer (ESA, Agilent E4448A).

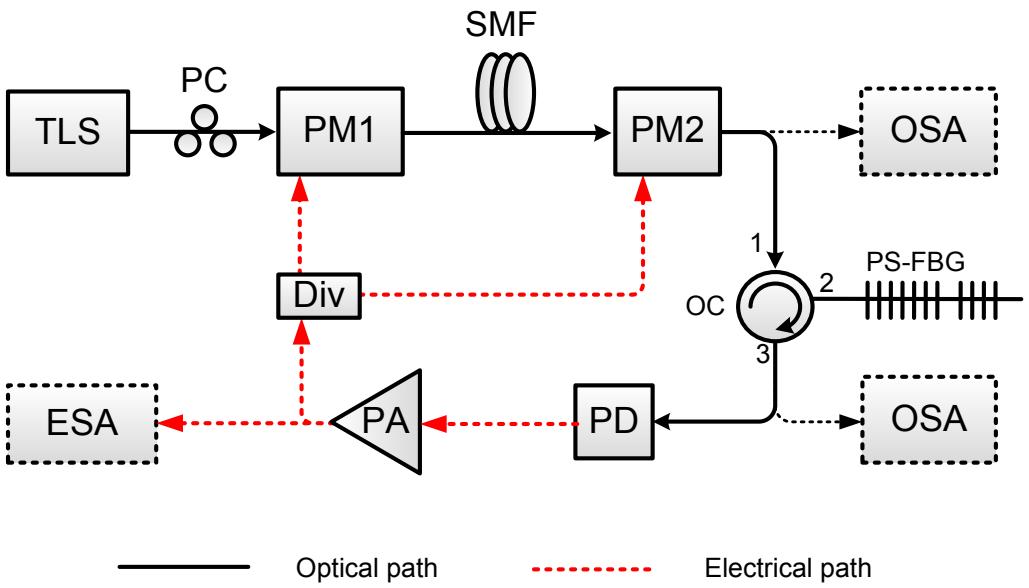

Fig. 6.1 Schematic of the proposed wideband frequency-tunable OEO.

To understand the operation and the frequency tuning of the OEO, we start our discussion from the equivalent wideband frequency-tunable microwave photonic bandpass filter that is

incorporated in the OEO loop. Based on the analysis in Chapter 5, the schematic of the equivalent microwave photonic bandpass filter in the proposed OEO is shown in Fig. 6.2. Its frequency response can be measured by a vector network analyzer (VNA). The VNA generates a microwave signal with its frequency sweeping over a frequency range of interest, and the received microwave signal at the output of the PD is sent back to the VNA.

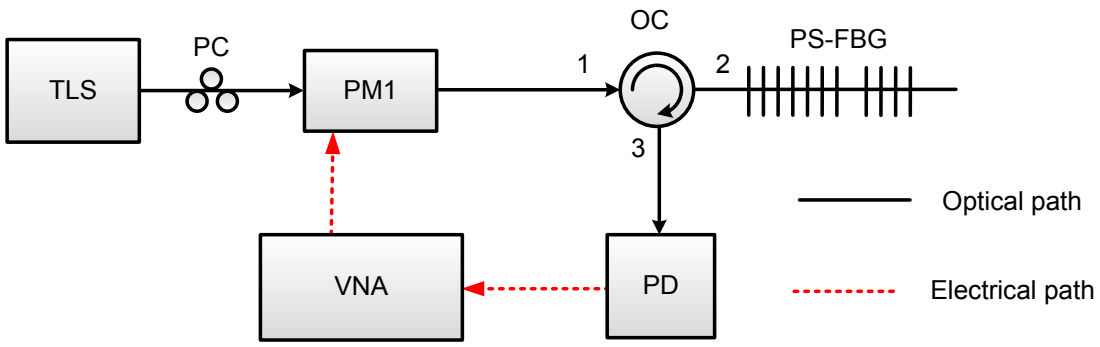

Fig. 6.2 Schematic of the equivalent wideband frequency-tunable microwave photonic bandpass filter in the proposed OEO.

From Chapter 5, we know that the output of PM1 contains an optical carrier and two first-order sidebands. If the light wave is directly applied to the PD, no signal would be detected except a dc since the beating between the optical carrier and the upper sideband will cancel completely the beating between the optical carrier and the lower sideband, due to the fact that the two beat signals are out of phase. However, when the amplitude and/or the phase profile of the phase-modulated light wave in its frequency domain is modified only over a small frequency range via the PS-FBG , the phase-modulated light wave can be converted to an intensity-modulated light wave, and PM-IM conversion has a transfer function corresponding to a microwave photonic bandpass filter with a narrow bandwidth.

The ultra-narrow passband only appears when one first-order sideband falls into the notch of the PS-FBG, and the central frequency of the passband is equal to the frequency spacing between the notch and the incident light wave. Since the notch of the PS-FBG can be controlled as narrow as a few MHz, accordingly the bandwidth of the microwave photonic BPF can be as narrow as a few MHz, thus a microwave photonic bandpass filter with a high-Q factor is achieved. The tunability of the microwave photonic bandpass filter can be easily realized by simply tuning the wavelength of the light wave from the TLS. Another important feature of the microwave photonic bandpass filter is the large frequency tunable range. The largest tunable range is limited by the reflection bandwidth of the PS-FBG, and the bandwidth of the PM, the PD and the PA. Since the bandwidths of the commercial PDs, PAs and PMs as well as the reflection bandwidth of the commercial PS-FBG can be tens of GHz now, the frequency tuning range of the microwave photonic bandpass filter could be also as large as tens of GHz. Therefore, due to the incorporation of the microwave photonic bandpass filter in the OEO loop, a microwave signal with an oscillation frequency that is tunable over a frequency range of tens of GHz can be generated.

The bandwidth of the microwave photonic bandpass filter can be further reduced if a second PM is employed (see Fig. 6.3). The two PMs are connected by a length of the SMF. If PM2 is connected to PM1 through the SMF, then the phase-modulated light wave is given by

$$
\begin{aligned}
E_{\mathrm{PM2}}(t) &= E_0 \exp\left\{ j\left[\omega_{\mathrm{o}} t + \pi \frac{V_{\mathrm{e}}}{V_\pi} \cos(\Omega t) + \pi \frac{V_{\mathrm{e}}}{V_\pi} \cos\left[\Omega(t+\tau)\right] \right] \right\} \\
&= E_0 \exp\left\{ j\left[\omega_{\mathrm{o}} t + \beta'(\Omega) \cdot \cos\left[\Omega t + \Omega\tau/2\right] \right] \right\} \\
&\approx E_0 \left\{ J_0\left[\beta'(\Omega)\right] \exp(j\omega_{\mathrm{o}} t) \right. \\
&\quad + J_1\left[\beta'(\Omega)\right] \exp\left[j(\omega_{\mathrm{o}} t + \Omega t + \Omega\tau/2 + \pi/2) \right] \\
&\quad \left. - J_1\left[\beta'(\Omega)\right] \exp\left[j(\omega_{\mathrm{o}} t - \Omega t - \Omega\tau/2 - \pi/2) \right] \right\}
\end{aligned}
\tag{6-1}
$$

where E_0 is the unit amplitude of the electrical field of the incident light wave, ω_{o} is the angular frequency of the incident light wave, V_π is the half-wave voltage of the PM, V_{e} is the amplitude and Ω is the frequency of the microwave applied to the PM, J_0 and J_1 are the 0^{th}- and 1^{st}-order Bessel functions of the first kind, $\tau = Ln_{\mathrm{o}}/c$ is the time delay introduced by the SMF, where L is the length of the SMF, c is the velocity of light in vacuum, n_{o} is the refractive index of the SMF, and $\beta'(\Omega) = 2\pi V_{\mathrm{e}} \cos(\Omega\tau/2)/V_\pi$ is an equivalent phase modulation index, which is not a constant but a sinusoidal function of Ω. Consequently, PM-IM conversion would have a transfer function that is equal to the product of the frequency response of the ultra-narrow microwave photonic bandpass and the frequency response of the sinusoidal comb filter, as shown in the zoom-in view of Fig. 6.3(b). The transmission peaks of the comb filter are located at the frequencies when $\left|\beta'(\Omega)\right| = 2\pi V_{\mathrm{e}}/V_\pi$, namely, $\Omega = 2\pi k/\tau$, where k is an integer. The distance between two adjacent peaks is $2\pi c/Ln_0$.

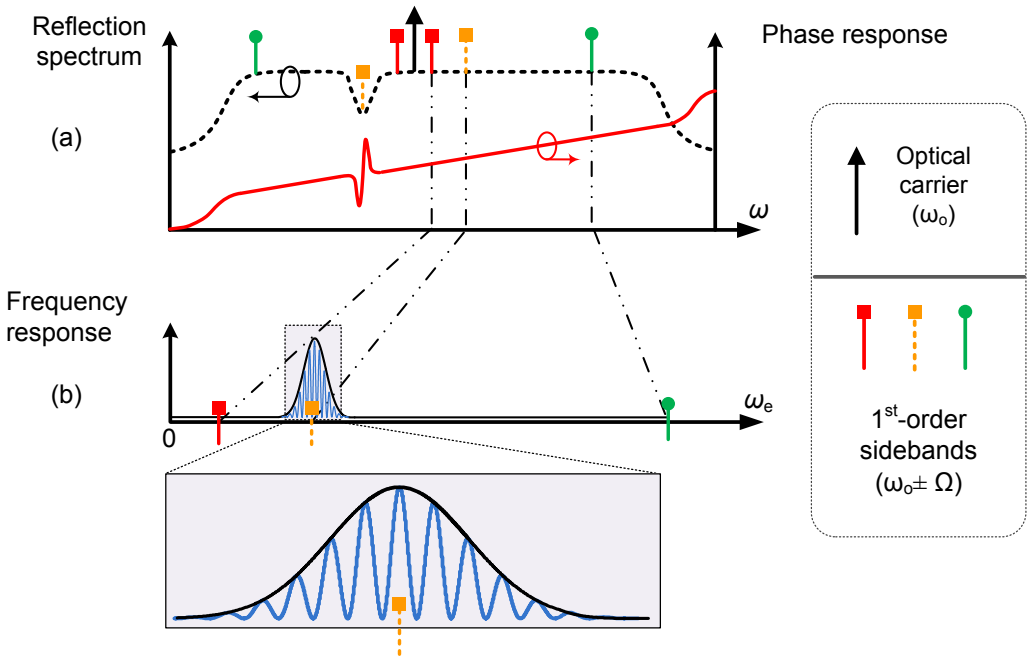

Fig. 6.3 The equivalent high-Q microwave photonic bandpass filter. (a) The reflection spectrum and phase response profile of the PS-FBG; (b) the frequency response of the photonic microwave bandpass filter.

After reflection by the PS-FBG, the electrical field $E_{\mathrm{IM}}(t)$ of the light wave at the input of the PD can be expressed as

$$\begin{aligned} E_{\mathrm{IM}}(t) \approx\ & E_0 J_0\left[\beta'(\Omega)\right]\exp\left(j\omega_{\mathrm{o}}t + j\omega_{\mathrm{o}}\tau'\right) \\ & + E_0 J_1\left[\beta'(\Omega)\right] \\ & \times\exp\left[j\left(\omega_{\mathrm{o}}t + \Omega t + \Omega\tau/2 + \pi/2 + \omega_{\mathrm{o}}\tau' + \Omega\tau'\right)\right] \\ & - E_0 r\left(\omega_{\mathrm{o}} - \Omega\right)\cdot J_1\left[\beta'(\Omega)\right] \\ & \times\exp\left[j\left(\omega_{\mathrm{o}}t - \Omega t - \Omega\tau/2 - \pi/2 + \omega_{\mathrm{o}}\tau' - \Omega\tau'\right)\right] \end{aligned} \tag{6-2}$$

where $r(\omega)$ is the reflection profile of the PS-FBG, where ω is the angular frequency of the light wave incident to the PS-FBG, $\tau' = L' n_{\mathrm{o}} / c$ is the time delay introduced by the short fiber between PM2 and the PD, where L' is the length of the short fiber. It is noticed that for

simplicity, we only consider the power reflection coefficient, and ignore the phase response of the PS-FBG in (6-2). Then, the microwave signal at the output of the PD can be expressed as

$$\begin{aligned} V(\Omega,t) &\propto \Re\left|E_{\mathrm{IM}}(t)\right|^2 \\ &= \Re\left[1-r(\omega_{\mathrm{o}}-\Omega)\right]J_0\left[\beta'(\Omega)\right]J_1\left[\beta'(\Omega)\right]\sin\left[\Omega t+\Omega\tau+\Omega\tau'\right] \\ &\approx \Re\left[1-r(\omega_{\mathrm{o}}-\Omega)\right]\pi V_{\mathrm{e}}/V_{\pi}\cos(\Omega\tau/2)\sin\left[\Omega t+\Omega\tau++\Omega\tau'\right] \end{aligned} \tag{6-3}$$

where $\Re$ is the photoresponsivity of the PD, $J_0\left[\beta'(\Omega)\right]\approx 1$ and $J_1\left[\beta'(\Omega)\right]\approx\beta'(\Omega)/2$ when $\beta'(\Omega)$ is small, say less than 0.5. Therefore, the frequency response $H(\Omega)$ can be given by

$$H(\Omega)=\frac{V(\Omega)^2}{V_{\mathrm{e}}^2}\approx\frac{\pi^2\Re^2}{V_{\pi}^2}\cdot\left[1-r(\omega_{\mathrm{o}}-\Omega)\right]^2\cdot\left[\frac{1+\cos(\Omega\tau)}{2}\right] \tag{6-4}$$

In (6-4), the term $\left[1-r(\omega_{\mathrm{o}}-\Omega)\right]^2$ represents the frequency response when only a single PM is used. The peak of the pass band appears when $r(\omega_{\mathrm{o}}-\Omega)=0$, which means that the lower sideband is completely suppressed. The other term, $[1+\cos(\Omega\tau)]/2$, is the frequency response of the comb filter.

If the gain in the loop is greater than the loss, once the loop is closed, the OEO will start to oscillate. The total output at the PD at any instant time is the summation of all circulating fields in the loop, which can be expressed as

$$\begin{aligned} V'(\Omega,t) &= \exp(j\Omega t)\times\sum_{m=0}^{\infty}\left\{\Re G(1-r)\pi V_{\mathrm{e}}/V_{\pi}\cos(\Omega\tau/2)\right\}^m \\ &\qquad\cdot\exp(jm\Omega\tau+jm\Omega\tau') \\ &= \exp(j\Omega t)\times\sum_{m=0}^{\infty}\left[G_{\mathrm{eff}}(\Omega)\right]^m\cdot\exp(jm\Omega\tau+jm\Omega\tau') \end{aligned} \tag{6-5}$$

where G is the voltage gain provided by the PA, m is the number of times the light wave circulates in the loop, and $G_{\text{eff}}(\Omega)$ is the effective open-loop gain, given by

$$G_{\text{eff}}(\Omega) = \Re G(1-r)\pi V_{\text{e}} / V_{\pi} \cos(\Omega\tau / 2) \tag{6-6}$$

After the OEO starts oscillation, the effective open-loop gain G_{eff} is little less than unity, Eq. (6-5) can then be simplified to

$$V'(\Omega, t) = \frac{\exp(j\Omega t)}{1 - G_{\text{eff}}(\Omega) \cdot \exp(j\Omega\tau + j\Omega\tau')} \tag{6-7}$$

The corresponding microwave power $P(\omega_{\text{e}}, t)$ is then given by

$$\begin{aligned} P(\Omega, t) &\propto \left|V'(\Omega, t)\right|^2 \\ &= \frac{1}{1 + G_{\text{eff}}^2(\Omega) - 2G_{\text{eff}}(\Omega) \cdot \cos(\Omega\tau + \Omega\tau')} \end{aligned} \tag{6-8}$$

Only when the two phase delays $\Omega\tau$ and $\Omega\tau'$ are multiples of 2π after each loop circulation, and $r(\omega_{\text{o}} - \Omega) = 0$, $|G_{\text{eff}}(\Omega)|$ would reach a maximum value, and the corresponding frequency will oscillate. At an oscillation frequency Ω_{osc}, Eq. (6-8) can be rewritten as

$$P(\Omega_{\text{osc}}, t) \propto \frac{1}{\left[1 - RG\pi V_{\text{e}} / V_{\pi}\right]^2} \tag{6-9}$$

Then, when the wavelength of the TLS, ω_{o}, is tuned to make $r(\omega_{\text{o}} - \Omega) = 0$, ω_{e} will automatically change to Ω' in the same direction of ω_{o}. If both $\Omega'\tau$ and $\Omega'\tau'$ are multiples of 2π, Ω' will be a new oscillation frequency, and frequency tuning is thus achieved.

6.3 Evaluation of the experimental results

An experiment based on the setup shown in Fig. 6.1 is performed (see Fig. 6.4). The TLS (Yokogawa AQ 2200-136) has a wavelength tunable range of 200 nm and a tuning step of 1 pm. The bandwidths of the PMs are 20 GHz. The PA in Fig. 6.1 consists of one Avanteck low-noise amplifier and an Agilent 83006A amplifier. The PD (Newport) has a bandwidth of 45 GHz. The PCs are used to minimize the polarization-dependent loss. The key device in the system is the PS-FBG, which is fabricated in a photosensitive fiber using a uniform phase mask by scanning an UV beam along the axial direction of the optical fiber. A phase shift can be introduced at the center of the grating by shifting the phase mask by half the corrugation width to create an ultra-narrow notch at the reflection spectrum. The PS-FBG is fabricated by introducing a phase shift during the fabrication process. An ultra-narrow transmission band in the reflection spectrum is thus generated.

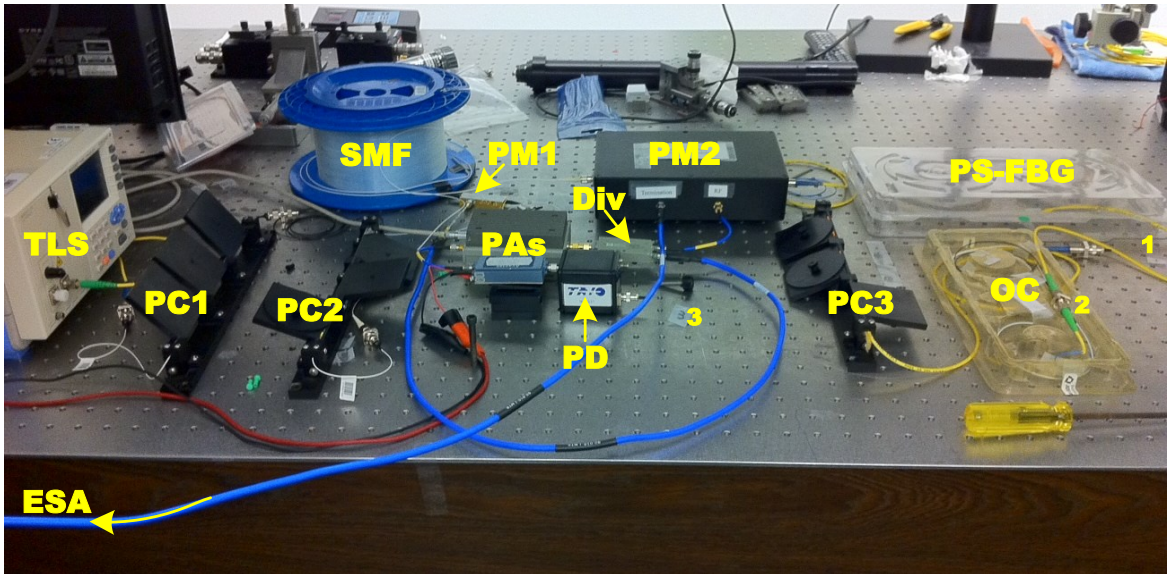

Fig. 6.4 Photograph of the experimental setup. Numbers 1, 2 and 3 in the photograph indicate port 1, port 2, and port 3 of the OC.

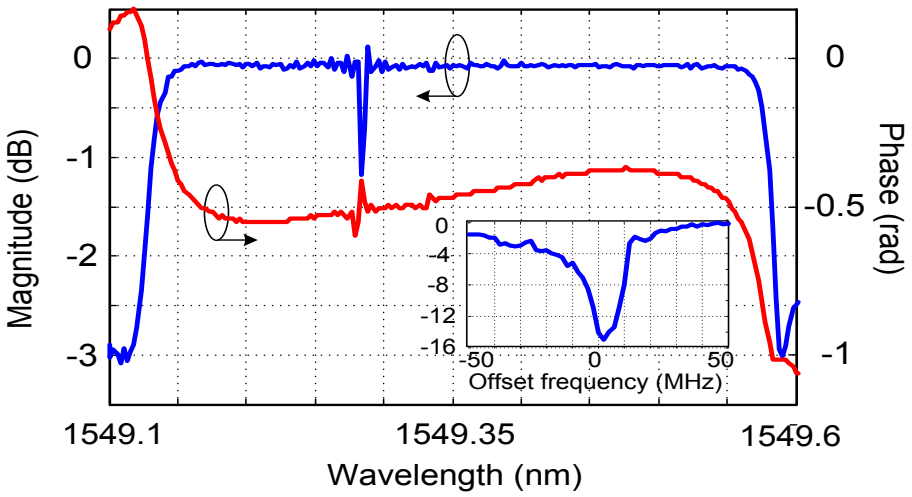

Fig. 6.5 Measured reflection magnitude response and phase response of the PS-FBG (resolution: 0.01nm). The inset gives a zoom-in view of the notch of the PS-FBG (resolution: 2 MHz).

The measured reflection magnitude response and phase response of the PS-FBG are shown in Fig. 6.5. The 3-dB reflection bandwidth is about 0.5 nm. The centre wavelength of the notch is about 1549.28 nm, with a full-width at half-maximum (FWHM) of only about 30 MHz. The maximum notch depth is more than 15 dB.

6.3.1 Frequency response of the microwave photonic filter

First of all, the frequency response of the equivalent wideband frequency-tunable photonic microwave bandpass filter based on PM-IM conversion is measured. To do so, the loop is opened at the output port of the PD, and only one PM is used. The frequency response is measured using a VNA (Agilent E8364A). The powers of the light wave sent to the PM and to the PD are measured to be about 5 dBm and 0 dBm, respectively. The wavelength of the optical carrier is set around 1549.28 nm, and the lower sideband will fall into the notch of the PS-FBG when the microwave frequency is equal to the difference between the frequency of the optical carrier and the center frequency of the notch. By increasing the wavelength of the optical carrier, the center frequency of the microwave photonic bandpass filter is increased.

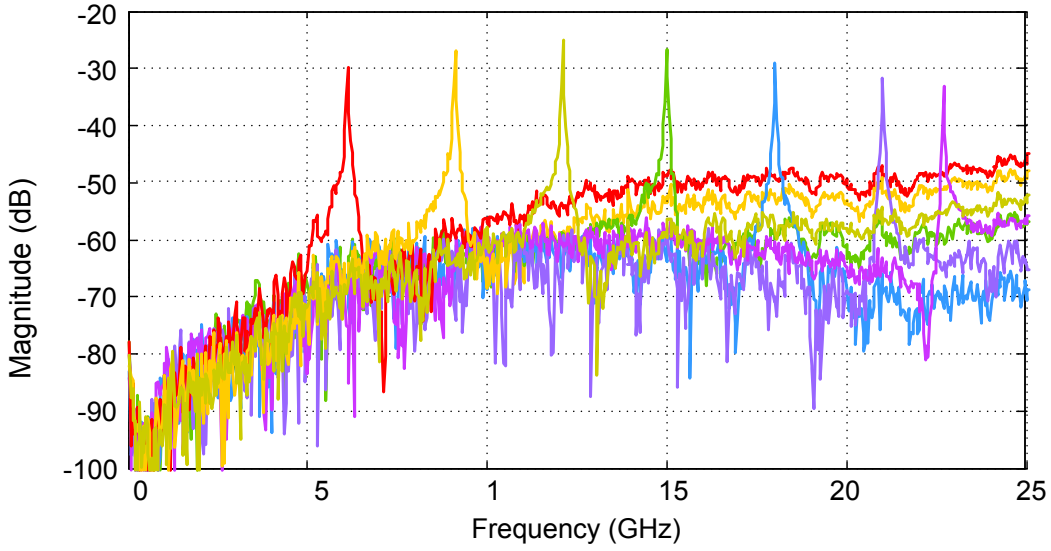

(a)

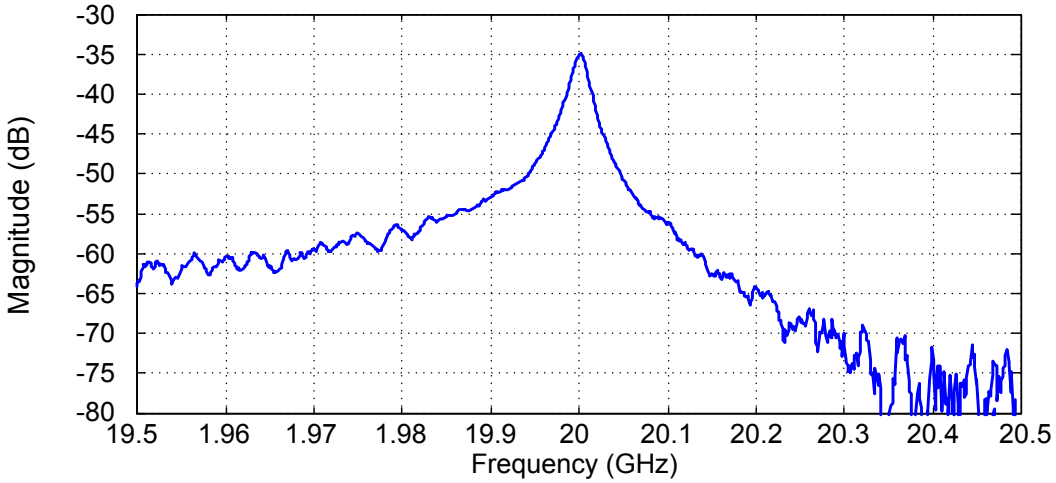

(b)

Fig. 6.6 (a) Measured frequency responses of the tunable MPF. (b) The zoom-in view of the frequency response when the center frequency is tuned at 20 GHz.

Fig. 6.6(a) shows the superimposed frequency responses of the microwave photonic bandpass filter with a tunable central frequency covering a range of about 20 GHz. This range can be increased if the reflection bandwidth of the PS-FBG is wider. From Fig. 6.6(a) we can see that the ratio of the transmission peak to the sidelobe can be as large as 30 dB, which is large enough to suppress undesired modes in the OEO. In Fig. 6.6(b), a zoom-in view of the

measured frequency response with a central frequency of 20 GHz is shown. The 3-dB bandwidth is about 20 MHz, corresponding to a Q-factor of 1000. If the index change of the grating is increased or the degree of the symmetry of the two sub-gratings separated by the phase shift section is improved, the PS-FBG would have a narrower notch and the 3-dB bandwidth of the microwave photonic filter can be further decreased.

6.3.2 Microwave generation of the wideband frequency-tunable optoelectronic oscillator

Then, when we close the OEO loop, single mode microwave generation can be obtained. The length of the SMF is about 500 m, corresponding to a time delay τ of about 2.43 μs. The length between PM2 and the power divider is about 10 m, corresponding to a time delay τ' of about 48.6 nm. The wavelength of the light wave is first set at 1549.36 nm, which is about 0.08 nm away from the central wavelength of the transmission band; thus Ω would be approximately equal to 10 GHz. By finely tuning the wavelength of the light wave and the delay to make $\Omega\tau$ and $\Omega\tau'$ are multiples of 2π, the OEO will start oscillation at 10 GHz. At the oscillation frequency, the phase modulation indices of PM1 and PM2 are about 0.25, giving an equivalent phase modulation index, $\beta'(\Omega_{osc})$ of 0.5.

Fig. 6.7 shows the measured optical spectrum at the outputs of PM2 and the PS-FBG. As expected, after reflection from the PS-FBG the power of the lower sideband of the phase-modulated light wave is attenuated, which is 10 dB lower than that of the upper sideband. Although the lower sideband is not completely removed, the residual power is very small, and an effective phase-modulation to intensity-modulation conversion is achieved. Fig. 6.8 shows

the spectrum of the generated 10-GHz signal with two different frequency spans of 25 GHz and 200 KHz. No other modes are observed.

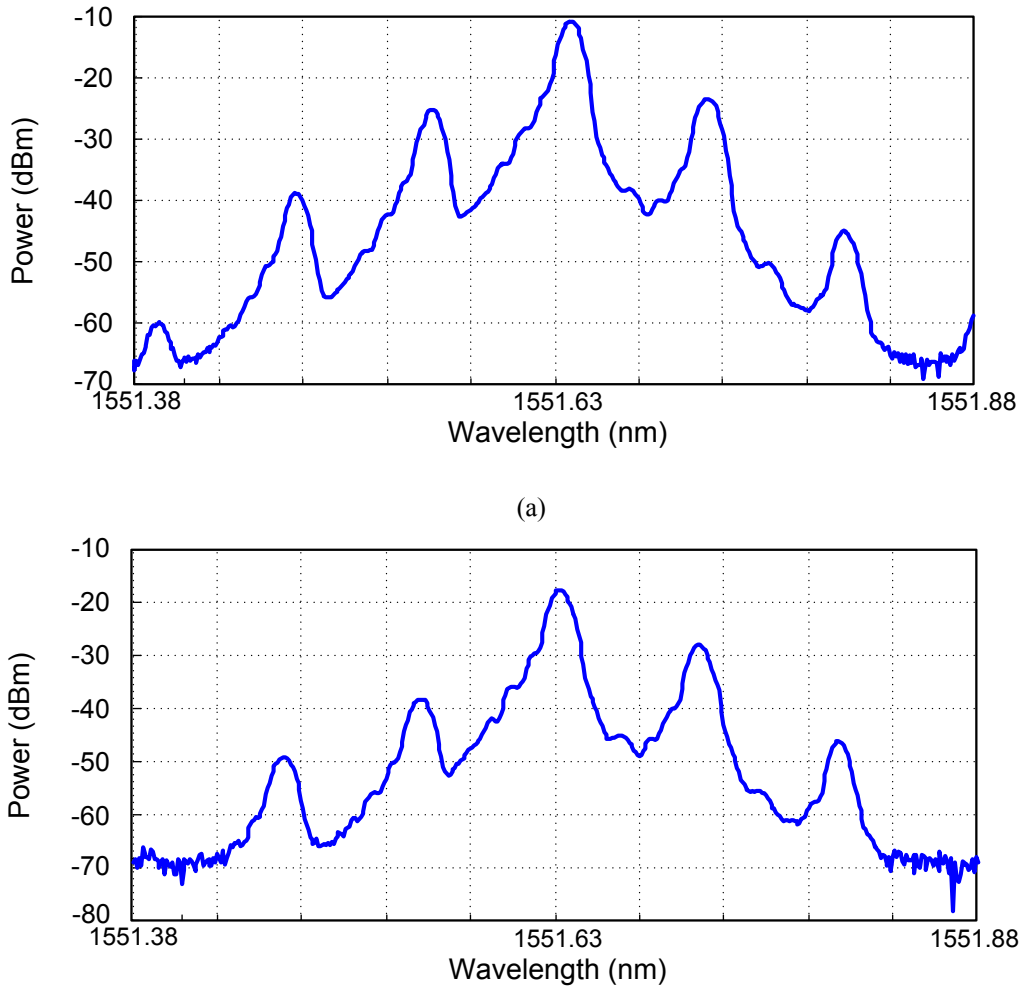

Fig. 6.7 (a) Optical spectrum at the output of PM2 when the OEO is operated at 10 GHz. (b) Optical spectrum at the output of the PS-FBG when the OEO is operated at 10 GHz.

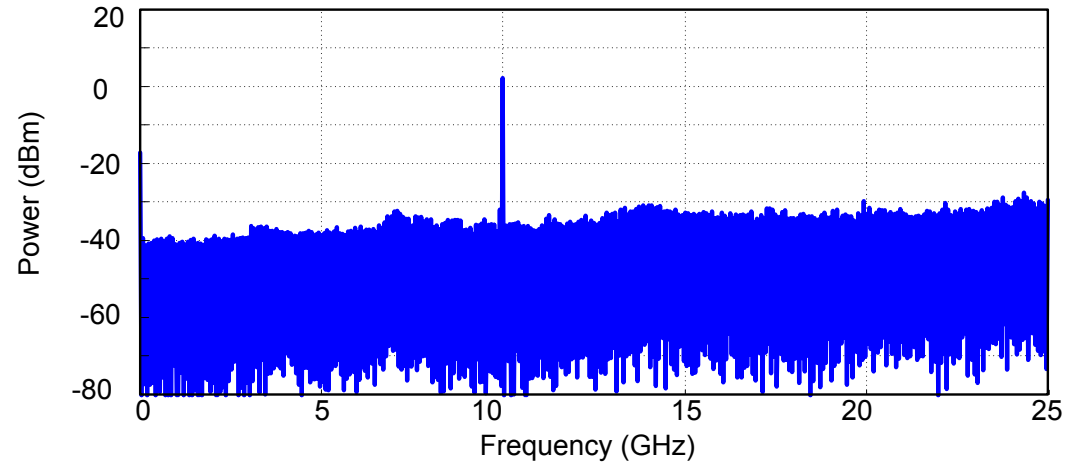

(a)

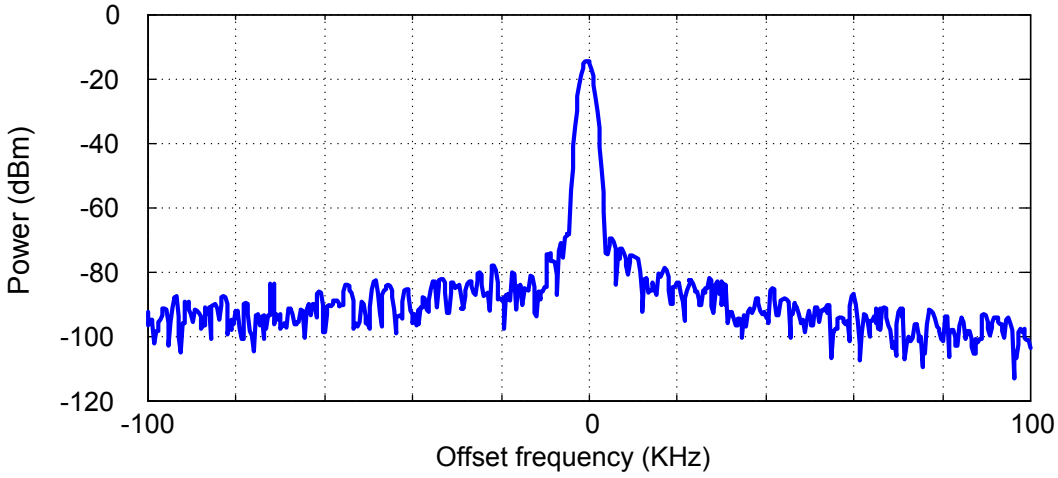

(b)

Fig. 6.8 Generation of a 10-GHz microwave signal using the proposed OEO. (a) Electrical spectrum of the generated 10-GHz signal (the frequency span is 30 GHz and the resolution bandwidth (RBW) is 3 MHz). (b) The zoom-in view of the 10-GHz signal (the frequency span is 200 KHz and the RBW is 1.8 KHz).

The stability of the system is evaluated. To do so, the system is allowed to operate in a room environment for a period of 10 min. The spectrum of the 10-GHz signal is shown on the ESA with negligible power fluctuations. The frequency stability is also evaluated. Due to the wavelength drift of the TLS and the spectrum drift of the unpackaged PS-FBG, a frequency shift of a few MHz is observed after an hour. The use of a wavelength-stabilized laser source and a packaged PS-FBG would increase significantly the frequency stability.

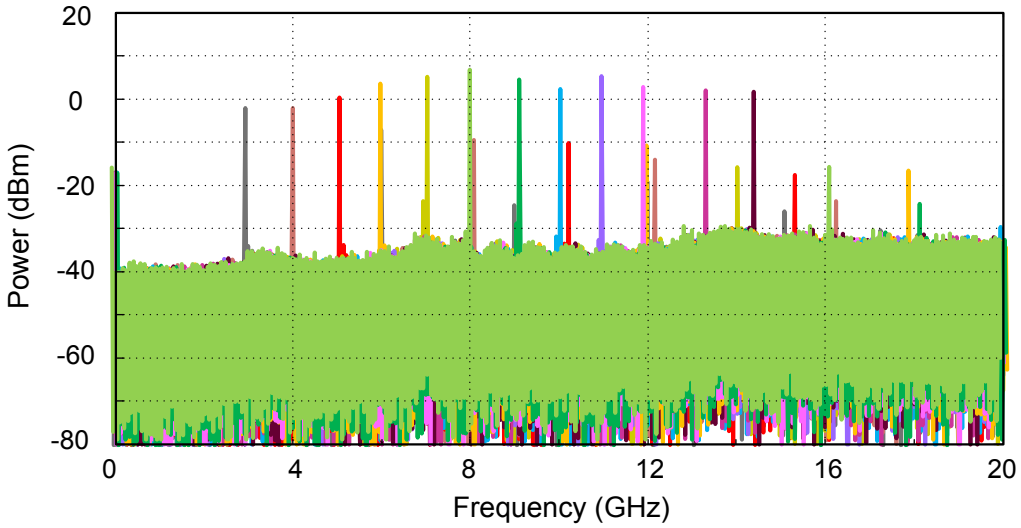
20
0
-20
-40
-60
-80
Power (dBm)
0
4
8
12
16
20
Frequency (GHz)

(a)

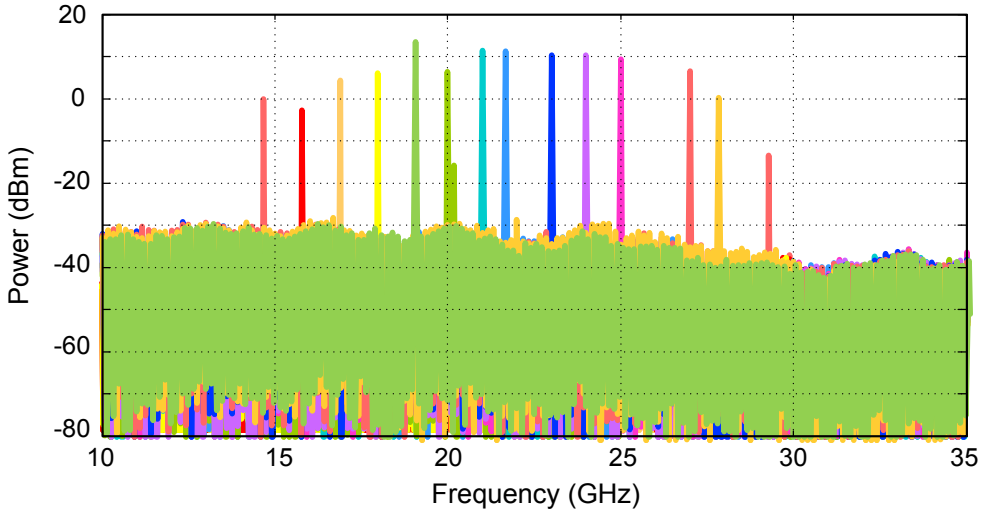
20
0
-20
-40
-60
-80
Power (dBm)
10
15
20
25
30
35
Frequency (GHz)

(b)

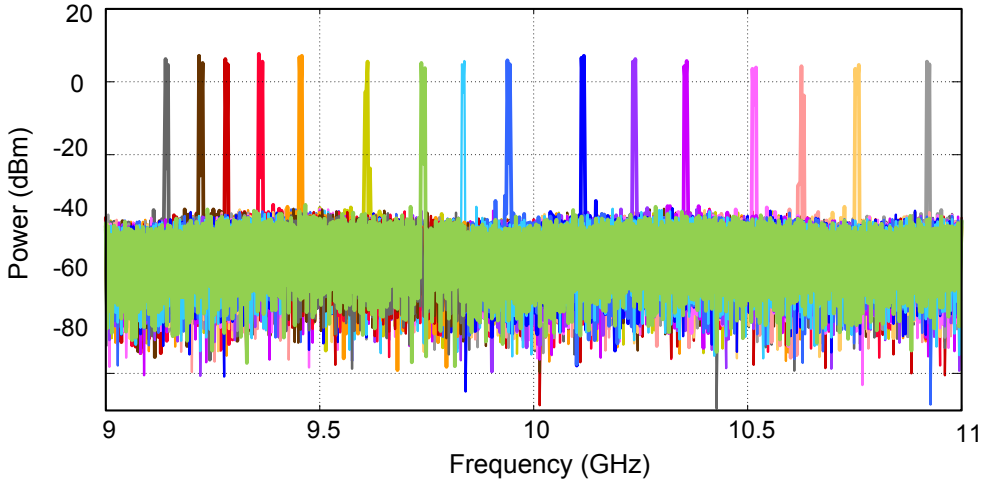
20
0
-20
-40
-60
-80
Power (dBm)
9
9.5
10
10.5
11
Frequency (GHz)

(c)

Fig. 6.9 Spectra of the generated microwave signal at different frequencies. (a) The frequency is coarsely tuned from 3 GHz to 14 GHz with a tuning step of 1 GHz; the RBW is 10 MHz. (b) The frequency is coarsely tuned from 15 GHz to 28 GHz with a tuning step of 1 GHz; the RBW is 3 MHz. (c) The frequency is finely tuned from 9.2 GHz to 10.8 GHz with a tuning step of about 125 MHz; the RBW is 3 MHz.

The frequency tunability of the proposed OEO is then investigated. Both coarse tuning and fine tuning are demonstrated. The tuning is realized by tuning the wavelength of the TLS. The smallest wavelength tuning step of the TLS is 1 pm, corresponding to a frequency tuning step of about 125 MHz. Fig. 6.9(a) shows the superimposed spectra of the generated microwave signal with the frequency coarsely tuned over a frequency range from 3 GHz to 14 GHz with a tuning step of 1 GHz. Fig. 6.9(b) shows the superimposed spectra of the generated microwave signal with the frequency coarsely tuned over a frequency range from 15 GHz to 28 GHz with a tuning step of 1 GHz. Thus, the total frequency tuning range of the proposed OEO is about 25 GHz. Fig. 6.9(c) shows the superimposed spectra with the frequency finely tuned from about 9.2 GHz to about 10.7 GHz with a tuning step of about 125 MHz. The tuning step can be smaller, but it is limited here by the wavelength tuning resolution of the TLS, which is 1 pm.

The main factor limiting the tunable range of the OEO is the limited reflection bandwidth of the PS-FBG. It is known that a wider reflection bandwidth can be achieved if the amplitude of the induced refractive index perturbation Δn is larger [212]. To achieve a large Δn, the fiber could be hydrogen loaded and the grating could be written by using IR femtosecond pulses [213], which potentially give a reflection bandwidth as large as a few nanometers. For example, if the reflection bandwidth of the PS-FBG is 2.4 nm, then the frequency tunable range of the microwave photonic filter can be 100 GHz, which also gives a frequency tunable range of the OEO of 100 GHz. If the PS-FBG is fabricated in a silicon-on-insulator waveguide by using deep-ultraviolet lithography, a wider reflection bandwidth as large as 10 nm can be

achieved [214]. Such a wide reflection bandwidth is capable of giving a tunable range of the OEO as large as hundreds of GHz.

The phase noise performance of the generated microwave signals is also studied. The analysis is done by modifying the phase noise power spectral density of an OEO discussed in Chapter 2. The modified equation gives a phase noise power spectral density with a better agreement with the experimental results. The phase noise power spectral density can be given by

$$S(f') = \frac{\delta}{(\delta/2\tau)^2 + (2\pi)^2 (\tau f')^2} \tag{6-10}$$

where f' is the frequency offset from the oscillation frequency, and δ is the input noise-to-signal ratio to the OEO, or the relative white noise level ρ_n in Section 2.2, given by

$$\delta = \rho_N G_A^2 / P_{\text{osc}} \tag{6-11}$$

where ρ_N is the equivalent input noise power density injected into the OEO from the input port of the PA, which has a typical value of 10^{-17} mW/Hz, P_{osc} is the power of the signal at the oscillation frequency applied to the PMs, and G_A is the voltage gain of the PA. Thus, P_{osc} / G_A^2 is the power of the oscillation frequency before the PA, which has a typical value of 10^{-4} mW. Therefore, δ has a typical value of 10^{-13}/Hz.

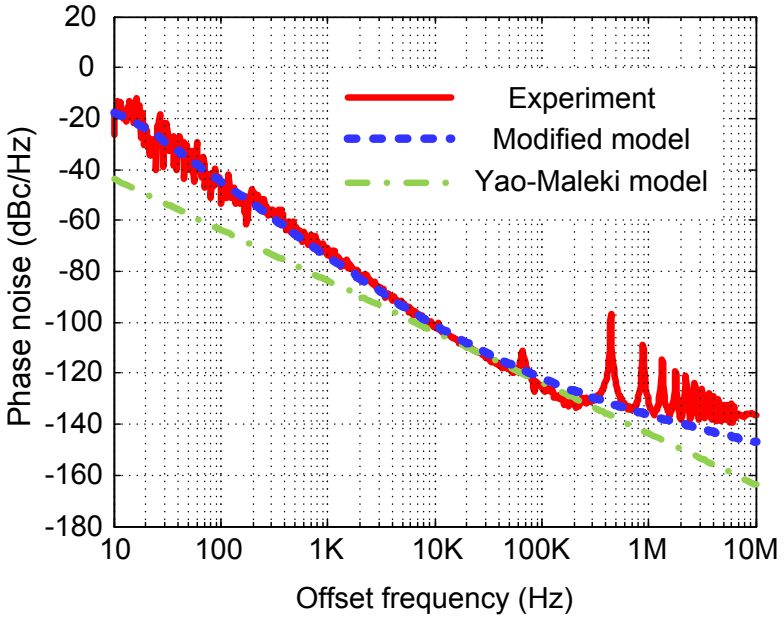

Fig. 6.10 A comparison of the phase noise based on the Yao-Maleki model, the modified model and experimental data for our proposed OEO.

Based on (6-10) and (6-11), we calculated the theoretical single-sideband phase noise spectrum of the generated microwave signal and compare it with the single-sideband phase noise spectrum of the experimentally generated 10-GHz microwave signal shown in Fig. 6.10. The single-sideband phase noise spectrum of the generated signal is measured by an Agilent E5052B signal source analyzer incorporating an Agilent E5053A downconverter. The theoretical phase noise spectrum is also shown in Fig. 10 as a dotted-dashed line. As can be seen the phase noise performance is under-estimated. The difference is due to the fact that in Chapter 2, we assume that the noise in the OEO is a strictly white noise source, and ignores other frequency-dependent noise sources which do exist in a real OEO. In our case, such frequency-dependent noise could be the relative intensity noise (RIN) of the TLS, the laser wavelength fluctuations, the length changing of the SMF, and the spectrum variations of the PS-FBG. Here in our analysis, we simply group all the frequency-dependent noise sources into two categories: the noise whose power density is inversely proportional to *f*' and the noise

whose power density is proportional to *f'* over only a small offset frequency range. Since all the noise sources are supposed to be independent, the power density of the input noise injected into the OEO can be written as

$$\rho_N' = \rho_N + \rho_{N1} / f' + \rho_{N2} \cdot f' \tag{6-12}$$

where ρ_{N1} and ρ_{N2} are two parameters of the input noise. The input noise-to-signal ratio to the OEO can also be rewritten as

$$\delta' = \rho_N' G_A^2 / P_{\text{osc}} = \delta + \delta_1 / f' + \delta_2 \cdot f' \tag{6-13}$$

where δ_1 and δ_2 are two parameters of the input noise-to-signal ratio. Thus the modified power density spectrum *S'(f')* is given by

$$\begin{aligned} S'(f') &= \frac{\delta'}{(\delta'/2\tau)^2 + (2\pi)^2 (\tau f')^2} \\ &= \frac{\delta}{(\delta'/2\tau)^2 + (2\pi)^2 (\tau f')^2} \\ &+ \frac{\delta_1 / f'}{(\delta'/2\tau)^2 + (2\pi)^2 (\tau f')^2} \\ &+ \frac{\delta_2 \cdot f'}{(\delta'/2\tau)^2 + (2\pi)^2 (\tau f')^2} \end{aligned} \tag{6-14}$$

To fit our experimental data, δ_1 and δ_2 are selected to be 8×10^{-9} and $4.5 \times 10^{-18}/\text{Hz}^2$. The calculated phase noise spectrum based on the modified model is shown in Fig. 6.10 as a dashed line.

From Fig. 6.10, we can also see that the measured phase noise is -102 dBc/Hz at a 10-KHz offset frequency. The peaks after 400-KHz offset frequency which have a frequency spacing

corresponding to a free spectral range of the OEO are resulted from the non-oscillating sidemodes. Another peak at 66-KHz is associated with an uncertain perturbation, and disappears from time to time. The phase noise performance can be further improved by using a wavelength-stabilized TLS and a packaged PS-FBG.

6.4 Conclusion

A novel approach to implementing a wideband frequency-tunable OEO using a PS-FBG was proposed and experimentally demonstrated. Due to the phase-modulation to intensity-modulation conversion in the PS-FBG, an equivalent high-Q tunable microwave photonic BPF in the OEO loop was established, which was employed to select one of the eigenmodes in the OEO, to achieve single-frequency oscillation. The central frequency of the equivalent microwave photonic bandpass filter could be easily tuned by tuning the wavelength of the TLS, thus leading to the tuning of the frequency of the generated microwave signal. The key significance of the proposed OEO is that it can provide large frequency tunability by simply tuning the optical wavelength. In addition, since no bias control is needed for the PMs, the operation stability is also better than using an MZM. The proposed OEO was verified by an experiment. The generation of a microwave signal with a frequency tunable from 3 GHz to 28 GHz was demonstrated. The generated microwave signal exhibited a good phase noise performance. A modified model was also developed to describe the phase noise performance of the proposed OEO. The phase noise performance of the proposed OEO can be further improved if a packaged PS-FBG and a wavelength-stabilized laser source are employed. The PMs and PS-FBG could be potentially integrated in a photonic integrated circuit (PIC) chip, which would significantly improve the overall performance of the proposed OEO.

CHAPTER 7 OPTICALLY TUNABLE FREQUENCY-MULTIPLYING OPTOELECTRONIC OSCILLATOR

An optically tunable frequency-multiplying optoelectronic oscillator (OEO) by combing the techniques of external modulation and the frequency-tunable OEO incorporating a tunable microwave photonic bandpass filter is proposed and experimentally demonstrated. The microwave photonic filter is implemented employing a phase-shifted fiber Bragg grating (PS-FBG), a polarization modulator (PolM) and a phase modulator (PM). The frequency tuning is realized by changing the wavelength of the light wave to the OEO loop. Frequency-doubling and quadrupling operations with large frequency tunability are experimentally demonstrated. The phase noise performance of the generated microwave signals is also investigated.

7.1 Tunable frequency-multiplying optoelectronic oscillator

From the discussion in Section 1.2.5, we know that microwave signal generation using an optoelectronic oscillator (OEO) has been considered a promising solution, and the two major limitations of a conventional OEO are that the frequency tunability is small and the frequency of the generated microwave signal is low. To solve these problems, many solutions have been proposed to either increase the frequency-tunable range by employing various microwave photonic filter or increase the frequency of the generated microwave signal by frequency doubling. However, no methods have been proposed to solve both problems simultaneously.

In this chapter, we proposed a new technique to simultaneously realize high frequency generation and wideband frequency tuning based on a tunable and frequency-multiplying OEO. In the proposed OEO, a tunable microwave photonic bandpass filter implemented based on phase-modulation to intensity modulation (PM-IM) conversion using a PolM, a phase modulator (PM), and a PS-FBG is incorporated in the OEO. The frequency tuning is simply done by tuning the wavelength of the light wave to the OEO. The frequency multiplying operation is achieved by taping part of the output from the PolM and sent it to an optical polarization analyzer (PolA). The joint operation of the PolM and the PolA corresponds to an intensity modulator (IM). Depending on the biasing point at the quadrature, the MITP or the MATP, the OEO will generate a fundamental, a frequency-doubled or a frequency-quadrupled microwave signal. An experiment is performed. A frequency-doubled microwave signal with a frequency tunable from 16 GHz to 28 GHz and a frequency-quadrupled signal with a frequency tunable from 30 to 42 GHz are generated. To the best of our knowledge, this is the widest frequency tunable range ever achieved. The phase noise performance of the OEO is also studied.

7.2 Principle of the tunable frequency-multiplying OEO

The schematic of the proposed optically tunable frequency-multiplying OEO is shown in Fig. 7.1. A light wave from a tunable laser source (TLS) is sent to a PolM via a polarization controller (PC1) which makes the polarization direction of the incident light wave have an angle of 45^{o} with respect to a principal axis of the PolM. The PolM is a special PM that supports both the transverse-electric and transverse-magnetic modes with opposite phase modulation indices. The light wave at the output of the PolM is then split into two paths:

1) One is sent to the PM through a polarization controller (PC3) and a length of SMF. Since one polarization axis of the PolM is aligned with the polarization axis of the PM by adjusting PC3, the PolM also functions as a PM that supports only one polarization direction. The phase-modulated light wave from the PM is then routed to a PS-FBG via an optical circulator (OC). The PS-FBG has an ultra-narrow notch in the reflection spectrum, which will remove one sideband of the phase-modulated light wave. The reflected light wave from the PS-FBG is detected by a photodetector (PD1), which leads to the implementation of a high-Q frequency-tunable microwave photonic bandpass filter due to PM-IM conversion as discussed in Chapter 5 and 6. The signal at the output of PD1 is amplified by a RF PA and applied to the PolM and the PM via a power divider (Div) to form a frequency-tunable OEO which would generate a fundamental frequency. Since the central frequency of the microwave photonic bandpass filter can be tuned by tuning the wavelength of the TLS, the frequency of the generated fundamental signal can also be tuned.

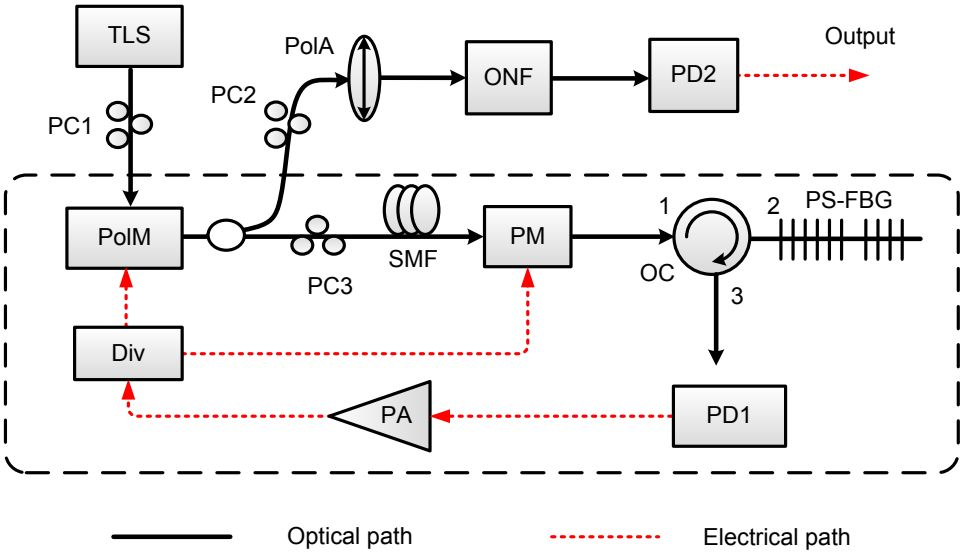

Fig. 7.1 The schematic of the optically tunable frequency-multiplying OEO.

2) The other is sent to a PolA followed by an optical notch filter (ONF) through a second PC (PC2) for achieving frequency multiplying.

If the principal axis of the PolA is oriented with an angle of 0˚ or 90˚ to the same principle axis of the PolM, the PolM functions in junction with the PolA as a PM. By using the ONF to remove the optical carrier of the phase-modulated light wave and beating the two first-order sidebands at PD2, a frequency-doubled microwave is generated.

If the principal axis of the PolA is oriented with an angle of 45˚ to the same principle axis of the PolM, the PolM functions in junction with the PolA as an IM. By adjusting a static phase introduced by PC2, the PolM-based IM can be biased to operate at the quadrature point, the minimum transmission point (MITP) or the maximum transmission point (MATP). When biased at the quadrature point, two first-order sidebands with the optical carrier are generated. By applying the optical signal at PD2, a microwave signal at the fundamental frequency is generated. When biased at the MITP, only two first-order sidebands are generated. By beating the two sidebands at PD2, a frequency-doubled microwave signal is generated. When biased at the MATP, two second-order sidebands with the optical carrier are generated. By using the ONF to remove the optical carrier and beating the two second-order sidebands at PD2, a frequency-quadrupled microwave is generated. The frequency of the frequency-multiplied signal can also be tuned by tuning the wavelength of the incident light wave with the tuning step determined by the wavelength tuning step of the TLS.

7.3 Performance evaluation of the tunable frequency multiplying

To evaluate the generation of the microwave frequency multiplication of the proposed OEO, an experiment based on the setup shown in Fig. 7.1 is performed. The length of the single mode fiber (SMF) is about 500 m, the length between the PM and the power divider is about 10 m. The reflection response of the PS-FBG and the frequency response of the microwave photonic bandpass filter are measured and shown in Fig. 7.2. To measure the frequency response, the loop is opened at the output port of PD1, and only the PM is used. The 3-dB bandwidth of the microwave photonic bandpass filter is about 40 MHz. It was shown in Chapter 6 that the use of two cascaded PMs would further decrease the bandwidth of the microwave photonic bandpass filter. By tuning the wavelength of the optical carrier, the center frequency of the microwave photonic bandpass filter is accordingly tuned.

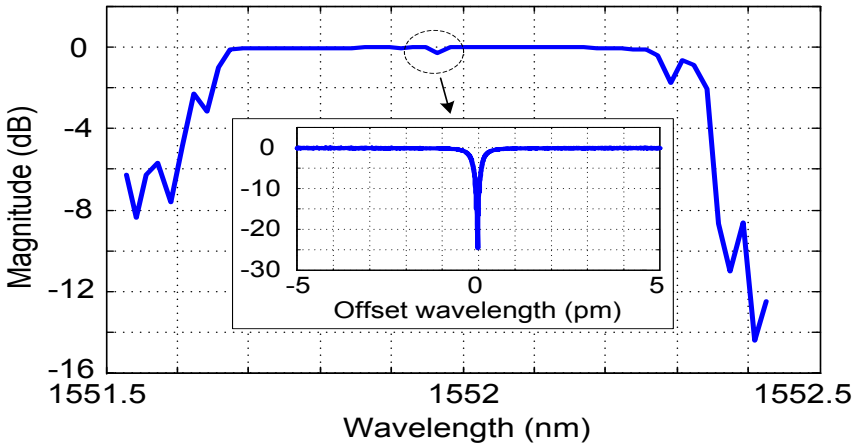

Fig. 7.2 Measured reflection magnitude response of the PS-FBG used in the proposed OEO. The inset is the zoom-in view of the notch with a high resolution.

7.3.1 Tunable microwave photonic bandpass filter

The frequency response of the equivalent wideband frequency-tunable microwave photonic bandpass filter based on PM-IM conversion is measured. To do so, the loop is opened at the

output port of the PD1, and only the PM is used. The frequency response is measured using a vector network analyzer (Agilent E8364A). The powers of the light wave sent to the PM and to the PD are measured to be about 10 and 2 dBm, respectively. The wavelength of the optical carrier is tuned around 1551.96 nm, ensuring that one sideband will fall into the notch of the PS-FBG and the other will be reflected by the PS-FBG. By increasing the wavelength difference between the optical carrier and the notch, the center frequency of the microwave photonic bandpass filter is accordingly increased.

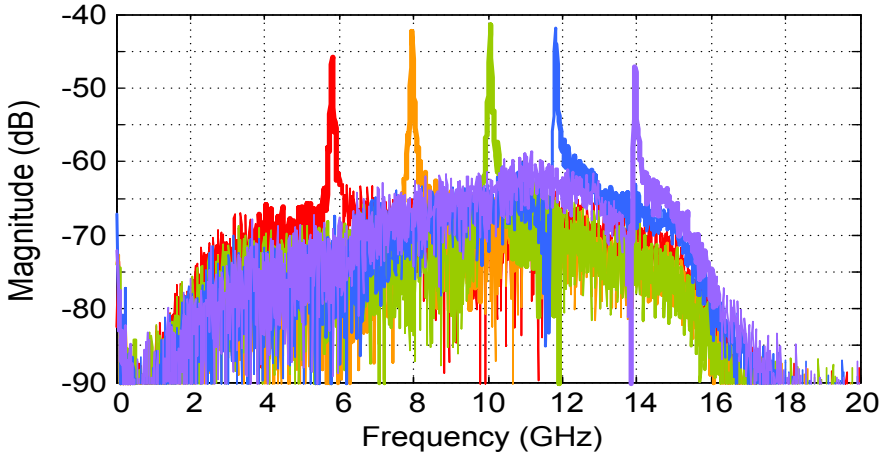

(a)

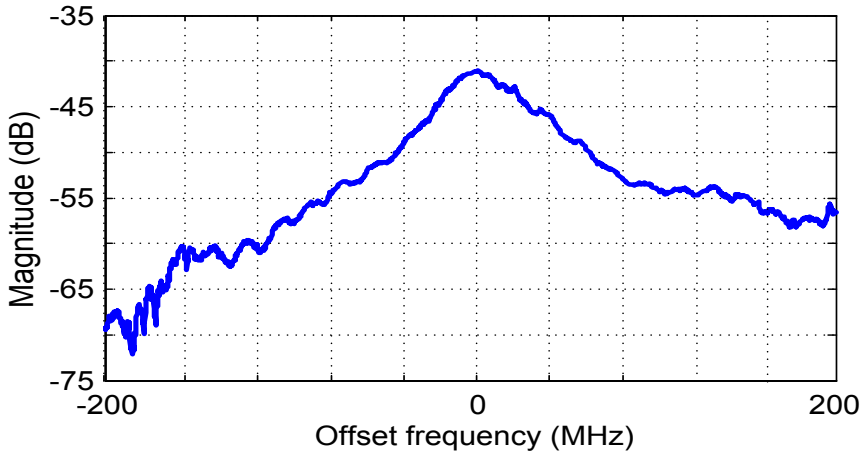

(b)

Fig. 7.3 (a) Measured frequency responses of the tunable microwave photonic bandpass filter. (b) The zoom-in view of the frequency response when the center frequency is tuned at 10 GHz.

Fig. 7.3(a) shows some superimposed frequency responses of the microwave photonic bandpass filter. From Fig. 7.3(a), we can see that the ratio of the transmission peak to the sidelobe can be as large as 15 ~ 20 dB, which is large enough to suppress undesired modes in the OEO. In Fig. 7.3(b), a zoom-in view of the measured frequency response of one photonic microwave bandpass filter with a central frequency of 10 GHz is shown. The 3-dB bandwidth is about 40 MHz. The 3-dB bandwidth can be further decreased by using a PS-FBG with a narrower notch.

7.3.2 Fundamental frequency generation

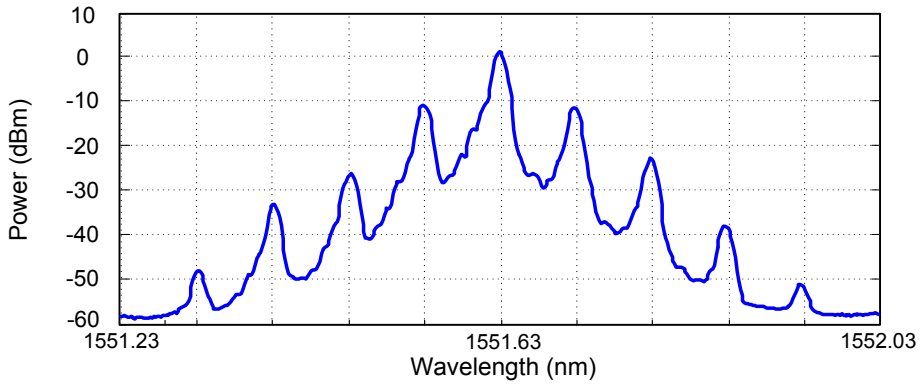

(a)

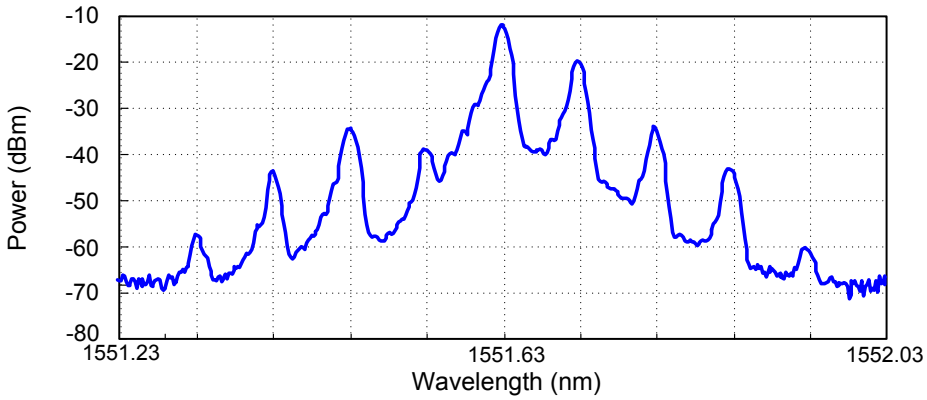

(b)

Fig. 7.4 (a) Optical spectrum at the output of PM2 when the OEO is operated at 10 GHz. (b) Optical spectrum at the output of the PS-FBG when the OEO is operated at 10 GHz.

When incorporating the microwave photonic bandpass filter in the OEO loop, a microwave signal at the fundamental frequency is generated at the output of PD1. In the experiment, the length of the SMF is about 500 meter, the length between the PM and the power divider is about 10 meters. The wavelength of the light wave is first set to be 0.08 nm away from the central wavelength of the notch of the PS-FBG; so that the oscillation frequency would be approximately equal to 10 GHz.

Fig. 7.4 shows the measured optical spectrum at the outputs of the PM and the PS-FBG after a 10-GHz signal starts oscillation in the OEO loop. As expected, after reflection of the PS-FBG, the power of one sideband of the phase-modulated light wave is 20 dB lower than that of the upper sideband. Although the higher order sideband can also be seen in Fig. 7.4, their powers are relatively low and will not affect the implementation of the microwave photonic bandpass filter and the generation of the fundamental frequency.

By tuning the wavelength of the TLS, the fundamental frequency is accordingly tuned. Fig. 7.5(a) shows the superimposed spectra of the generated microwave signal with the frequency coarsely tuned over a frequency range from 6 GHz to 14 GHz with a tuning step of 1 GHz with a frequency span of 20 GHz. The tuning step is determined by the wavelength tuning resolution of the TLS, which is 1 pm here. Fig. 7.5(b) shows the zoom-in view of the generated 10-GHz microwave signal.

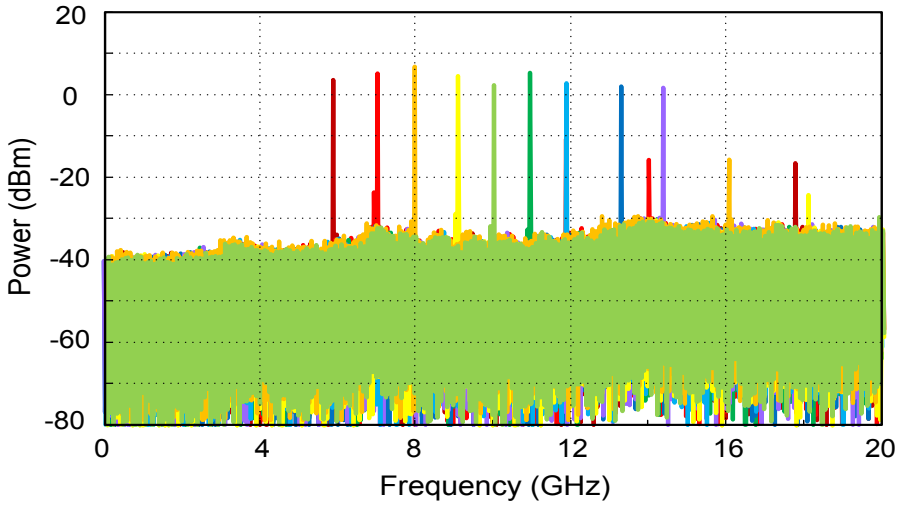

(a)

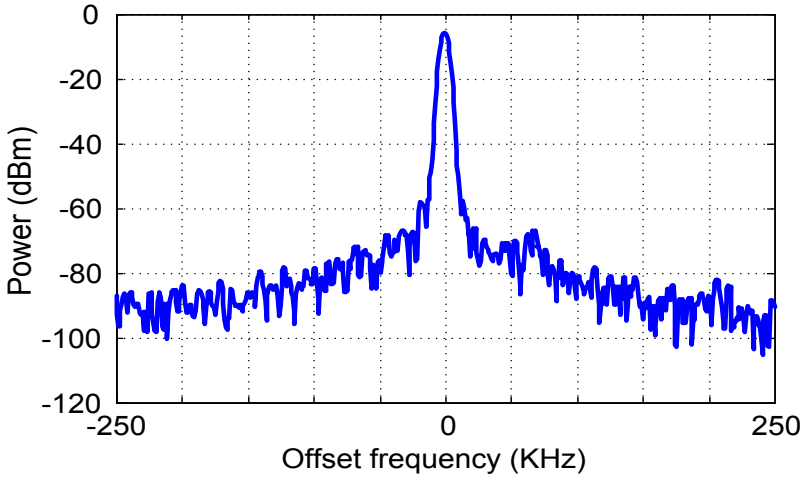

(b)

Fig. 7.5 (a) Electrical spectrum of the generated microwave signal at different fundamental frequencies with a frequency span of 20 GHz and a resolution bandwidth (RBW) of 3 MHz. (b) The zoom-in view of the 10-GHz signal with a frequency span of 500 KHz and a RBW of 4.7 KHz.

7.3.3 Frequency doubling

Once the fundamental frequency is oscillating in the OEO loop, a frequency-doubled signal can be generated at the output of PD2. Since there are two ways to enable frequency doubling, both are demonstrated here.

In the first method, the PolM functions as a PM. The optical spectrum at the output of the ONF is shown in Fig. 7.6 when the fundamental frequency is 10 GHz. From Fig. 7.6, we can see that the optical carrier from the TLS is suppressed and only two first-order sidebands become dominant.

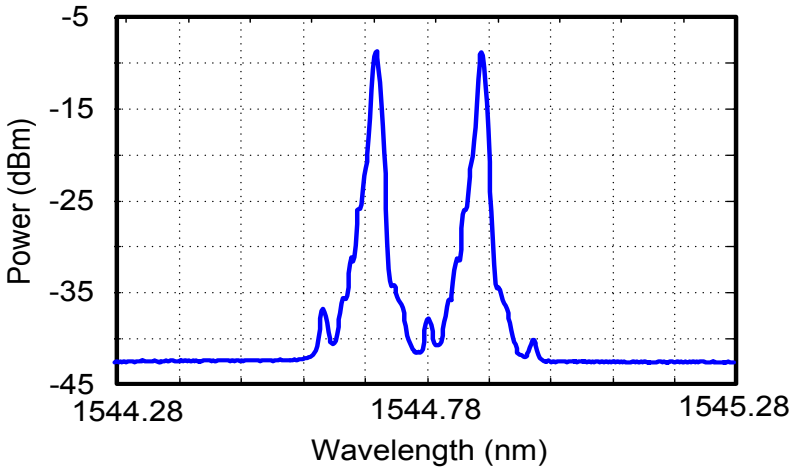

Fig. 7.6 Optical spectrum at the output of the ONF when the OEO is operated at 10 GHz and the PolM operates as a PM.

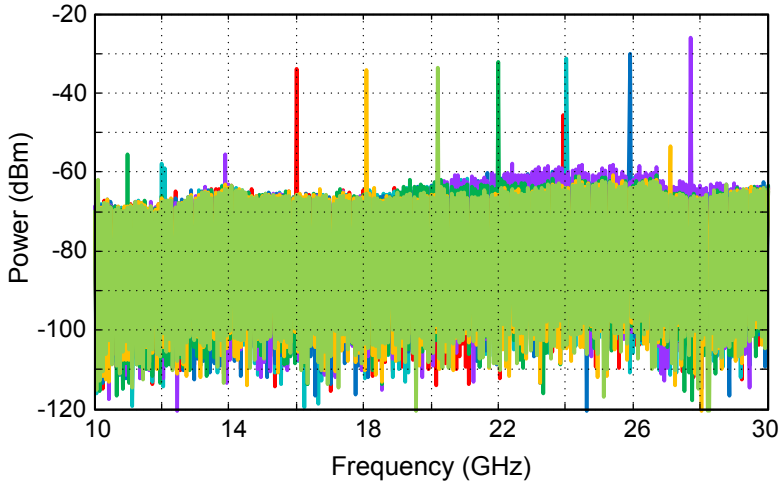

(a)

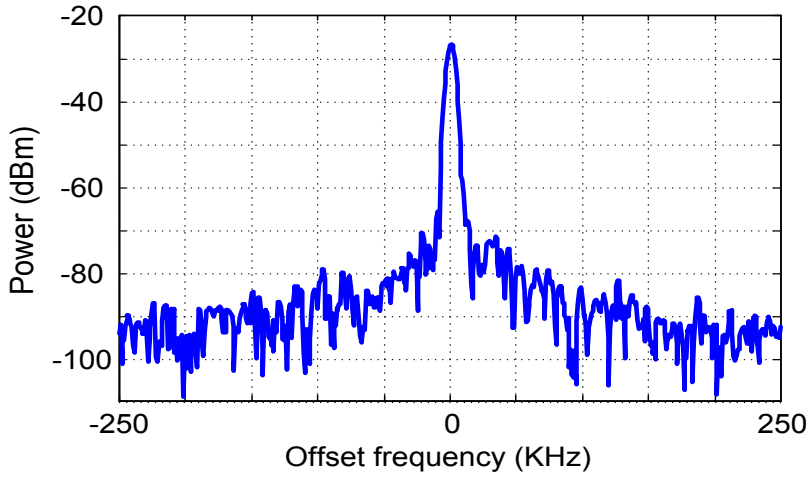

(b)

Fig. 7.7 (a) Electrical spectrum of the generated frequency-doubled microwave signal at different frequencies with a resolution bandwidth (RBW) of 3 MHz. (b) The zoom-in view of the 20-GHz signal (the frequency span is 500 KHz and the RBW is 4.7 KHz).

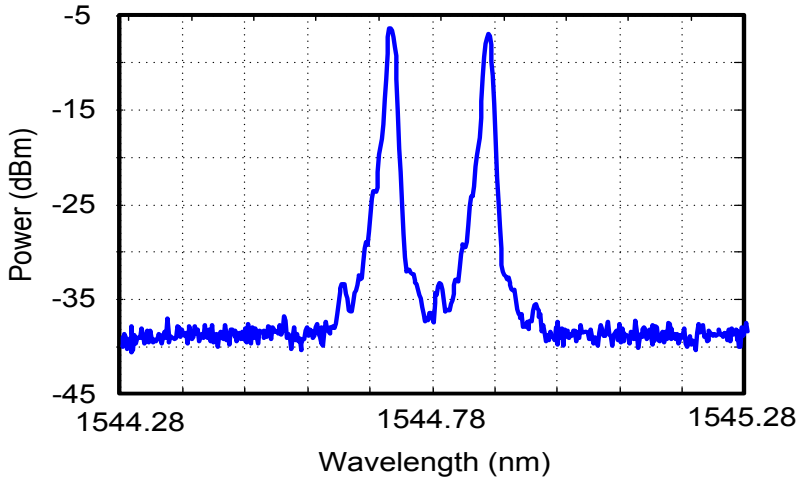

Fig. 7.8 Optical spectrum at the output of the PolA when the OEO is operated at 10 GHz and the PolM operates as an IM biased at the MITP.

By beating these two sidebands, a frequency-doubled signal at 20 GHz can be generated. The frequency can also be tuned by tuning the wavelength of the TLS. Fig. 7.7(a) shows the superimposed spectra of the generated microwave signal with the frequency tuned over a

frequency range from 16 GHz to 28 GHz with a tuning step of 2 GHz. Fig. 7.7(b) shows the zoom-in view of the 20-GHz microwave signal.

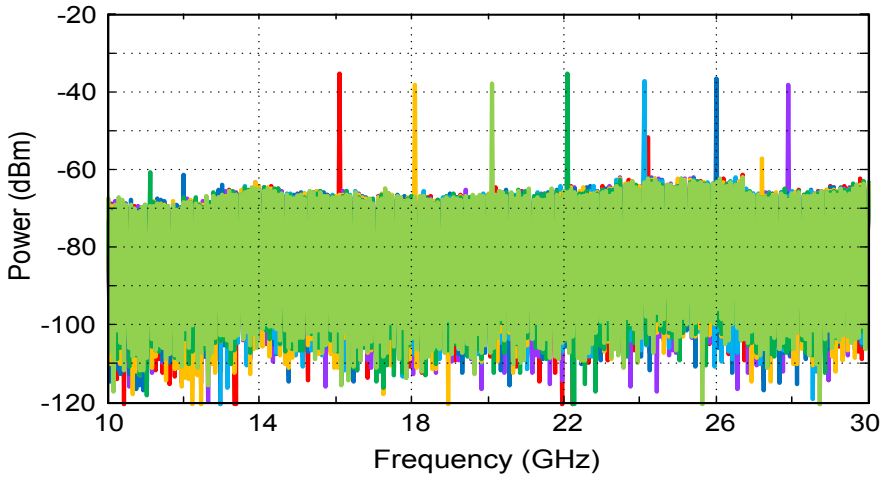

(a)

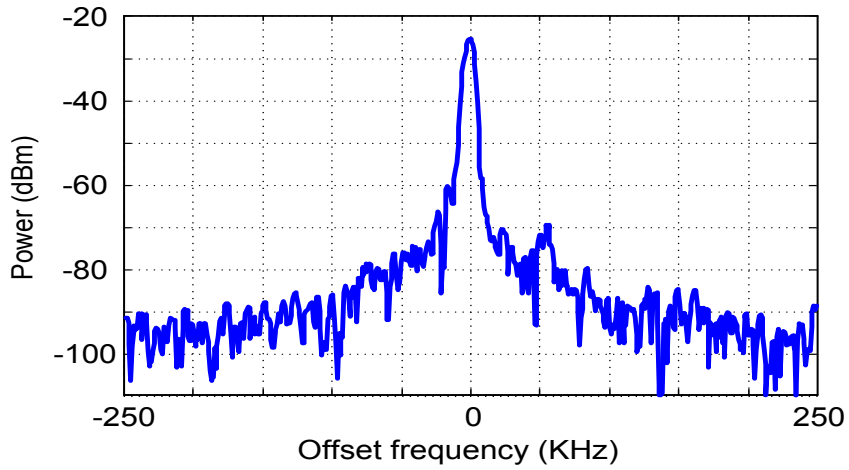

(b)

Fig. 7.9 Electrical spectrum of the generated frequency-doubled microwave signal at different frequencies with a resolution bandwidth (RBW) of 3 MHz. (b) The zoom-in view of the 20-GHz signal with a the frequency span of 500 KHz and the RBW of 4.7 KHz).

In the second method, the PolM functions as an IM biased at the MITP. Only the PolA is required. The optical spectrum at the output of the PolA is shown in Fig. 7.8 when the

fundamental frequency is 10 GHz. Similar to the spectrum shown in Fig. 7.6, there are only two dominant first-order sidebands.

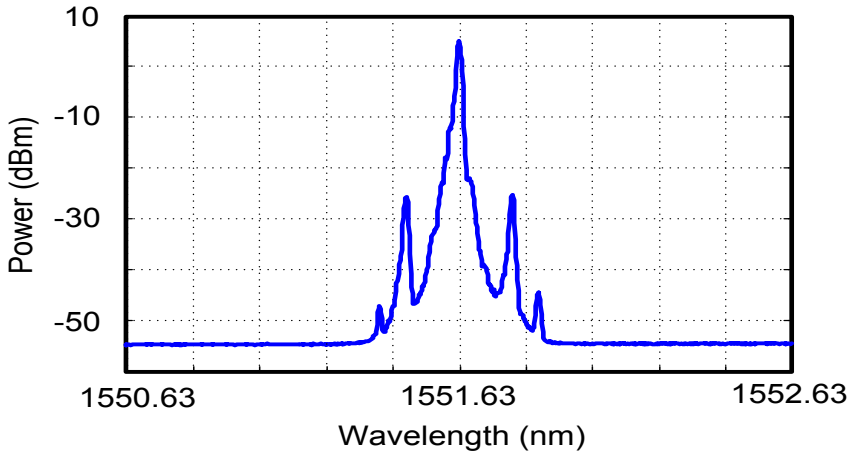

(a)

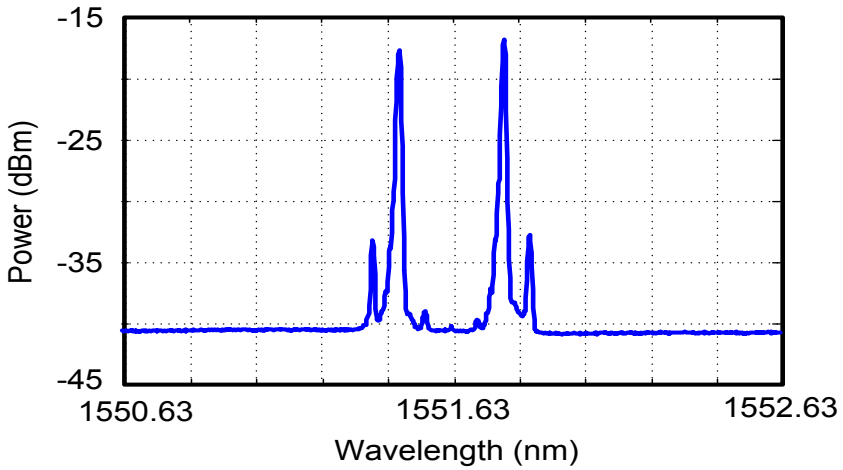

(b)

Fig. 7.10 (a) Optical spectrum at the output of the PolA. (b) Optical spectrum at the output of the ONF. The OEO is operated at 10 GHz and the PolM operates as an MZM biased at the MATP.

By beating these two sidebands, a frequency-doubled signal at 20 GHz can also be generated, whose frequency can also be tuned by simply tuning the wavelength of the TLS. Fig. 7.9(a) shows the superimposed spectra of the generated microwave signal with the frequency tuned

over a frequency range from 16 GHz to 28 GHz. And Fig. 7.9(b) also shows the zoom-in view of the 20-GHz microwave signal.

Comparing the two sets of optical and electrical spectra, we can see that the two methods for the frequency doubling are quite similar. In the first method where the PolM-based PM is used, the ONF with a large notch depth and narrow notch bandwidth is required to suppress the residual optical carrier. In the second method, no ONF is needed and the PolM-based IM is biased at the MITP by using two PCs. The bias state of the PolM-based IM is much more stable than that of a conventional IM whose bias state is controlled by an active dc power supplier. However, in order to significantly suppress the optical carrier, the extinction ration of the PolM-based IM must be very high, which is not easy to realize and maintain due to the imbalance of the power of the light waves of the two modes and the polarization fluctuations of the light wave. Therefore, combing two methods for the frequency doubling would be a promising solution to solve the problems in each one.

7.3.4 Frequency quadrupling

When the PolM-based MZM is biased at the MATP, all the odd-order sidebands can be suppressed, leading to the dominance of the optical carrier and the two second-order sidebands in the frequency domain. By using the ONF to remove the optical carrier and beating the two second-order sidebands that remain, frequency quadrupling will be realized.

The optical spectrum at the output of the PolA is shown in Fig. 7.10(a) when the fundamental frequency is 10 GHz. From Fig. 7.10(a), we can see that the first-order sidebands are suppressed while the optical carrier and the two second-order sidebands become dominant.

Fig. 7.10(b) shows the optical spectrum at the output of the ONF, from which we can see that only the two second-order sidebands remain while the optical carrier is removed.

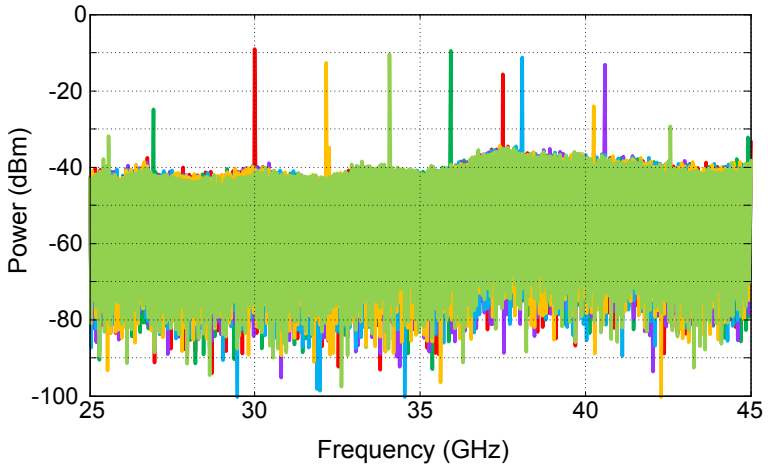

(a)

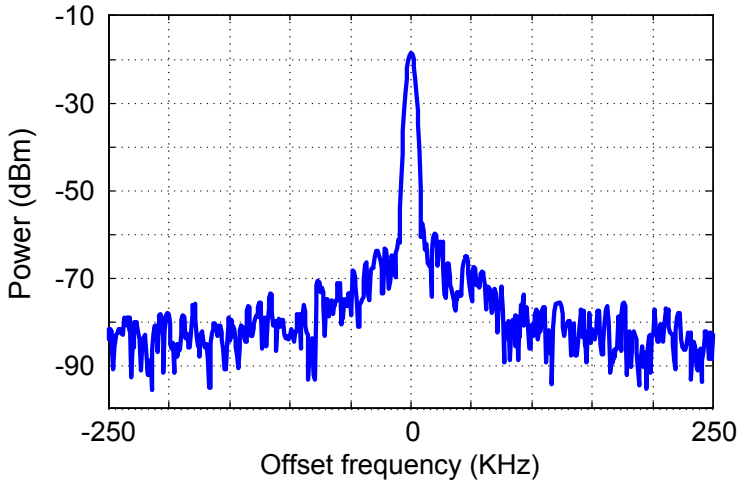

(b)

Fig. 7.11 (a) Electrical spectrum of the generated frequency-doubled microwave signal at different frequencies with a resolution bandwidth (RBW) of 3 MHz. (b) The zoom-in view of the 40-GHz signal (the frequency span is 500 KHz and the RBW is 4.7 KHz).

By beating these two sidebands, a frequency-doubled signal at 40 GHz can be generated. The frequency can also be tuned by tuning the wavelength of the TLS. Fig. 7.11(a) shows the superimposed spectra of the generated microwave signal with the frequency tuned over a

frequency range from 30 to 42 GHz with a tuning step of about 2 GHz. Fig. 7.11(b) shows the zoom-in view of the 20-GHz microwave signal with a span of 500 KHz.

In the case of frequency quadrupling, the power of the second-order sidebands is relative low; therefore, before beating them at PD2, an EDFA is required to increase the power of the two sidebands. And the frequency tuning range is mainly determined by the bandwidth of the PolM and the PM, the PD and the PA. All of these components with a 40-GHz bandwidth are commercially available now, therefore, the proposed frequency-multiplying OEO can be used to generate a microwave signal with a frequency tunable range of 160-GHz.

7.3.5 Stability and phase noise performance

The stability of the generated frequency-multiplied microwave signal greatly relies on the stability of the fundamental frequency. Therefore, the stability of the fundamental frequency is very important. To evaluate it, the system is configured to generate a 10-GHz fundamental signal and operates in a room environment for a period of 20 min. The spectrum of the 10-GHz tone is stably shown on the ESA with negligible power variations. However, due to instability of the microwave photonic BPF caused by the wavelength drifts of the TLS and the notch drifts of the unpackaged PS-FBG, a frequency shift of a few MHz, even mode hopping can be observed after hours.

The phase noise curves of the fundamental frequency and the frequency-multiplied microwave signal are also measured by an Agilent E5052B signal source analyzer incorporating an Agilent E5053A downconverter and compared in Fig. 7.12. From Fig. 7.12, we can see that the measured phase noise of the fundamental frequency is -113.4 dBc/Hz at a 100-kHz offset

frequency. The peaks after 400-KHz offset frequency and its integer multiples correspond to the sidemodes of the OEO given that the total loop length is close to 500 meters.

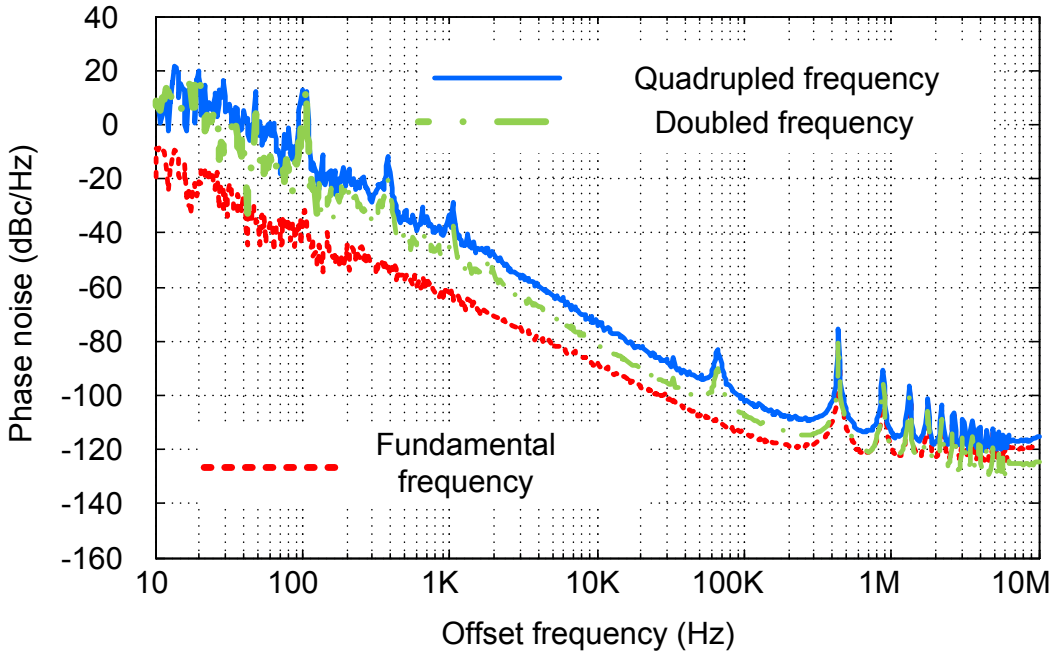

Fig. 7.12 A comparison of the phase noise curves of the fundamental frequency, doubled frequency and the quadrupled frequency.

The phase noise for the doubled and quadrupled frequency is -107.1 dBc/Hz and -101.7 dBc/Hz at a 100-kHz offset frequency, respectively. Thus, the frequency-doubled and frequency-quadrupled signals have a 6-dB and a 12-dB phase noise degradation compared with the fundamental frequency signal. Theoretically, the phase noise of a frequency-doubled and a frequency-quadrupled signal should have a phase noise degradation of about $20\log_{10}2 \approx 6.0$ dB, and $20\log_{10}4 \approx 12.0$ dB, respectively. The experimental results are consistent well with the theoretical results. However, the phase noise curves of the frequency-doubling and frequency-quadrupling at other offset frequencies are a little worse than the theoretical prediction, which could be contributed from additional phase noise introduced by polarization fluctuations.

Another peak at 66-KHz is associated with an uncertain perturbation, and disappears from time to time.

The stability of the generated microwaves and their phase noise performance can be further improved by using a wavelength-stabilized TLS and a packaged PS-FBG which could be immune to the environmental changes. The use of a long fiber delay line in the loop could also improve the phase noise performance, but a PS-FBG with a narrower notch is also required to ensure single mode oscillation.

7.4 Conclusion

A simple and novel wideband tunable frequency-doubling or frequency-quadrupling OEO combining the technique of external modulation and a frequency-tunable OEO based on a microwave photonic bandpass filter has been proposed and experimentally demonstrated. The key features of the proposed OEO are: 1) the generation of a high frequency microwave signal can be achieved by using low-frequency components in the OEO; 2) wideband microwave frequency tuning can be realized by simply tuning the wavelength of the incident light wave. In addition, no bias control is needed which greatly simplifies the implementation and improves the operation stability. The experiments were performed. The generations of a fundamental oscillation with a frequency from 6 GHz to 14 GHz, a frequency-doubled microwave signal with a frequency from 16 GHz to 28 GHz, a frequency-quadrupled microwave signal with a frequency from 30 GHz to 42 GHz were demonstrated. Totally, the frequency tunable range is about 42 GHz, which is, to the best of our knowledge, the widest frequency-tunable range ever achieved. The phase noise performances of the generated fundamental frequency, doubled frequency and the quadrupled frequency were also evaluated.

CHAPTER 8 SUMMARY AND FUTURE RESEARCH

8.1 Summary

The work of the thesis was focused on the investigation of photonic generation of ultra-low phase noise, frequency-tunable microwave and mm-wave signals based on two techniques: external modulation and optoelectronic oscillation.

External modulation, as known as microwave frequency multiplication using electro-optical (EO) modulators, has been demonstrated to be a promising technique to generate a high frequency microwave or mm-wave signal from a low frequency microwave signal. The system is simple with large frequency tunability. However, conventional external modulation can only provide a small frequency multiplication factor (FMF). Although there are various methods to increase the FMF, the large FMF is at the cost of limited frequency tuning range. Therefore, we proposed to use two Mach-Zehnder modulators (MZMs) to realize microwave frequency multiplication with a FMF as large as 8. A comprehensive study was presented to prove that two-MZM-based external modulation is capable of achieving frequency sextupling and octupling with large frequency tunability. To further increase the FMF, optical nonlinear effects are employed. A joint use of external modulation, four-wave mixing (FWM) and stimulated-Brillouin-scattering-assisted (SBS-assisted) adaptive filtering was demonstrated to achieving frequency twelvetupling. FWM is used to triple the FMF obtained using conventional external modulation, and stimulated-Brillouin-scattering-assisted (SBS-assisted) adaptive filtering is incorporated to remove undesired sidebands. Since an SBS-assisted-filter

is wavelength-independent, it ensures a larger frequency tunable range. By combing the two-MZM-based external modulation, FWM and SBS-assisted filtering, even a larger FMF of 24 can be potentially achieved. Based on the commercially available 40-GHz EO modulators, 40-GHz microwave amplifiers, and terahertz photomixers, an mm-wave or terahertz signal of a frequency up to 1THz could be generated, and the frequency tuning range could be as large as hundreds of GHz.

An OEO is another promising technique for photonic microwave and mm-wave generation. A conventional OEO using an electrical bandpass filter has two major limitations, limited frequency tunability and low frequency of the generated signal. To address two problems simultaneously, we first proposed a wideband frequency tunable microwave photonic filter (MPF) which was implemented based on PM-IM conversion and achieved a widest frequency-tunable range ever obtained. Then the proposed wideband frequency-tunable MPF was incorporated in an OEO, replacing the electrical bandpass filter, to form an optically frequency-tunable OEO. The generation of a frequency-tunable microwave and mm-wave signal has been successfully demonstrated. Finally, to increase the frequency of the generated microwave or mm-wave signal, external modulation techniques were merged with the frequency-tunable OEO to implement an optically tunable frequency-multiplying OEO which simultaneously eliminates the two limitations of a conventional OEO. In the experiment, the generation of a frequency-doubled microwave signal and a frequency-quadrupled microwave signal have been demonstrated. Totally, a frequency tunable range of more than 40 GHz was demonstrated, which is, to the best of our knowledge, the widest frequency-tunable range ever achieved.

8.2 Future research

In this research work, photonic microwave and mm-wave generation based on external modulation and optoelectronic oscillation was investigated and demonstrated. In the case of external modulation, the obtained FMF is still not large enough for the generation of a high-frequency mm-wave or a terahertz wave signal using low-cost, low-frequency microwave components. Seeking photonic solutions to significantly increase FMF will be the next research focus. In addition, as observed in some experiments, some undesired sidebands are not completed suppressed, and unwanted harmonics at the output of the photodetector will appear, which could cause negative results in many practical applications. Thus, effectively removing undesired sidebands without using complicated optical filtering system is also a challenge.

For the frequency-tunable OEO, the frequency tunability is excellent and capable of covering a frequency range of tens of GHz. However, the phase noise performance is still a few dB worse than that of the commercialized microwave generators based on multiplied-up quartz oscillators or dielectric resonator oscillators. Using a well-packaged PS-FBG with a narrower notch and a wavelength-stabilized TLS are very necessary to further reduce the phase noise. Given all the devices in our proposed OEO can be integrated based on the photonic integrated circuit technologies, developing an integrated frequency-tunable OEO is also well worth being investigated.

Furthermore, the proposed OEO can also find some applications in optical sensing, since the unpackaged PS-FBG used in the OEO is quite sensitive to the environmental changes, like

temperature and stress, which can be easily interrogated by measuring the oscillation frequency of the OEO. The relevant researches will also be studied.

REFERENCES

[1] V. L. Granastein, *Physical Principles of Wireless Communications*, 2012 : Auerbach Publications.

[2] M. Fabbri, P. Faccin,"Radio over Fiber Technologies and Systems: New Opportunities," *Transparent Optical Networks, 2007*. ICTON '07. 9th Int. Conf. on vol. 3, pp. 230-233, Jul. 2007.

[3] A. Hirata, M. Harada, and T. Nagatsuma, "120-GHz Wireless Link using photonic techniques for generation, modulation, and emission of millimeter-wave signals," *J. Lightw. Tech.*, vol. 21, no. 10, pp. 2145-2153, Oct. 2003.

[4] H. A. Raweshidy and S. Komaki, *Radio over fiber technologies for mobile communications networks*, 2002: Artech House.

[5] M. J. Fice, E. Rouvalis, F. van Dijk, A. Accard, F. Lelarge, C. C. Renaud, G. Carpintero, and A. J. Seeds, "146-GHz millimeter-wave radio-over-fiber photonic wireless transmission system," *Opt. Exp*., vol. 20, no. 2, pp. 1769–1774, Jan.2012.

[6] V. Sharma, A. Singh, A. K. Sharma, "Challenges to radio over fiber (RoF) technology and its mitigation schemes – A review, *Optik - International Journal for Light and Electron Optics*, vol. 123, no. 4, pp. 338-342, Feb. 2012.

[7] R. J. Sullivan, *Microwave Radar Imaging and Advanced Concepts,* 2000 :Artech House.

[8] http://www.thintri.com/Millimeter-Waves-brochure-2012.pdf

[9] B. Fleming, "Recent advancement in automotive radar systems," *IEEE Veh. Technol. Mag.,* vol.7, no.1, pp.4-9, Mar. 2012.

[10] J. Hasch, E. Topak, R. Schnabel, T. Zwick, R. Weigel, and C. Waldschmidt, "Millimeter-wave technology for automotive radar sensors in the 77 GHz frequency band," *IEEE Trans. Microw. Theory Tech.*, vol. 60, no. 3, pp. 845–860, Mar. 2012.

[11] S. O. Tatu, B. Boukari, E. Moldovan, R. G. Bosisio, W. Ke, "Millimeter-wave multi-port radar sensor with integrated receiver front-end for automotive applications," *Microwave Symposium Digest (MTT), 2012 IEEE MTT-S Int.*, pp.1-3, 17-22 Jun. 2012.

[12] M. Klemm, J. A. Leendertz, D. Gibbons, I. J. Craddock, A. Preece, and R. Benjamin, "Microwave radar-based breast cancer detection: Imaging in inhomogeneous breast phantoms," *IEEE Antennas Wireless Propag.Lett.,* vol.8, pp.1349-1352, 2009.

[13] J. D. Shea, B. D. Van Veen, S. C Hagness, "A TSVD Analysis of Microwave Inverse Scattering for Breast Imaging," *IEEE Trans. Biomed. Eng.,* vol. 59, no. 4, pp. 936-945, Apr. 2012.

[14]http://finance.yahoo.com/news/infonetics-research-millimeter-wave-gear-165800449.html.

[15] M. Z. Win, D. Dardari, A. F. Molisch, W. Wiesbeck, and J. Zhang, "History and applications of UWB," *Proceedings of the IEEE*, vol. 97, no. 2, pp. 198-204, 2009.

[16] J. G. Proakis, *Spread Spectrum Signals for Digital Communications*. 2003: Wiley.

[17] D. K. Barton, *Radar System Analysis and Modeling*, 2005: Artech House.

[18] M. Kolber, "Predict phase noise effects in digital communications systems," *Microwaves and RF*, vol. 210, pp. 59-70, Sep. 1999.

[19] A. Richardson, *WCDMA Design Handbook*, 2005: Cambridge University Press.

[20] A. P. S. Khanna, "Microwave oscillators: the state of the technology," *Microwave journal,* vol. 49, no. 4, pp. 22-44, Apr. 2006.

[21] D. A. Howe and A. Hati, "Low-noise X-band oscillator and amplifier technologies: Comparison and status," *in Proceedings of the Joint IEEE Int. Frequency Control Symp. and Precise Time and Time Interval (PTTI) Systems and Applications Meeting,* Vancouver, Canada, Aug. 2005, pp. 481-487.

[22] V. Bottom, *Introduction to Quartz Crystal Unit Design*. New York, 1982: VanNostrand Reinhold.

[23] I. Bahl and P. Bhartia, *Microwave Solid State Circuit Design,*1988 :Wiley

[24] M. Tobar, E. Ivanov, P. Blondy, D. Cros, and P. Guillon, "High-Q whispering gallery traveling wave resonators for oscillator frequency stabilization," *IEEE Trans. Ultrason., Ferroelectr., Freq. Control*, vol. 47, no. 2, pp.421-426, Mar.2000.

[25] G. K. Montress, T. E. Parker, M. J. Loboda, J. A. Greer, "Extremely low-phase-noise SAW resonators and oscillators: design and performance," *IEEE Trans. Ultrason. Ferroelectr. Freq. Control,* vol.35, no.6, pp.657-667, Nov. 1988.

[26] A. P. S. Khanna et al, "A film bulk acoustic resonator (FBAR) L band low noise oscillator for digital communications," *Technical Digest, EuMC,* 2002.

[27] J. G Hartnett, N. R Nand, C. Wang, J. M Le Floch, "Cryogenic sapphire oscillator using a lowvibration design pulse-tube cryocooler: first results," *IEEE Trans. Ultrason. Ferroelectr. Freq. Control,* vol. 57, no. 5, pp. 1034-1038, May 2010.

[28] S. Grop, P.Y. Bourgeois, R. Boudot, Y. Kersale, E. Rubiola, V. Giordano, "10 GHz cryocooled sapphire oscillator with extremely low phase noise," *Electron Lett.*, vol. 46, no. 6, pp. 420-422, Mar. 2010.

[29] A. P. S. Khanna, and J. Buenrostro, "2-22 GHz low phase noise silicon bipolar YIG tuned oscillator using composite feedback," *Microwave Symposium Digest (MTT), 1992 IEEE MTT-S Int.*, vol.3, pp.1297-1299, Jun. 1992.

[30] A. P. S. Khanna, J. Hauptman, "18-40 GHz 13 dBm low noise GaAs FET YIG tuned oscillator," *Microwave Symposium Digest (MTT), 1991 IEEE MTT-S Int.*, vol. 1, pp.209-212, Jul. 1991.

[31] A. Chenakin, *Frequency Synthesizers - Concept to Product*, 2011: Artech House.

[32] A. J. Seeds, "Microwave photonics," *IEEE Trans. Microw. Theory Tech.,* vol. 50, no. 3, pp. 877-887, Mar. 2002.

[33] A. J. Seeds and K. J. Williams, "Microwave photonics," *J. Lightwave Technol.,* vol. 24, no. 12, pp. 4628-4641, Dec. 2006.

[34] J. Capmany and D. Novak, "Microwave photonics combines two worlds," *Nat. Photon.,* vol. 1, no. 6, pp. 319-330, Jun. 2007.

[35] J. P. Yao, "Microwave Photonics," *J. Lightwave Technol.,* vol. 27, no. 1-4, pp. 314-335, Feb. 2009.

[36] I. Gasulla, J. Lloret, J. Sancho, S. Sales, J. Capmany, "Recent breakthroughs in microwave photonics," *IEEE Photon. J.,* vol. 3, no. 2, pp. 311-315, Apr. 2011.

[37] B. E. A. Saleh and M. C. Teich, *Fundamentals of Photonics*, 1991 :Wiley.

[38] L. Goldberg, H. F. Taylor, J. F. Weller and D. M. Bloom, "Microwave signal generation with injection locked laser diodes," *Electron Lett.*, vol. 19, no. pp. 491-493, Jun. 1983.

[39] L. Goldberg, A. Yurek, H. F. Taylor and J. F. Weller, "35 GHz microwave signal generation with injection locked laser diode," *Electron Lett*., vol. 21, no. 18, pp. 714-715, Aug.1985.

[40] W. Lee and P. J. Delfyett, "Dual-mode injection locking of two independent modelocked semiconductor lasers," *Electron. Lett.*, vol. 40, no. 19, pp.1182 -1183, Sep. 2004.

[41] L. Chrostowski, X. Zhao, and C. Chang-Hasnain, "Microwave Performance of Optically Injection-locked VCSELs," *IEEE Trans. Microw. Theory Tech.,* vol. 54, no. 2, pp. 788-796, Feb. 2006.

[42] A. Quirce and A. Valle, "High-frequency microwave signal generation using multi-transverse mode VCSELs subject to two-frequency optical injection," *Opt. Exp.*, vol. 20, no. 12, pp. 13390-13401, May 2012.

[43] J. Harrison and A. Mooradian, "Linewidth and offset frequency locking of external cavity GaAlAs lasers," *IEEE J. Quantum Electron.*, vol. 25, no. 6, pp. 1252–1255, Jun. 1989.

[44] M. Z. Win, C.-C. Chen, and R. A. Scholtz, "Optical phase-locked loop (OPLL) for an amplitude modulated communications link using solid-state lasers," *IEEE J. Select. Areas Commun*., vol. 13, no. 3, pp. 569–576, Apr. 1995.

[45] R. T. Ramos and A. J. Seeds, "Fast heterodyne optical phase-lock loop using double quantum well laser diodes," *Electron. Lett.,* vol. 28, no. 1, pp. 82–83, Jan. 1992.

[46] U. Gliese, N. T. Nielsen, M. Bruun, E. L. Christensen, K. E. Stubkjaer, S. Lindgren, and B. Broberg, "A wideband heterodyne optical phaselocked loop for the generation of 3-18 GHz microwave carriers," *IEEE Photon. Technol. Lett*., vol. 4, no. 8, pp. 936–938, Aug.1992.

[47] A. C. Bordonalli, C. Walton, and A. J. Seeds, "High-Performance phase locking of wide linewidth semiconductor lasers by combined use of optical injection locking and optical phase-lock loop," *J. Lightwave Technol.*, vol. 17, no. 2, pp. 328–342, Feb. 1999.

[48] L. N. Langley, M. D. Elkin, C. Edge, M. J. Wale, U. Gliese, X. Huang, and A. J. Seeds, "Packaged semiconductor laser optical phase-locked loop (OPLL) for photonic generation, processing and transmission of microwave signals," *IEEE Trans. Microw. Theory Tech.*, vol. 47, no. 7, pp.1257-1264, Jul. 1999.

[49] S. Ristic , A. Bhardwaj , M. J. Rodwell , L. A. Coldren and L. A. Johansson, "An optical phase-locked loop photonic integrated circuit," *J. Lightw. Technol.*, vol. 28, no. 4, pp. 526-538, Feb. 2010.

[50] R. J. Steed , L. Ponnampalam , M. J. Fice , C. C. Renaud , D. C. Rogers , D. G. Moodie , G. D. Maxwell , I. F. Lealman , M. J. Robertson , L. Pavlovic , L. Naglic , M. Vidmar and A. J. Seeds, "Hybrid integrated optical phase-lock loops for photonic terahertz sources," *IEEE J. Sel. Topics Quantum Electron.*, vol. 17, no. 1, pp.210-217, Jan-Feb. 2011.

[51] M. Lu, H. Park, E. Bloch, A. Sivananthan, A. Bhardwaj, Z. Griffith, L. A. Johansson, M. J. Rodwell, and L. A. Coldren, "Highly integrated optical heterodyne phase-locked loop with phase/frequency detection," *Opt. Exp.*, vol. 20, no. 9, pp. 9736-9741, Apr. 2012.

[52] R. T. Ramos, P. Gallion , D. Erasme, A. J. Seeds and A. C. Bordonalli, "Optical injection locking and phase-lock loop combined systems," *Opt. Lett.*, vol. 19, no. 1, pp.4-6, Jan. 1994.

[53] A. C. Bordonalli, C.Walton, and A. J. Seeds, "High performance phase locking of wide linewidth semiconductor lasers by combined use of optical injection locking and optical phase-lock loop," *J. Lightw. Technol.,* vol. 17, pp. 328-342, Feb. 1999.

[54] L. A. Johansson and A. J. Seeds, "Millimeter-wave modulated optical signal generation with high spectral purity and wide locking bandwidth using a fiber-integrated optical phase-lock loop," *IEEE Photon. Technol. Lett.*, vol. 12, no. 6, pp. 690-693, Jun. 2000.

[55] C. C. Renaud , M. Dser , C. F. C. Silva , B. Puttnam , T. Lovell , P. Bayvel and A. J. Seeds, "Nanosecond channel-switching exact optical frequency synthesizer using an optical injection phase-locked loop (OIPLL)," *IEEE Photon. Technol. Lett., vol*. 16, no. 3, pp. 903-905, Mar. 2004.

[56] Y. Shoji, M. Fice, Y. Takayama, A. J. Seeds, "A pilot-carrier coherent LEO-to-ground downlink system using an optical injection phase lock loop (OIPLL) technique," *J. Lightw. Technol.,* vol. 30, no. 6, pp. 2696-2706, Aug. 2012.

[57] J. J. O'Reilly, P. M. Lane, R. Heidemann, and R. Hofstetter, "Optical generation of very narrow linewidth millimeter wave signals," *Electron. Lett.,* vol. 28, no. 25, pp. 2309–2311, Dec. 1992.

[58] J. J. O'Reilly, P. M. Lane, "Fiber-supported optical generation and delivery of 60 GHz signals," *Electron. Lett.,* vol. 30, no. 16, pp. 1329–1330, Aug. 1994.

[59] G. Qi, J. P. Yao, J. Seregelyi, C. Bélisle, and S. Paquet, "Generation and distribution of a wide-band continuously tunable millimeter-wave signal with an optical external modulation technique," *IEEE Trans. Microw. Theory Tech.,* vol. 53, no. 10, pp. 3090-3097, Oct. 2005.

[60] G. Qi, J. P. Yao, J. Seregelyi, S. Paquet and C. Bélisle,, "Optical generation and distribution of continuously tunable millimeter-wave signals using an optical phase modulator," *J. Lightw. Technol.*, vol. 23, no. 9, pp. 2687-2695, Sep. 2005.

[61] J. Zhang, H. Chen, M. Chen, T. Wang, and S. Xie, "Photonic generation of a millimeter-wave signal based on sextuple-frequency multiplication," *Opt. Lett.*, vol. 32, no. 9, pp. 1020-1022, Apr. 2007.

[62] J. Zhang, H. Chen, M. Chen, T. Wang, S. Xie, "A photonic microwave frequency quadrupler using two cascaded intensity modulators with repetitious optical carrier suppression," *IEEE Photon. Technol. Lett.,* vol. 19, no. 14, pp. 1057-1059, Jul. 2007.

[63] Y. Zhao, X. Zheng, H. Wen, and H. Zhang, "Simplified optical millimeter-wave generation configuration by frequency quadrupling using two cascaded Mach–Zehnder modulators," *Opt. Lett.*, vol. 34, no. 21, pp. 3250-3252, Nov. 2009.

[64] M. Mohamed, X. Zhang, B. Hraimel, and K. Wu, "Frequency sextupler for millimeter-wave over fiber systems," *Opt. Exp.,* vol. 16, no. 14, pp. 10141-10151, Jun. 2008.

[65] W. Li and J. P. Yao, "Microwave frequency multiplication using two cascaded Mach-Zehnder modulators," *Proc. 2009 Asia-Pacific Microwave Photonics Conf.,* Beijing, China, Apr. 2009.

[66] W. Li and J. P. Yao, "Microwave generation based on optical-domain microwave frequency octupling," *IEEE Photon. Technol. Lett.*, vol. 22, no. 1, pp. 24-26, Jan. 2010.

[67] W. Li and J. P. Yao, "Investigation of photonically assisted microwave frequency multiplication based on external modulation," *IEEE Trans. Microw. Theory Tech.*, vol. 58, no. 11, pp. 3259-3268, Nov. 2010.

[68] J. Ma, X. Xin, J. Yu, C. Yu, K. Wang, H. Huang, and L. Rao, "Optical millimeter wave generated by octupling the frequency of the local oscillator," *J. Opt. Netw.* vol. 7, no. 10, pp. 837-845, Oct. 2008.

[69] X. Yin, A. Wen, Y. Chen, and T. Wang, "Studies in an optical millimeter-wave generation scheme via two parallel dual-parallel Mach-Zehnder modulators," *J. Mod. Optic.*, vol. 58, no. 8, pp. 665–673, Mar. 2011.

[70] C. T. Lin , P. T. Shih , J. Chen , W. Q. Xue , P. C. Peng, and S. Chi, "Optical millimeter-wave signal generation using frequency quadrupling technique and no optical filtering," *IEEE Photon. Technol. Lett.*, vol. 20, pp. 1027-1029, Jun. 2008.

[71] C. Lin, P. Shih, W. Jiang, J. Chen, P. Peng, and S. Chi, "A continuously tunable and filterless optical millimeter-wave generation via frequency octupling," *Opt. Exp.*, vol. 17, no. 22, pp. 19749-19756, Oct. 2009.

[72] C. T. Lin, J. Chen, P.T. Shih, W.J. Jiang, and S. Chi, "Ultra-high data-rate 60 GHz radio-over-fiber systems employing optical frequency multiplication and OFDM formats," *J. Lightw. Technol.,* vol. 28, no. 16, pp. 2296-2306, Aug. 2010.

[73] T. Kawanishi, S. Oikawa, and M. Izutsu,, "Reciprocating optical modulation for millimeter-wave generation by using a dual-section fiber Bragg grating," *J. Lightw. Technol*., vol. 20, no.8, pp. 1408-1415, Aug. 2002.

[74] T. Kawanishi, S. Shinada, T. Sakamoto, S. Oikawa, K. Yoshiara, and M. Izutsu, "Reciprocating optical modulator with resonant modulating electrode," *Electron. Lett.*, vol. 41, no. 5, pp. 271-272, Mar. 2005.

[75] H. J. Song , N. Shimizu , T. Furuta , K. Suizu , H. Ito and T. Nagatsuma, "Broadband-frequency-tunable sub-terahertz wave generation using an optical comb, AWGs, optical switches, and a uni-traveling carrier photodiode for spectroscopic applications," *J. Lightw. Technol.*, vol. 26, no. 15, pp. 2521-2530, Aug. 2008.

[76] H. J. Song, N. Shimizu and T. Nagatsuma, "Generation of two-mode optical signals with broadband frequency tunability and low spurious signal level," *Opt. Exp.*, vol. 15, no. 22, pp. 14901-14906, Oct. 2007.

[77] A. Wiberg, P. P-Millán, M. V. Andres, and P. O. Hedekvist, "Microwave-photonic frequency multiplication utilizing optical four-wave mixing and fiber Bragg gratings," *J. Lightw. Technol.*, vol. 24, no. 1, pp. 329-334, Jan. 2006.

[78] Q. Wang, H. Rideout, F. Zeng, and J. P. Yao, "Millimeter-wave frequency tripling based on four-wave mixing in a semiconductor optical amplifier," *IEEE Photon. Technol. Lett.,* vol. 18, no. 23, pp. 2460-2462, Dec. 2006.

[79] T. Wang, H. Chen, M. Chen, J. Zhang, and S. Xie, "High-spectral-purity millimeter-wave signal optical generation," *J. Lightw. Technol.,* vol. 27, no. 12, pp. 2044-2051, Jun. 2009.

[80] G. P. Agrawal, *Nonlinear Fiber Optics*, 2001: Academic.

[81] S. Preu, G. H. Dohler, S. Malzer, L. J. Wang, and A. C. Gossard, "Tunable, continuous-wave Terahertz photomixer sources and applications," *J. Appl. Phys.,* vol. 109, no. 6, pp. 061301-1-061301-56, Mar. 2011.

[82] K. Ajito, Y. Muramoto, A. Wakatsuki, T. Nagatsuma, N. Kukutsu, "Uni-travelling-carrier photodiode module generating 300 GHz power greater than 1 mW," *IEEE Microw. Wireless Compon. Lett.,* vol. 22, no. 7, pp. 363-365, Jul. 2012.

[83] H. Tanoto, J. H. Teng, Q. Y. Wu, M. Sun, Z. N. Chen, S. A. Maier, B. Wang, C. C. Chum, G. Y. Si, A. J. Danner, and S. J. Chua, "Greatly enhanced continuous-wave terahertz emission by nano-electrodes in a photoconductive photomixer," *Nat. Photon.,* vol. 6, no. pp. 121-126, Feb. 2012.

[84] N. Kim, S.-P. Han, H. Ko, Y. A. Leem, H.-C. Ryu, C. W. Lee, D. Lee, M. Y. Jeon, S. K. Noh, and K. H. Park, "Tunable continuous-wave terahertz generation/detection with compact 1.55 μm detuned dual-mode laser diode and InGaAs based photomixer," *Opt. Exp.,* vol. 19, no. 16, pp. 15397-15403, Aug. 2011.

[85] B. A. Garcia, L. G. Munoz, D. S. Vargas, S. Bauerschmidt, G. Dohler, S. Preu, S. Malzer, L. Hong, A. C. Gossard, "High power terahertz photomixer arrays," *Antennas and Propagation (EUCAP), 2012 6th European Conf. on*, pp. 1007-1010, Mar. 2012.

[86] C. L. Wang and C. L. Pan, "Tunable multiterahertz beat signal generation from a two-wavelength laser-diode array," *Opt. Lett*., vol. 20, no. 11, pp. 1292-1294, Jun.1995.

[87] P. Pellandini, R. P. Stanley, R. Houdrè, U. Oesterle, M. Ilegems, and C. Weisbuch, "Dual-wavelength laser emission from a coupled semiconductor microcavity," *Appl. Phys. Lett.,* vol. 71, no. 7, pp. 864-866, Aug. 1997.

[88] S. Hoffmann, M. Hofmann, E. Bründermann, M. Havenith, M. Matus, J. V. Moloney, A. S. Moskalenko, M. Kira, S. W. Koch, S. Saito, and K. Sakai, "Four-wave mixing and direct terahertz emission with two-color semiconductor lasers," *Appl. Phys. Lett*., vol. 84, no. 18, pp. 3585-3587, May, 2004.

[89] M. Tani, O. Morikawa, S. Matsuura, and M. Hangyo, "Generation of terahertz radiation by photomixing with dual- and multiple-mode lasers," *Semicond. Sci. Technol.*, vol. 20, no. 7, pp. S151-S163, Jul. 2005.

[90] A. Klehr , J. Fricke , A. Knauer , G. Erbert , M. Walther , R. Wilk , M. Mikulics, and M. Koch, "High-power monolithic two-mode DFB laser diodes for the generation of THz radiation," *IEEE J. Sel. Top. Quantum Electron.*, vol. 14, no. 2, pp. 289 -294 Mar.-Apr. 2008.

[91] S. Zolotovskaya, V. I. Smirnov, G. B. Venus, L. B. Glebov, and E. U. Rafailov, "Two-color output from InGaAs laser with multiplexed reflective Bragg mirror," *IEEE Photon. Technol. Lett.*, vol. 21, no. 15, pp. 1093-1095, Aug. 2009.

[92] N. Kim, J. Shin, E. Sim, C. W. Lee, D. S. Yee, M. Y. Jeon, Y. Jang, and K. H. Park, "Monolithic dual-mode distributed feedback semiconductor laser for tunable continuous-wave terahertz generation," *Opt. Exp.*, vol. 17, no. 16, pp.13851 -13859, Aug. 2009.

[93] N. A. Naderi , F. Grillot, K. Yang , J. B. Wright, A. Gin, and L. F. Luke, "Two-color multi-section quantum dot distributed feedback laser," *Opt. Exp.*, vol. 18, no. 26, pp. 27028-27035, Dec. 2010.

[94] E. H. Bernhardi, R. Khan, C. Roeloffzen, H. van Wolferen, K. Wörhoff, R. M. de Ridder, and M. Pollnau, "Optical generation of microwave signals with a dual-phase-shifted Al_2O_3:Yb^{3+} distributed-feedback laser," in *CLEO: Applications and Technology*, 2012, paper JW2A.36, 2012.

[95] J. Liu, J. P. Yao, J. Yao, and T. H. Yeap, "Single longitudinal mode multi-wavelength fiber ring laser," *IEEE Photon. Technol. Lett.*, vol. 16, no.4, pp.1020-1022, Apr. 2004.

[96] X. Chen, J. P. Yao, and Z. Deng, "Ultra-narrow dual-transmission-band fiber Bragg grating filter and its application in a dual-wavelength single-longitudinal-mode fiber ring laser," *Opt. Lett.*, vol. 30, no. 16, pp. 2068-2070, Aug. 2005.

[97] Y. Dai, X. Chen, J. Sun, Y. Yao, and S. Xie, "Dual-wavelength DFB fiber laser based on a chirped structure and the equivalent phase shift method," *IEEE Photon. Technol. Lett.*, vol. 18, pp. 1964-1966, Sep. 2006.

[98] S. Pan and J. Yao, "A wavelength-switchable single-longitudinal-mode dual-wavelength erbium-doped fiber for switchable microwave generation," *Opt. Exp.*, vol. 17, no. 7, pp. 5414-5419, Mar. 2009.

[99] H. Maestre, A. J. Torregrosa, C. R. Fernandez-Pousa, J. A. Pereda, and J. Capmany, "Widely tuneable dual-wavelength operation of a highly doped erbium fiber laser based on diffraction gratings," *IEEE J. Quantum Electron.*, vol.47, no.9, pp. 1238-1243, Sept. 2011.

[100] R. Kim; S. Chu; and Y. Han, "Stable and widely tunable single-longitudinal-mode dual-wavelength erbium-doped fiber laser for optical beat frequency generation," *IEEE Photon. Technol. Lett.*, vol.24, no.6, pp. 521-523, Mar. 2012.

[101] G. Liang, T. Wang, X. Zhou, Q. Li, and S. Qian, "A novel switchable dual-wavelength ring erbium-doped fiber laser operating in single-longitudinal-mode," *Electronics and Optoelectronics (ICEOE), 2011 Int. Conf. on*, vol.1, pp.V1-69-V1-71, Jul. 2011.

[102] S. Pan, X. Zhao, and C. Lou, "Switchable single-longitudinal-mode dual-wavelength erbium-doped fiber ring laser incorporating a semiconductor optical amplifier," *Opt. Lett.*, vol. 33, no. 8, pp. 764-766, Apr. 2008.

[103] X. Chen, Z. Deng, and J. P. Yao, "Photonic generation of microwave signal using a dual-wavelength single-longitudinal-mode fiber ring laser," *IEEE Trans. Microw. Theory Tech.*, vol. 54, no. 2, pp. 804-809, Feb. 2006.

[104] M. Tang, H. Minamide, Y. Wang, T. Notake, S. Ohno, and H. Ito, "Tunable terahertz-wave generation from DAST crystal pumped by a monolithic dual-wavelength fiber laser," *Opt. Exp.,* vol. 19, no. 2, pp. 779-786, Jan. 2011.

[105] M. C. Gross , P. T. Callahan , T. R. Clark , D. Novak , R. B. Waterhouse, and M. L. Dennis, "Tunable millimeter-wave frequency synthesis up to 100 GHz by dual-wavelength Brillouin fiber laser," *Opt. Exp.*, vol. 18, no. 13, pp. 13321 -13330, Jun. 2010.

[106] G. Ducournau, P. Szriftgiser, T. Akalin, A. Beck, D. Bacquet, E. Peytavit, and J. F. Lampin, "Highly coherent terahertz wave generation with a dual-frequency Brillouin fiber laser and a 1.55 μm photomixer," *Opt. Lett.*, vol. 36, no. 10, pp. 2044-2046, Jun. 2011.

[107] H. Maestre, A. J. Torregrosa, C. R. Fernandez-Pousa, J. A. Pereda, and J. Capmany, "Widely tuneable dual-wavelength operation of a highly doped erbium fiber laser based on diffraction gratings," *IEEE J. Quantum Electron.*, vol.47, no.9, pp. 1238-1243, Sep. 2011.

[108] Y. G. Shee, M. H. Al-Mansoori, S. Yaakob, A. Man, A. K. Zamzuri, F. R. Mahamd Adikan, and M. A. Mahdi, "Millimeter wave carrier generation based on a double-Brillouin-frequency spaced fiber laser," *Opt. Exp.*, vol. 20, no. 12, pp. 13402-13408, Jun. 2012.

[109] J. Liu; L. Zhan, P. Xiao, Q. Shen, G. Wang, Z. Wu, X. Liu, and L. Zhang, "Optical generation of tunable microwave signal using cascaded Brillouin fiber lasers," *IEEE Photon. Technol. Lett.*, vol.24, no.1, pp. 22-24, Jan. 2012.

[110] Y. Dai , X. Chen , L. Xia , Y. Zhang, and S. Xie, "Sampled Bragg grating with desired response in one channel by use of a reconstruction algorithm and equivalent chirp," *Opt. Lett.*, vol. 29, no. 12, pp. 1333-1335, Jun. 2004.

[111] Y. Dai and J. P. Yao, "Numerical study of a DFB semiconductor laser and laser array with chirped structure based on the equivalent chirp technology," *IEEE J. Quantum Electron.,* vol. 44, no. 10, pp. 938-945, Oct. 2008.

[112] E. Desurvire, *Erbium-Doped Fiber Amplifiers*, 1994: Wiley.

113 S. Yamashita and K. Hotate, "Multiwavelength erbium-doped fiber laser using intracavity etalon and cooled by liquid nitrogen," *Electron. Lett.*, vol. 32, no. 14, pp. 1298-1299, Jul. 1996.

[114] A. Neyer and E. Voges, "Hybrid electro-optical multivibrator operating by finite feedback delay," *Electron. Lett.*, vol.18, no.2, pp. 59-60, Jan. 1982.

[115] X. S. Yao and L. Maleki, "Optoelectronic microwave oscillator," *J. Opt. Soc. Amer. B,* vol. 13, no. 8, pp. 1725-1735, Aug. 1996.

[116] X. S. Yao and L. Maleki, "Optoelectronic oscillator for photonic systems," *IEEE J. Quantum Electron.*, vol. 32, no. 7, pp. 1141-1149, Jul. 1996.

[117] T. Berceli and P. Herczfeld, "Microwave photonics—a historical perspective," *IEEE Trans. Microw. Theory Tech.,* vol. 58, no. 11, pp. 2992-3000, Nov. 2010.

[118] X. S. Yao and L. Maleki, "Multiloop optoelectronic oscillator," *IEEE J. Quantum Electron.,* vol. 36, no. 1, pp. 79-84, Jan. 2000.

[119] Y. Jiang, J. Yu, Y. Wang, L. Zhang, and E. Yang, "An optical domain combined dual-loop optoelectronic oscillator," *IEEE Photon. Technol. Lett.,* vol. 19, no. 11, pp. 807-809, Jun. 2007.

[120] E. Shumakher and G. Eisenstein, "A novel multiloop optoelectronic oscillator," *IEEE Photon. Technol. Lett.*, vol. 20, no. 22, pp. 1881-1883, Nov. 2008.

[121] E. Shumakher, "The optoelectronic oscillator: Review and recent advances," *Microwaves, Communications, Antennas and Electronics Systems, 2009. COMCAS 2009. IEEE Int. Conf. on*, pp. 1-5, Nov. 2009.

[122] X. Liu, W. Pan, X. Zou, B. Luo, L. Yan, and B. Lu, "A reconfigurable optoelectronic oscillator based on cascaded coherence-controllable recirculating delay lines," *Opt. Exp.,* vol. 20, no. 12, pp. 13296-13301, Jun. 2012.

[123] W. H. Tseng and K. M. Feng, "Enhancing long-term stability of the optoelectronic oscillator with a probe-injected fiber delay monitoring mechanism," *Opt. Exp.*, vol. 20, no. 2, pp. 1597-1607, Jan. 2012.

[124] W. Zhou and G. Blasche, "Injection-locked dual opto-electronic oscillator with ultra-low phase noise and ultra-low spurious level," *IEEE Trans. Microw. Theory Tech.*, vol. 53, no. 3, pp. 929-933, Mar. 2005.

[125] K. H. Lee, J. Y. Kim, and W. Y. Choi, "Injection-locked hybrid optoelectronic oscillators for single-mode oscillation," *IEEE Photon. Technol. Lett.*, vol. 20, pp. 1645-1647, Oct.2008.

[126] O. Okusaga, W. Zhou, E. C. Levy, M. Horowitz, G. M. Carter, and C. R. Menyuk, "Experimental and simulation study of dual injection-locked OEOs," *in IEEE Freq. Cont. Symp*., pp. 875–879, 2009.

[127] O. Okusaga, E. J. Adles, E. C. Levy, W. Zhou, G. M. Carter, C. R. Menyuk, and M. Horowitz, "Spurious mode reduction in dual injection-locked optoelectronic oscillators," *Opt. Exp.*, vol. 19, no. 7, pp. 5839–5854, Mar. 2011.

[128] V. S. Ilchenko and A. B. Matsko, "Optical resonators with whispering-gallery modes—Part II: applications," *IEEE J. Sel. Top. Quantum Electron.*, vol. 12, no. 1, pp. 15-32, Jan.-Feb. 2006.

[129] A. B. Matsko, L. Maleki, A. A. Savchenkov, and V. S. Ilchenko, "Whispering gallery mode based optoelectronic microwave oscillator," *J. Mod. Opt.,* vol. 50, no-15-17, pp. 2523-2542, Jan. 2003.

[130] K. Volyanskiy, P. Salzenstein, H. Tavernier, M. Pogurmirskiy, Y. K. Chembo, and L. Larger, "Compact optoelectronic microwave oscillators using ultra-high Q whispering gallery mode disk-resonators and phase modulation," *Opt. Exp.,* vol. 18, no. 21, pp. 22358-22363, Oct 2010.

[131] A. A. Savchenkov, V. S. Ilchenko, J. Byrd, W. Liang, D. Eliyahu, A. B. Matsko, D. Seidel, and L. Maleki, "Whispering-gallery mode based optoelectronic oscillators," *in IEEE Freq. Cont. Symp*., pp. 554–557, 2011.

[132] K. Saleh, P. Merrer, O. Llopis, and G. Cibiel, "Optical scattering noise in high Q fiber ring resonators and its effect on optoelectronic oscillator phase noise," *Opt. Lett.,* vol. 37, no. 4, pp. 518-520, Feb. 2012.

[133] http://www.oewaves.com

[134] L. Maleki, "Sources: The optoelectronic oscillator," *Nat. Photon.,* vol. 5, no. 12, pp. 28–730, Dec. 2011.

[135] S. Poinsot, H. Porte, J. Goedgebuer, W. T. Rhodes, and B. Boussert, "Continuous radio-frequency tuning of an optoelectronic oscillator with dispersive feedback," *Opt. Lett.*, vol. 27, no. 15, pp. 1300-1302, Aug. 2002.

[136] E. Shumakher, S. Ó. Dúill, and G. Eisenstein, "Optoelectronic oscillator tunable by an SOA based slow light element," *J. Lightw. Technol.*, vol. 27, no. 18, pp. 4063-4068, Sep. 2009.

[137] I. Ozdur, D. Mandridis, N. Hoghooghi, and P. J. Delfyett, "Low noise optically tunable optoelectronic oscillator with Fabry-Perot etalon," *J. Lightw. Technol.*, vol. 28, no. 21, pp. 3100 -3106, Nov. 2010.

[138] D. Eliyahu and L. Maleki, "Tunable, ultralow phase noise YIG based optoelectronic oscillator," *Proc. IEEE MTT-S Int. Microw. Symp. Dig.*, vol. 3, pp. 2185 -2187 2003.

[139] D. Zhu; S. Pan; D. Ben, "Tunable frequency-quadrupling dual-loop optoelectronic oscillator," *IEEE Photon. Technol. Lett*., vol. 24, no. 3, pp. 194-196, Feb. 2012.

[140] S. Pan and J. P. Yao, "Wideband and frequency-tunable microwave generation using an optoelectronic oscillator incorporating a Fabry–Perot laser diode with external optical injection," *Opt. Lett.*, vol. 35, no. 11, pp. 1911-1913, Jun. 2010.

[141] B. Yang, X. Jin, X. Zhang, S. Zheng, H. Chi, Y, Wang, "A wideband frequency-tunable optoelectronic oscillator based on a narrowband phase-shifted FBG and wavelength tuning of laser," *IEEE Photon. Technol. Lett.*, vol.24, no.1, pp.73-75, Jan.1, 2012.

[142] W. Li and J. P. Yao, "An optically tunable optoelectronic oscillator," *J. Lightw. Technol.*, vol. 28, no. 18, pp. 2640-2645, Sep. 2010.

[143] W. Li and J. P. Yao, "Wideband frequency-tunable optoelectronic oscillator incorporating a tunable microwave-photonic filter based on phase-modulation to intensity-modulation conversion using a phase-shifted fiber-Bragg grating," *IEEE Trans. Microw. Theory Tech.*, vol. 60, no. 6, pp. 1735-1742, Jun. 2012.

[144] M. Li, W. Li, and J. P. Yao, "Tunable optoelectronic oscillators incorporating a high-Q spectrum-sliced photonic microwave transversal filter," *IEEE Photon. Technol. Lett.*, vol. 24, no. 14, pp. 1251-1253, Jul. 2012.

[145] Z. Tang, S. Pan; D. Zhu, R. Guo, Y. Zhao; M. Pan, D. Ben, and J. P. Yao, "Tunable optoelectronic oscillator based on a polarization modulator and a chirped FBG," *IEEE Photon. Technol. Lett.,* vol. 24, no. 17, pp. 1487-1489, Sept. 2012.

[146] H. Shahoei, M. Li , and J. P. Yao, "Continuously tunable time delay using an optically pumped linearly chirped fiber Bragg grating," *J. Lightw. Technol.*, vol. 29, no. 10, pp. 1465-1472, May 2011

[147] M. Li and J. P. Yao, "Photonic generation of continuously tunable chirped microwave waveforms based on a temporal interferometer incorporating an optically-pumped linearly-chirped fiber Bragg grating," *IEEE Trans. Microw. Theory Tech.*, vol. 59, no. 12, pp. 3531-3537, Dec. 2011.

[148] K. Noguchi, H. Miyazawa, and O. Mitomi, "75 GHz broadband Ti:$LiNbO_3$ optical modulator with ridge structure," *Electron. Lett.*, vol.30, no.12, pp. 949-951, Jun. 1994.

[149] G. K. Gopalakrishnan, C. H. Bulmer, W. K. Burns, R. W. McElhanon, and A. S. Greenblatt, "40 GHz, low half-wave voltage Ti:$LiNbO_3$ intensity modulator," *Electron. Lett.*, vol. 28, no.9, pp. 826-827, Apr. 1992.

[150] Y. Tang, H. Chen, J. Peters, U. Westergren, and J. Bowers, "Over 40 GHz traveling-wave electroabsorption modulator based on hybrid silicon platform," *in Optical Fiber Communication Conference* 2011, paper OWQ3.

[151] M. Shin, V. S. Grigoryan and P. Kumar, "Frequency-doubling optoelectronic oscillator for generating high-frequency microwave signals with low phase noise," *Electron. Lett.*, vol. 43, no. 4, pp. 242 -244 2007.

[152] S. L. Pan and J. P. Yao, "A frequency-doubling optoelectronic oscillator using a polarization modulator," *IEEE Photon. Technol. Lett.*, vol. 21, no. 13, pp. 929 -931, Jul. 2009.

[153] S. Cai , S. Pan , D. Zhu , Z. Tang , P. Zhou, and X. Chen, "Coupled frequency-doubling optoelectronic oscillator based on polarization modulation and polarization multiplexing," *Opt. Commun.*, vol. 285, no. 16, pp. 1140-1143, Mar. 2012.

[154] W. Li and J. P. Yao, "An optically tunable frequency-multiplying optoelectronic oscillator," *IEEE Photon. Technol. Lett.*, vol. 24, no. 10, pp. 812-814, May 2012.

[155] J. D. Bull, N. A. Jaeger, H. Kato, M. Fairburn, A. Reid, and P. Ghanipour, "40-GHz electro-optic polarization modulator for fiber optic communications systems," *in Proc. SPIE,* Dec. 2004, vol. 5577, pp. 133-143.

[156] P. T. Callahan, M. C. Gross, and M. L. Dennis, "Phase noise measurements of a dual-wavelength Brillouin fiber laser," *Proc. IEEE Topical Meet. Microw. Photon.*, pp. 155-158, 2010.

[157] T. M. Ramond, S. A. Diddams, L. Hollberg, and A. Bartels, "Phase-coherent link from optical to microwave frequencies by means of the broadband continuum from a 1-GHz Ti:sapphire femtosecondoscillator," *Opt. Lett.*, vol. 27, no. 20, pp. 1842-1844, Oct. 2002.

[158] A. Bartels, S. A. Diddams, C. W. Oates, G. Wilpers, J. C. Bergquist, W. H. Oskay, and L. Hollberg, "Femtosecond-laser-based synthesis of ultrastable microwave signals from optical frequency references," *Opt. Lett.*, vol. 30, no. 6, pp. 667-669, Mar. 2005.

[159] W. Zhang, Z. Xu, M. Lours, R. Boudot, Y. Kersalé, A. N. Luiten, Y. Le Coq, and G. Santarelli, "Advanced noise reduction techniques for ultra-low phase noise opticalto-microwave division with femtosecond fiber combs," *IEEE Trans. Ultrason. Ferroelectr. Freq. Control,* vol. 58, no.5, pp. 900- 908, May 2011.

[160] J. Millo, R. Boudot, M. Lours, P. Y. Bourgeois, A. N. Luiten, Y. Le Coq, Y. Kersalé, and G. Santarelli, "Ultra-low-noise microwave extraction from fiber-based optical frequency comb," *Opt. Lett.,* vol. 34, no. 23, pp. 3707-3709, Dec. 2009.

[161] W. C. Swann, E. Baumann, F. R. Giorgetta, and N. R. Newbury, "Microwave generation with low residual phase noise from a femtosecond fiber laser with an intracavity electro-optic modulator," *Opt. Exp.,* vol. 19, no. 24, pp. 24387-24395, Nov. 2011.

[162] T. M. Fortier, M. S. Kirchner, F. Quinlan, J. Taylor, J. C. Bergquist, T. Rosenband, N. Lemke, A. Ludlow, Y. Jiang, C. W. Oates, and S. A. Diddams, "Generation of ultrastable microwaves via optical frequency division," *Nat. Photon.*, vol. 5, no. 7, pp. 425-429, Jul. 2011.

[163] F. Quinlan, T. M. Fortier, M. S. Kirchner, J. A. Taylor, M. J. Thorpe, N. Lemke, A. D. Ludlow, Y. Jiang, and S. A. Diddams, "Ultralow phase noise microwave generation with an Er:fiber-based optical frequency divider," *Opt. Lett.,* vol. 36, no. 16,pp. 3260-3262, Aug. 2011.

[164] T. Kawanishi, T. Sakamoto, M. Tsuchiya, M. Izutsu, S. Mori, and K. Higuma, "70dB extinction-ratio LiNbO3 optical intensity modulator for two-tone lightwave generation," i*n Proc. OFC* 2006, Anaheim, CA, 2006, paper OWC4.

[165] T. Kawanishi, T. Sakamoto, A. Chiba, M. Tsuchiya, and H. Toda, "Ultra high extinction-ratio and ultra low chirp optical intensity modulation for pure two-tone lightwave signal generation," *Proc. CLEO*, 2008.

[166] Y. Ogiso, Y. Tsuchiya, S. Shinada, S. Nakajima, T. Kawanishi, and H. Nakajima, "High extinction-ratio integrated Mach–Zehnder modulator with active Y-branch for optical SSB signal generation," *IEEE Photon. Technol. Lett.*, vol. 22, no. 12, pp. 941-943, Jun. 2010.

[167] A. Demir, A. Mehrotra, and J. Roychowdhury, "Phase noise in oscillators: A unifying theory and numerical methods for characterization," *IEEE Trans. Circuits Syst. I, Fund. Theory Appl.*, vol. 47, no. 5, pp. 655-674, May 2000.

[168] E. Rubiola, *Phase Noise and Frequency Stability in Oscillators*, 2008: Cambridge Univ. Press.

[169] D. Eliyahu, D. Seidel, and L. Maleki, "RF amplitude and phase-noise reduction of an optical link and an optoelectronic oscillator," *IEEE Trans. Microw. Theory Tech.*, vol. 56, no. 2, pp. 449 -456, Feb. 2008.

[170] K. Volyanskiy , Y. K. Chembo , L. Larger, and E. Rubiola, "Contribution of laser frequency and power fluctuations to the microwave phase noise of optoelectronic oscillators," *J. Lightw. Technol.*, vol. 28, no. 18, pp. 2730-2735, Sep. 2010.

[171] E. N. Ivanov, M. E. Tobar, and R. A. Woode, "Microwave interferometry: Application to precision measurements and noise reduction techniques," *IEEE Trans. Ultrason., Ferroelect., Freq. Control*, pp.1526-1536, Nov. 1997.

[172] D. L. Creedon, M. E. Tobar, E. N. Ivanov, J. G. Hartnett, "High-resolution flicker-noise-free frequency measurements of weak microwave signals," *IEEE Trans. Microw. Theory Tech.*, vol. 59, no. 6, pp. 1651-1657, Jun. 2011.

[173] E. Rubiola and V. Giordano, "Dual carrier suppression interferometer for the measurement of phase noise," *Electron. Lett.*, vol. 36, no. 25, pp. 2073-2075, Dec. 2000.

[174] R. D. Esman and K. J. Williams, "Wideband efficiency improvement of fiber optic systems by carrier subtraction," *IEEE Photon. Technol. Lett.,* vol. 7, no. 2, pp. 218-220, Feb. 1995.

[175] L. Liu , S. Zheng , X. Zhang , X. Jin, and H. Chi, "Performances improvement in radio over fiber link through carrier suppression using stimulated Brillouin scattering," *Opt. Exp.*, vol. 18, no. 11, pp. 11827-11837, May 2010.

[176] A. Kobyakov , M. Sauer and D. Chowdhury, "Stimulated Brillouin scattering in optical fibers," *Adv. Opt. Photon.*, vol. 2, no. 1, pp.1 -59, Mar. 2010.

[177] Y. C. Shen, X. M. Zhang, and K. S. Chen, "Optical carrier-suppression of microwave signals with stimulated Brillouin scattering in long fiber ring," *Microw. Opt. Technol. Lett.,* vol. 43, No. 3, pp. 258-260, Sep. 2004.

[178] C. K. Madsen and J. H. Zhao, *Optical Filter Design and Analysis, a Signal Processing Approach*, 1999: Wiley.

[179] J. Capmany, B. Ortega, and D. Pastor, "A tutorial on microwave photonic filters," *IEEE J. Lightw. Technol.,* vol. 24, no. 1, pp. 201-229, Jan. 2006.

[180] A. A. Savchenkov, L. Wei, V. S. Ilchenko, A. B. Matsko, D. Seidel, and L. Maleki, "RF photonic signal processing components: From high order tunable filters to high stability tunable oscillators," *IEEE Radar Conference, 2009*, pp. 1-6, May 2009.

[181] X. Yi and R. Minasian, "Photonic approaches for processing high frequency microwave signals," *Information, Communications and Signal Processing (ICICS) 2011 8th Int. Conf. on*, pp.1-4, Dec. 2011.

[182] Y. Dai and J. P. Yao, "Nonuniformly-spaced photonic microwave delay-line filter," *Opt. Exp.*, vol. 16, no. 7, pp. 4713-4718, Mar. 2008.

[183] B. Vidal, T. Mengual, C. Ibanez-Lopez, and J. Marti, "WDM photonic microwave filter with variable cosine windowing based on a DGD module," *IEEE Photon. Technol. Lett.,* vol.18, no.21, pp.2272-2274, Nov. 2006.

[184] Y. Dai and J. P. Yao, "Nonuniformly spaced photonic microwave delay-line filters and applications," *IEEE Trans. Microw. Theory Tech.*, vol. 58, no. 11, pp. 3279-3289, Nov. 2010.

[185] D. Pastor, B. Ortega, J. Capmany, S. Sales, A. Martinez, and P. Muñoz, "Optical microwave filter based on spectral slicing by use of arrayed waveguide gratings," *Opt. Lett.,* vol. 28, no. 19, pp. 1802-1804, Oct. 2003.

[186] J. Mora, B. Ortega, A. Díez, J. L. Cruz, M. V. Andrés, J. Capmany, and D. Pastor, "Photonic microwave tunable single-bandpass filter based on a Mach-Zehnder interferometer," *J. Lightw. Technol.,* vol. 24, no. 7, pp. 2500-2509, Jul. 2006.

[187] K. Zhu, H. Ou, H. Fu, E. Remb, and S. He, "A simple and tunable single-bandpass microwave photonic filter of adjustable shape," *IEEE Photon. Technol. Lett.,* vol. 20, no. 23, pp. 1917-1919, Dec. 2008.

[188] J. H. Lee, Y. M. Chang, Y. G. Han, S. B. Lee, and H. Y. Chung, "Fully reconfigurable photonic microwave transversal filter based on digital micromirror device and continuous-wave, incoherent supercontinuum source," *Appl. Opt.,* vol. 46, no. pp. 5158-5167, Aug. 2007.

[189] E. Hamidi, D. E. Leaird, and A. M. Weiner, "Tunable programmable microwave photonic filters based on an optical frequency comb," *IEEE Trans. Microw. Theory and Tech.,* vol. 58, no.11, pp. 3269-3278, Nov. 2010.

[190] M. Song, V. T. Company, A. J. Metcalf, and A. M. Weiner, "Multitap microwave photonic filters with programmable phase response via optical frequency comb shaping," *Opt. Lett.,* vol. 37, no. 5, pp. 845-847, Mar. 2012.

[191] V. R. Supradeepa, C. M. Long, R. Wu, F. Ferdous, E. Hamidi, D. E. Leaird, and A. M. Weiner, "Comb-based radiofrequency photonic filters with rapid tunability and high selectivity," *Nat. Photon.*, vol. 6, no. 3, pp. 1186-194, Mar. 2012.

[192] N. You and R. A. Minasian, "A novel high-Q optical microwave processor using hybrid delay-line filters," *IEEE Trans. Microw. Theory Tech.,* vol. 47, no7, pp.1304-1308, Jul. 1999.

[193] J. Capmany, "On the cascade of incoherent discrete-time micro-wave photonic filters," *J. Lightw. Technol.*, vol. 24, no. 7, pp. 2564-2578, Jul. 2006.

[194] B. Ortega, J. Mora, J. Capmany, D. Pastor, and R. Garcia-Olcina, "Highly selective microwave photonic filters based on active optical recirculating cavity and tuned modulator hybrid structure," *Electron. Lett.*, vol. 41, no. 20, pp. 1133-1135, Sep. 2005.

[195] E. Xu, X. Zhang, L. Zhou, Y. Zhang, Y. Yu, X. Li, and D. Huang, "Ultrahigh-Q microwave photonic filter with Vernier effect and wavelength conversion in a cascaded pair of active loops," *Opt. Lett.,* vol. 35, no. 8, pp. 1242-1244, Apr. 2010.

[196] M. Sagues, A. Loayssa, and J. Capmany, "Multitap complex-coefficient incoherent microwave photonic filters based on stimulated Brillouin scattering," *IEEE Photon. Technol. Lett.*, vol. 19, no. 16, pp.1194-1196, Aug. 2007.

[197] B. Vidal, M. A. Piqueras, and J. Martí, "Tunable and reconfigurable photonic microwave filter based on stimulated Brillouin scattering," *Opt. Lett.,* vol. 32, no. 1, pp. 23-24, Jan. 2007.

[198] S. Chin, L, Thevenaz, J. Sancho, S. Sales, J. Capmany, P. Berger, J. Bourderionnet, and D. Dolfi, "Broadband true time delay for microwave signal processing, using slow light based on stimulated Brillouin scattering in optical fibers," *Opt. Exp.,* vol. 18, no. 21, pp. 22599-22613, Oct. 2010.

[199] R. Pant, A. Byrnes, E. Li, D. Choi, C. G. Poulton, S. Fan, S. J. Madden, B. Luther-Davies, and B. J. Eggleton, "Photonic chip based tunable and dynamically reconfigurable microwave photonic filter using stimulated Brillouin scattering," in *Bragg Gratings, Photosensitivity, and Poling in Glass Waveguides*, 2012, paper JW4D.5.

[200] A. Byrnes, R. Pant, C. G. Poulton, E. Li, D. Choi, S. J. Madden, B. Luther-Davies, and B. J. Eggleton, "On-chip, tunable, narrow-bandpass microwave photonic filter using stimulated Brillouin scattering (SBS)," in *CLEO: Science and Innovations*, 2012, paper CTu2A.6.

[201] X. Yi and R. A. Minasian, "Microwave photonic filter with single bandpass response," *Electron. Lett.,* vol. 45, no. 7, pp. 362-363, Mar. 2009.

[202] J. Palací, G. E. Villanueva, J. V. Galán, J. Martí, and B. Vidal, "Single bandpass photonic microwave filter based on a notch ring resonator," *IEEE Photon. Technol. Lett.,* vol. 22, no. 17. pp. 1276-1278, Sep. 2010.

[203] W. Li, M. Li, and J. P. Yao, "A narrow-passband and frequency-tunable micro-wave photonic filter based on phase-modulation to intensity-modulation conversion using a phase-shifted fiber Bragg grating," *IEEE Trans. Microw. Theory Tech.*, vol. 60, no. 5, pp.1287-1296, May 2012.

[204] F. Zeng and J. P. Yao, "Investigation of phase modulator based all-optical bandpass microwave filter," *IEEE J. Lightw. Technol.*, vol. 23, no. 4, pp. 1721-1728, Apr. 2005.

[205] H. Chi, X. Zou, and J. Yao, "Analytical models for phase-modulation-based microwave photonic systems with phase modulation to intensity modulation conversion using a dispersive device," *J. Lightw. Technol.*, vol. 27, no. 5, pp. 511-521, Mar. 2009.

[206] Y. Painchaud, M. Aubé, G. Brochu, and M. Picard, "Ultra-narrowband notch filtering with highly resonant fiber Bragg gratings," *in Bragg Gratings, Photosensitivity, and Poling in Glass Waveguides*, OSA Technical Digest (CD), paper BTuC3, 2010.

[207] Y. Painchaud, M. Poulin, C. Latrasse, N. Ayotte, M. Picard, and M. Morin, "Bragg grating notch filters in silicon-on-insulator waveguides," in *Bragg Gratings, Photosensitivity, and Poling in Glass Waveguides*, OSA Technical Digest (CD), paper BW2E.3, 2012.

[208] T. Erdogan, "Fiber grating spectra," *J. Lightw. Technol.,* vol. 15, no. 8, pp. 277-1294, Aug. 1997.

[209] C. L. Goldsmith, G. A. Magel, B. M. Kanack, and R. J. Baca, "Coherent combining of RF signals in a traveling-wave photodetector array," *IEEE Photon. Technol. Lett.,* vol. 9, no.7, pp. 988-990, Jul. 1997

[210] V. E. Houtsma, T. Hu, N. Weimann, R. Kopf, A. Tate, J. Frackoviak, R. Reyes, Y. Chen, and L. Zhang, "A 1 W linear high-power InP balanced uni-traveling carrier photodetector," in *37th European Conference and Exposition on Optical Communications*, 2011, paper Tu.3.LeSaleve.6.

[211] A. Ramaswamy, M. Piels, N. Nunoya, T. Yin, and J. E. Bowers, "High power silicon-germanium photodiodes for microwave photonic applications," *IEEE Trans. Microw. Theory and Tech.,* vol. 58, no. 11, pp. 3336-3343, Nov. 2010.

[212] P. St. J. Russell, J. L. Archambault, and L. Reekie, "Fiber gratings," *Physics World,* vol. 6, no. 10, pp. 41-46, Oct.1993.

[213] M . Bernier, Y. Sheng, and R. Vallee, “Ultrabroadband fiber Bragg gratings written with a highly chirped phase mask and Infrared femtosecond pulses,” *Opt. Exp.,* vol. 17, no. 5, pp. 3285-3290, Mar. 2009.

[214] X. Wang, W. Shi, S. Grist, H. Yun, N. A. F. Jaeger, and L. Chrostowski, “Narrow-band transmission filter using phase-shifted Bragg gratings in SOI waveguide,” *Photonics Conference (PHO), 2011 IEEE ,* paper ThZ1, pp.869-870, Oct. 2011.

PUBLICATION LIST

Refereed journal papers

1 **W. Li** and J. P. Yao, "Spurious-free dynamic range improvement of a microwave photonic link based on bidirectional use of a polarization modulator in a Sagnac loop," *Opt. Express,* submitted.

2 F. Kong, **W. Li** and J. P. Yao, "Transverse load sensing based on a dual-frequency optoelectronic oscillator," *Opt. Lett.*, submitted.

3 X. Chen, **W. Li** and J. P. Yao, "Microwave photonic link with improved dynamic range using a polarization modulator," *IEEE Photon. Technol. Lett.,* submitted.

4 W. Liu, **W. Li**, and J. P. Yao, "An ultra-wideband microwave photonic phase shifter with a full 360^{o} phase tunable range," *IEEE Photon. Technol. Lett.*, under revisions.

5 **W. Li**, W. Zhang, and J. P. Yao, "A wideband 360^{o} photonic-assisted microwave phase shifter using a polarization modulator and a polarization-maintaining fiber Bragg grating," *Opt. Express*, vol. 20, no. 28, pp. 29838-29843, Dec. 2012.

6 M. Li, **W. Li**, and J. P. Yao, "Tunable optoelectronic oscillator incorporating a high-Q spectrum-sliced photonic microwave transversal filter," *IEEE Photon. Technol. Lett.*, vol. 24, no. 14, pp. 1251-1253, July 2012.

7 **W. Li** and J. P. Yao, "Wideband frequency-tunable optoelectronic oscillator incorporating a tunable microwave-photonic filter based on phase-modulation to intensity-modulation conversion using a phase-shifted fiber-Bragg grating," *IEEE Trans. Microw. Theory Tech.*, vol. 60, no. 6, pp. 1735-1742, June 2012.

8 **W. Li** and J. P. Yao, "An optically tunable frequency-multiplying optoelectronic oscillator," *IEEE Photon. Technol. Lett.*, vol. 24, no. 10, pp. 812-814, May 2012.

9 **W. Li**, M. Li, and J. P. Yao, "A narrow-passband and frequency-tunable micro-wave photonic filter based on phase-modulation to intensity-modulation conversion using a

phase-shifted fiber Bragg grating," *IEEE Trans. Microw. Theory Tech.*, vol. 60, no. 5, pp. 1287-1296, May 2012.

10 X. Zou, **W. Li**, W. Pan, B. Luo, L. Yan, and J. P. Yao, "A photonic approach to the measurement of time-difference-of-arrival and angle-of-arrival of a microwave signal," *Opt. Lett.*, vol. 37, no. 4, pp. 755-757, Feb. 2012.

11 M. Qasymeh, **W. Li**, and J. P. Yao, "Frequency-tunable microwave generation based on time-delayed optical combs," *IEEE Trans. Microw. Theory Tech.*, vol. 59, no. 11, pp. 2987-2993, Nov. 2011.

12 Z. Li, **W. Li**, H. Chi, X. Zhang, and J. P. Yao, "A continuously tunable microwave fractional Hilbert transformer based on a photonic microwave delay-line filter using a polarization modulator," *IEEE Photon. Technol. Lett.*, vol. 23, no. 22, pp. 1694-1699, Nov. 2011.

13 W. Liu, **W. Li**, and J. P. Yao, "Real-time interrogation of a linearly chirped fiber Bragg grating sensor for simultaneous measurement of strain and temperature," *IEEE Photon. Technol. Lett.*, vol. 23, no. 18, pp. 1340-1342, Sep 2011.

14 Z. Li, **W. Li**, H. Chi, X. Zhang, and J. P. Yao, "Photonic generation of phase-coded microwave signal with large frequency tunability," *IEEE Photon. Technol. Lett.*, vol. 23, no. 11, pp. 712-714, Jun. 2011.

15 Z. Li, **W. Li,** H. Chi, X. Zhang, and J. P. Yao, "Optical single-sideband modulation using a fiber-Bragg-grating-based optical Hilbert transformer," *IEEE Photon. Technol. Lett.*, vol. 23, no. 9, pp. 558-560, May 2011.

16 **W. Li** and J. P. Yao, "Microwave and terahertz generation based on photonically assisted microwave frequency twelvetupling with large tunability," *IEEE Photon. J.*, vol. 2, no. 6, pp. 954-959, Dec. 2010.

17 **W. Li** and J. P. Yao, "Investigation of photonically assisted microwave frequency multiplication based on external modulation," *IEEE Trans. Microw. Theory Tech.*, vol. 58, no. 11, pp. 3259-3268, Nov. 2010.

18 M. Li, C. Wang, **W. Li**, and J. P. Yao, "An unbalanced temporal pulse shaping system for chirped microwave waveform generation," *IEEE Trans. Microw. Theory Tech.*, vol. 58, no. 11, pp. 2968-2975, Nov. 2010.

19 **W. Li** and J. P. Yao, "An optically tunable optoelectronic oscillator," *IEEE/OSA J. Lightw. Technol.*, vol. 28, no. 18, pp. 2640-2645, Sep. 2010.

20 **W. Li** and J. P. Yao, "Microwave generation based on optical-domain microwave frequency octupling," *IEEE Photon. Technol. Lett.*, vol. 22, no. 1, pp. 24-26, Jan. 2010.

21 **W. Li** and J. P. Yao, "Optical frequency comb generation based on repeated frequency shifting using two Mach-Zehnder modulators and an asymmetric Mach-Zehnder interferometer," *Opt. Express*, vol. 17, no. 26, pp. 23629-23636, Dec. 2009.

22 **W. Li** and J. P. Yao, "Edge-triggered bi-phase modulation for the generation and modulation of UWB pulses," *IEEE Photon. Technol. Lett.*, vol. 20, no. 20, pp. 1691-1693, Oct. 2008.

Conference Papers

1 **W. Li**, W. Zhang, and J. P. Yao "An ultra-wideband 360^{o} photonic-assisted microwave phase shifter*," OFC 2013*, 17-21 March 2013, Anaheim, CA, USA, paper OTu2H.4.

2 **W. Li** and J. P. Yao "A narrow-passband frequency-tunable microwave photonic filter with an improved dynamic range," *OFC 2013*, 17-21 March 2013, Anaheim, CA, USA, paper OTu2H.3.

3 M. Li, **W. Li**, J. P. Yao, and J. Azana "Femtometer-resolution wavelength interrogation using an optoelectronic oscillator," *IPC 2012*, 23-27 September 2012, Burlingame, California, USA, paper TuK2.

4 M. Li, **W. Li,** J. P. Yao, and J. Azana, "Femtometer-resolution wavelength interrogation of a phase-shifted fiber Bragg grating sensor using an optoelectronic oscillator," *2012 OSA Topical Meeting on Bragg Gratings, Photosensitivity, and Poling in Glass Waveguides*, 17-21 June 2012, Cheyenne Mountain Resort, Colorado Springs, Colorado, USA, paper BTu2E.3

5 **W. Li** and J. P. Yao, "An optically tunable frequency-doubling optoelectronic oscillator incorporating a phase-shifted-fiber- Bragg-grating-based frequency-tunable photonic microwave filter," *2011 IEEE Microwave Photonics Conference*, Singapore, Oct. 2011, pp.429-432.

6 M. Li, **W. Li,** and J. P. Yao, "A tunable optoelectronic oscillator based on a high-Q spectrum-sliced photonic microwave transversal filter," *2011 IEEE Microwave Photonics Conference*, Singapore, Oct. 2011, pp. 304-307.

7 **W. Li** and J. P. Yao, "An optically tunable frequency-quadrupling optoelectronic oscillator," *2011 IEEE Photonics Conference*, Oct. 2011, Arlington, USA, pp. 475-476.

8 **W. Li** and J. P. Yao, "A wideband frequency tunable optoelectronic oscillator incorporating a tunable photonic microwave filter based on a phase-shifted fiber Bragg grating," *Proc. SPIE 8007, Photonics North 2011*, Ottawa, Canada, May 2011, pp. 80070F-1-80070F-7.

9 **W. Li** and J. P. Yao, "Optical frequency comb generation based on repeated frequency shifting," *The 22nd IEEE Lasers and Electro Optics Society Annual Meeting (LEOS 2009)*, paper WO4.

10 **W. Li** and J. P. Yao, "Microwave frequency multiplication using two cascaded Mach-Zehnder modulators," *Asia-Pacific Microwave Photonics Conference*, Beijing, China, 22-24 April 2009.